CL-Windcon

Closed Loop Wind Farm Control

DELIVERABLE REPORT

Classification of control-oriented models for wind farm control applications

Deliverable No.	D1.4	Work Package No.	WP1	Tasks No.	1.4
Work Package Title		Wind farm control-oriented model development			
Linked Tasks Title		Model classification			
Status		**Draft Final**			
Dissemination level		**public**			
Due date deliverable		2018-09-30	Submission date		2018-10-01
Deliverable version		1.6			

This project has received funding from the European Union's Horizon 2020 research and innovation programme under grant agreement No 727477

DOCUMENT CONTRIBUTORS

Deliverable responsible	USTUTT
Contributor	**Organization**
Steffen Raach	USTUTT
Filippo Campagnolo	TUM
Bharath Kodiyala Ramamurthy	GE Renewable Energy
Stefan Kern	GE Renewable Energy
Sjoerd Boersma	Delft University of Technology
Bart Doekemeijer	Delft University of Technology
Jan-Willem van Wingerden	Delft University of Technology
Torben Knudsen	Aalborg University
Maria Aparicio-Sanchez	CENER
Pedro Correia	CENER
Stoyan Kanev	ECN-TNO
Roberto Chávez	CENER
Sugoi Gomez-Iradi	CENER
David Astrain	CENER
Elena Cantero	CENER
Paolo Schito	POLIMI

Reviewer	**Organization**
Giancarlo Potenza	ENEL
Stefano Cacciola	POLIMI

CONTENTS

List of Figures . . . 5

List of Tables . . . 10

1 Executive Summary . . . 11

2 Model Classification . . . 12
2.1 Introduction . . . 12
2.2 SOWFA . . . 12
2.2.1 General model description . . . 12
2.3 FLORIS . . . 15
2.3.1 General model description . . . 15
2.3.2 General model classification . . . 15
2.4 Model based on data reduction techniques . . . 16
2.4.1 General description . . . 16
2.4.2 General model classification . . . 16
2.5 SimWindFarm . . . 17
2.5.1 General description . . . 17
2.5.2 General model classification . . . 17
2.6 WindFarmSimulator . . . 18
2.6.1 General model description . . . 18
2.6.2 General model classification . . . 19
2.7 FAST.Farm . . . 19
2.7.1 General description . . . 19
2.7.2 General model classification . . . 20
2.8 FarmFlow . . . 21
2.8.1 General model description . . . 21
2.8.2 General model classification . . . 21
2.9 DNV GL model based on LongSim . . . 22
2.9.1 Generel model description . . . 22
2.9.2 General model classification . . . 22
2.10 Wake Dissipation Model . . . 24
2.10.1 General model description . . . 24
2.10.2 General model classification . . . 24
2.11 Summary . . . 25

3 SOWFA base reference simulations . . . 30
3.1 SOWFA precursor simulations . . . 30
3.1.1 Numerical set-up . . . 31
3.1.2 Analysis of the A4 case . . . 32
3.1.3 Results for the rest of scenarios . . . 35

4 Calibration and Parameter tuning of FLORIS and WFSim . . . 41
4.1 FLORIS . . . 41
4.1.1 Calibration methodology . . . 41
4.1.2 Calibration results . . . 42
4.1.3 Validation results . . . 43

4.2 WFSim . . . 47
4.2.1 Tuning parameters in the WFSim model . . . 47
4.2.2 Validation of the WFSim model with SOWFA . . . 47
4.2.3 Validation of the WFSim model with PALM . . . 50

5 Sensitivity analysis with FAST.Farm . . . 54
5.1 Introduction . . . 54
5.1.1 HWkDflO analysis . . . 57
5.1.2 HWkDflOY analysis . . . 57
5.1.3 CNearWake analysis . . . 58
5.1.4 HWkDflx analysis . . . 60
5.1.5 HWkDflxY analysis . . . 62
5.1.6 vShr analysis . . . 64
5.1.7 vAmb analysis . . . 68
5.1.8 Conclusions . . . 70
5.2 Comparison FLORIS/FAST.Farm . . . 71
5.2.1 FLORIS configuration . . . 71
5.2.2 Results comparison . . . 71
5.3 Conclusions . . . 74

6 Validation of the FLORIS steady-state wind farm model . . . 76
6.1 Introduction . . . 76
6.2 Model description . . . 76
6.3 Validation of FLORIS with respect to CFD data. . . . 77
6.3.1 Simulation environment . . . 78
6.3.2 Performed simulations . . . 79
6.3.3 Model parameters tuning . . . 79
6.3.4 Comparison between CFD and FLORIS-predicted wake flow. . . . 81
6.3.5 Comparison between CFD and FLORIS-predicted turbulence intensity. . . . 86
6.4 Conclusions . . . 91

7 Validation of a model based on data reduction techniques . . . 92
7.1 Introduction . . . 92
7.2 Validation of ROMs with respect to CFD data . . . 92
7.2.1 Simulation environment . . . 93
7.2.2 Comparisons ROM - CFD SOWFA simulation . . . 95
7.3 Validation of ROMs with respect to wind tunnel experiments . . . 95
7.4 Conclusions . . . 105

8 Single wake model benchmark with field data . . . 106
8.1 Introduction . . . 106
8.2 Description of benchmark data set . . . 106
8.2.1 Setup of the experiment and instrumentation . . . 106
8.2.2 Postprocessing . . . 108
8.2.3 Benchmark cases . . . 108
8.3 Models included in the benchmark and procedure followed to generate predictions . . . 109
8.3.1 FarmFlow . . . 109
8.3.2 FLORIS . . . 110
8.4 Approach for comparing the wake models with lidar data . . . 111
8.5 Results . . . 112

8.5.1 Wake recovery . . . 113
8.5.2 Variation of atmospheric conditions . . . 116
8.5.3 Variation of turbine operation . . . 116
8.6 Conclusions . . . 121

9 Conclusions . . . 123

References . . . 123

LIST OF FIGURES

Figure 1. Instantaneous horizontal wind speed [ms^{-1}] in the first time step of the recorded precursor (t=91000s), from the A4 case study, at hub height, i.e. 119 m above the surface (a) and in a x-direction plane midway through the domain (b). 33

Figure 2. Evolution in time of the averaged wind speed (left) and turbulence intensity (right) of the A4 case study. The averaged values are based on 1000s intervals. 34

Figure 3. Evolution in time of the averaged wind speed (top panels) and turbulence intensity (bottom panels) of the A4 case study. Comparison among different averaging windows are shown for the wind speed and derived turbulence intensity values at hub height (left panels), and for other relevant heights (5m, 45m, 195m and 795m) on the right panels. . 34

Figure 4. Vertical profile of the wind direction averaged on the last 1×10^4 seconds of the precursor A4 simulation. 35

Figure 5. Evolution in time of the friction velocity (left) and resolved turbulent kinetic energy (right) throughout all the domain height (top panels) and at specifically certain heights above ground (bottom panels). 36

Figure 6. Evolution in time of the resolved turbulent kinetic energy (solid line) and the subgrid tke accounted by the model (dashed line) in the A4 case study. 36

Figure 7. Vertical profiles of turbulence intensity (left) friction velocity (center) and wind speed (right) for the A4 case study. The profiles correspond to different periods of the evolution of the precursor simulation (i.e. at the 30, 60 and 90×10^3-th seconds) from the simulated velocity averaged every 5000 seconds. Additionally, the vertical profiles obtained with the Monin-Obukhov Similarity Theory (MOST) are shown for reference. 37

Figure 8. Vertical profiles of turbulence intensity (left) and wind speed (right) for the A1 and A2 cases. These cases share the same 4.5 m/s target velocity at hub height. Similar to Figure 7, the profiles correspond to different periods of the evolution of the precursor simulation (i.e. at the 30, 60 and 90×10^3-th seconds) from the simulated velocity averaged every 5000 seconds. Additionally, the vertical profiles obtained with the Monin-Obukhov Similarity Theory (MOST) are shown for reference. 38

Figure 9. Vertical profiles of turbulence intensity (left) and wind speed for the A5 and A6 cases. These cases share the same 7.7 m/s target velocity at hub height. Similar to Figure 7, the profiles correspond to different periods of the evolution of the precursor simulation (i.e. at the 30, 60 and 90×10^3-th seconds) from the simulated velocity averaged every 5000 seconds. Additionally, the vertical profiles obtained with the Monin-Obukhov Similarity Theory (MOST) are shown for reference. 39

Figure 10. Vertical profiles of turbulence intensity (left) and wind speed for the A7 and A8 cases. These cases share the same 11.4 m/s target velocity at hub height. Similar to Figure 7, the profiles correspond to different periods of the evolution of the precursor simulation (i.e. at the 30, 60 and 90×10^3-th seconds) from the simulated velocity averaged every 5000 seconds. Additionally, the vertical profiles obtained with the Monin-Obukhov Similarity Theory (MOST) are shown for reference. 40

Figure 11. Inflow comparison. In gray are all vertical profiles along the spatial domain, upon which a single mean profile is fit using spline interpolation. 42

Figure 12. Wake comparison at 5D downstream. The black dots in the top subplot show the locations of the measurements that will be used to calibrate the surrogate model with SOWFA. . . . 43
Figure 13. Validation of the surrogate model with SOWFA: time-averaged flow field at turbine hub height. Units are ms^{-1}. . . . 45
Figure 14. Validation of the surrogate model with SOWFA: wind speed at hub height at different distances downstream 46
Figure 15. Validation of the surrogate model with SOWFA: time-averaged power capture per turbine 46
Figure 16. Time series of the thrust coefficients. 48
Figure 17. Wind farm power from SOWFA (blue dashed) and WFSim (black). 49
Figure 18. Topology simulated wind farm (a) and mean flow centreline at four time instances through the first row (b). 49
Figure 19. Mean flow centreline at four time instances through the second row (a) and third row (b) of turbines. The vertical red dashed lines indicate the positions of the turbines. . . . 50
Figure 20. Longitudinal flow fields at hub height from SOWFA (below) and WFSim (above) at arbitrarily time step. 50
Figure 21. Time series of the thrust coefficients. 51
Figure 22. Wind farm power from PALM (blue dashed) and WFSim (black). 52
Figure 23. Mean flow centreline at four time instances through the farm. The vertical red dashed lines indicate the positions of the turbines. 52
Figure 24. Longitudinal flow fields at hub height from PALM (below) and WFSim (above) at arbitrarily time step. Flow is flowing from left to right in this picture, with two turbines: one at $x = 200$ m, and one around $x = 950$ m. 53
Figure 25. Reference Systems for the sensitivity analysis 56
Figure 26. Wake Center position for different values of HWkDflO (case yaw=0^o) 57
Figure 27. Wake center position at turbine for different values of HWkDflO (case yaw=0^o) . . . 57
Figure 28. Wake profile at 3D (left) and 5D (right) for different values of HWkDflO (case yaw=0^o) 58
Figure 29. Wake Center position for different values of HWkDflOY (case yaw=20^o) 58
Figure 30. Wake center position (y) at turbine for different values of HWkDflOY (case yaw=20^o) 59
Figure 31. Wake profile at 3D (left) and 7D (right) for different values of HWkDflOY (case yaw=20^o) 59
Figure 32. Wake Center position for different values of CNearWake (case yaw=0^o) 60
Figure 33. Wake profile at 0D (left) and 3D (right) for different values of CNearWake (case yaw=0^o) 60
Figure 34. Wake profile at 5D (left) and 10D (right) for different values of CNearWake (case yaw=0^o) 61
Figure 35. Wake map of velocities for baseline (up), NearWake1 (left) and NearWake2 (right)(FAST.Farm reference system) 61
Figure 36. Wake Center position for different values of HWkDflx (case yaw=0^o) 62

Figure 37. Wake center position with respect to baseline for different values of HWkDflx (0D, 5D, 10D, case yaw=0^o) . . . 62
Figure 38. Wake profile at 5D (left) and 10D (right) for different values of HWkDfx (case yaw=0^o) 63
Figure 39. Wake Center position for different values of HWkDflxY (left) and positions with respect to baseline for 5D and 10D (right) (case yaw=20^o) . . . 63
Figure 40. Wake profile at 3D (left) and 10D (right) for different values of HWkDfxY (case yaw=0^o) 64
Figure 41. Wake map of velocities for baseline (up), HWkDflxY1 (left) and HWkDflxY2 (right), case yaw = 20^o (FAST.Farm reference system) . . . 65
Figure 42. Wake Center position for different sets of vShr (case yaw=0^o) . . . 65
Figure 43. Wake profile at 3D (left) and 5D (right) for different sets of vShr (case yaw=0^o) at Wake Centers . . . 66
Figure 44. Wake profile at 7D (left) and 10D (right) for different sets of vShr (case yaw=0^o) at Wake Centers . . . 66
Figure 45. Wake map of velocities for baseline (up), vShr1 (left) and vShr2 (right)(FAST.Farm reference system) . . . 67
Figure 46. Wake Center position for different sets of vAmb (case yaw=0^o) . . . 68
Figure 47. Wake profile at 3D (left) and 5D (right) for different sets of vShr (case yaw=0^o) at Wake Centers . . . 69
Figure 48. Wake profile at 7D (left) and 10D (right) for different sets of vShr (case yaw=0^o) at Wake Centers . . . 69
Figure 49. Wake map of velocities for baseline (up), vAmb1 (left) and vAmb2 (right)(FAST.Farm reference system) . . . 70
Figure 50. Floris (Jensen) wind map for (case yaw=0^o; v=7.7m/s and TI=5%) . . . 72
Figure 51. Wake Center position comparison (case yaw=0^o) . . . 73
Figure 52. Comparison of wake profiles at 0D and 3D for FLORIS and FAST.Farm . . . 73
Figure 53. Comparison of wake profiles at 5D and 7D for FLORIS and FAST.Farm . . . 74
Figure 54. Comparison of wake profiles at 10D for FLORIS and FAST.Farm . . . 74
Figure 55. Visualization of iso-vorticity field for the precursor and turbine cluster simulations. 78
Figure 56. Porté-Agel flow velocity predictions for mid-TI, $\gamma = 0°$, $C_T = 0.902$ . . . 81
Figure 57. Porté-Agel flow velocity predictions for mid-TI, $\gamma = 0°$, $C_T = 0.789$ . . . 82
Figure 58. Porté-Agel flow velocity predictions for mid-TI, $\gamma = -30°$ . . . 82
Figure 59. Porté-Agel flow velocity predictions for mid-TI, $\gamma = -20°$ . . . 82
Figure 60. Porté-Agel flow velocity predictions for mid-TI, $\gamma = 10°$ . . . 83
Figure 61. Porté-Agel flow velocity predictions for mid-TI, $\gamma = 20°$ . . . 83
Figure 62. Porté-Agel flow velocity predictions for mid-TI, $\gamma = 30°$ . . . 83
Figure 63. Porté-Agel flow velocity predictions for high-TI, $\gamma = 0°$, $C_T = 0.718$ . . . 84
Figure 64. Porté-Agel flow velocity predictions for high-TI, $\gamma = 0°$, $C_T = 0.686$ . . . 84
Figure 65. Porté-Agel flow velocity predictions for high-TI, $\gamma = -30°$ . . . 84

Figure 66. Porté-Agel flow velocity predictions for high-TI, $\gamma = -20°$ . . . 85
Figure 67. Porté-Agel flow velocity predictions for high-TI, $\gamma = -10°$ . . . 85
Figure 68. Porté-Agel flow velocity predictions for high-TI, $\gamma = 10°$ . . . 85
Figure 69. Porté-Agel turbulence intensity predictions for mid-TI, $\gamma = 0°$, $C_T = 0.902$ . . . 86
Figure 70. Porté-Agel turbulence intensity predictions for mid-TI, $\gamma = 0°$, $C_T = 0.789$ . . . 87
Figure 71. Porté-Agel turbulence intensity predictions for mid-TI, $\gamma = -30°$ . . . 87
Figure 72. Porté-Agel turbulence intensity predictions for mid-TI, $\gamma = -20°$ . . . 87
Figure 73. Porté-Agel turbulence intensity predictions for mid-TI, $\gamma = 10°$ . . . 88
Figure 74. Porté-Agel turbulence intensity predictions for mid-TI, $\gamma = 20°$ . . . 88
Figure 75. Porté-Agel turbulence intensity predictions for mid-TI, $\gamma = 30°$ . . . 88
Figure 76. Porté-Agel turbulence intensity predictions for high-TI, $\gamma = 0°$, $C_T = 0.718$ . . . 89
Figure 77. Porté-Agel turbulence intensity predictions for high-TI, $\gamma = 0°$, $C_T = 0.686$ . . . 89
Figure 78. Porté-Agel turbulence intensity predictions for high-TI, $\gamma = -30°$ . . . 89
Figure 79. Porté-Agel turbulence intensity predictions for high-TI, $\gamma = -20°$ . . . 90
Figure 80. Porté-Agel turbulence intensity predictions for high-TI, $\gamma = -10°$ . . . 90
Figure 81. Porté-Agel turbulence intensity predictions for high-TI, $\gamma = 10°$ . . . 90
Figure 82. Rotor disk partitioned into four sectors or quadrants (S1, S2, S3, and S4) as defined by the SEWS wake observer. . . . 94
Figure 83. Wind farm layout. Two-turbine cluster aligned with the incoming wind. . . . 94
Figure 84. Comparison between ROM-reconstructed and CFD-obtained power outputs . . . 96
Figure 85. Comparison between the SEWSs output of ROM and CFD for the S1 and S3 sectors of WT2 . . . 97
Figure 86. Comparison between the SEWSs output of ROM and CFD for the S2 and S4 sectors of WT2 . . . 98
Figure 87. Comparison of the stream-wise velocity component on the horizontal plane between the CFD flow (top), ROM-predicted flow with KF-p state observer (middle), and ROM-predicted flow without state observer (bottom) at one instant in time (γ = 23 deg) . . . 99
Figure 88. Comparison of the stream-wise velocity component on the vertical plane between the CFD flow (top), ROM-predicted flow with KF-p state observer (middle), and ROM-predicted flow without state observer (bottom) at one instant in time ($gamma$ = 23 deg) . . . 99
Figure 89. Case with aligned wind turbines: comparison between ROM and Wind tunnel (EXP.) power outputs. . . . 101
Figure 90. Case with aligned wind turbines: comparison between the SEWSs output of ROM and Wind tunnel (EXP.) for the S1 and S3 sectors of WT2 . . . 102
Figure 91. Case with laterally displaced wind turbines: comparison between ROM and Wind tunnel (EXP.) power outputs. . . . 103
Figure 92. Case with laterally displaced wind turbines: comparison between the SEWSs output of ROM and Wind tunnel (EXP.) for the S1 and S3 sectors of WT2 . . . 104

Figure 93. (a) Layout of the test turbine and its immediate neighbors (b) Wind direction distribution at the test site . . . 107
Figure 94. Sketch of the instrumentation setup for the test turbine . . . 107
Figure 95. Sketch of the locations where measurement data and model predictions are compared (red dots). . . . 109
Figure 96. Example of hub-height velocity deficit profiles from lidar measurements at different downstream distances for neutral (left), stable (center) and unstable (right) atmospheric conditions. Black arrows indicate the observed s-shaped path of the center of the time averaged velocity deficit and error bars provide the 95% confidence interval for the mean of the measurements . . . 113
Figure 97. Example of orthogonal regression fit of a Gaussian curve to a measured velocity deficit profile . . . 113
Figure 98. Hub-height velocity deficit profiles for 6-8m/s at 3.4 and 5D downstream for neutral, stable, and unstable atmospheric conditions. . . . 114
Figure 99. Hub-height velocity deficit profiles for 6-8m/s at 7 and 11D downstream for neutral, stable, and unstable atmospheric conditions. . . . 115
Figure 100. Hub-height velocity deficit profiles for 6-8m/s at 5D for different elevations above ground (z/HH) and neutral, stable, and unstable atmospheric conditions. . . . 117
Figure 101. Variation of hub-height wake centerline peak velocity deficit with atmospheric conditions. . . . 118
Figure 102. Variation of hub-height wake width with atmospheric conditions. . . . 119
Figure 103. Variation of hub-height wake centerline peak velocity deficit with turbine operation at 6-8m/s. The top row shows results for baseline operation, the second row shows results for thrust-reduced operation, and the bottom row quantifies the delta centerline peak velocity deficit between the two operation modes. . . . 120
Figure 104. Variation of hub-height wake width with turbine operation at 6-8m/s. The top row shows results for baseline operation, the second row shows results for thrust-reduced operation, and the bottom row quantifies the delta wake width between the two operation modes. . . . 121

LIST OF TABLES

Table 1. Overall conditions for the simulated scenarios. The total simulated time is the addition of the Initial precursor time and the Recorded precursor time. . . . 30
Table 2. Optimal parameters Ψ_{opt} for the surrogate model after calibration using high-fidelity simulation data . . . 44
Table 3. Nomenclature. . . . 47
Table 4. Tuning parameters of the WFSim model. . . . 47
Table 5. Summary of the SOWFA simulation set-up. . . . 48
Table 6. Summary of the WFSim simulation set-up. . . . 48
Table 7. Summary of the PALM simulation set-up. . . . 51
Table 8. Summary of the WFSim simulation set-up. . . . 51
Table 9. Parameters for FAST.Farm . . . 55
Table 10. Definition of the cases for calibration . . . 56
Table 11. CFD Data Cases . . . 79
Table 12. Porté-Agel model parameters before calibration . . . 80
Table 13. Porté-Agel turbulence model parameters before calibration . . . 80
Table 14. Porté-Agel model parameters after calibration . . . 81
Table 15. Porté-Agel model parameters after calibration . . . 86
Table 16. Cases used for comparisons with wind tunnel experiments . . . 100
Table 17. Parameter settings used for the “Zones” model in FLORIS . . . 111
Table 18. Parameter settings used for the “Larsen” model in FLORIS . . . 111
Table 19. Parameter settings used for the “Jensen Gaussian” model in FLORIS . . . 112
Table 20. Parameter settings used for the “Porté-Agel” model in FLORIS . . . 112

1 EXECUTIVE SUMMARY

The design and operation of a wind farm must account for physical phenomena that can be typically neglected when it comes to stand-alone machines. Indeed, complex interactions take place between the atmospheric flow and the wind farm, as well as within the wind power plant itself. In fact, wakes represent a major form of coupling within the plant, and can have a significant influence on power capture and loading, with in turn may imply consequences on life and maintenance.

In recent years, interest has grown past the control of single wind turbines, which remains nevertheless a problem of primary importance, and research has moved into the area of cooperative control of wind turbines within a farm. From this point of view, one may for example seek to maximize the total wind farm power (in contrast to the power maximization of each individual wind turbine), or to achieve a given power set point while minimizing fatigue loading, or other goals that require some form of coordination among the wind turbines.

This deliverable deals with the classification and the analysis of the wake models set in the CL-Windcon project. The wake models of task 1.2 are classified with respect to their capabilities with various aspects. First, the deliverable gives a general overview on each model as well as a written classification description. Then a spreadsheet comparison is given in which the status of each model is analyzed as well as the application area and the future plans are stated.

In the following chapters different aspects of validation and tuning are studied. Calibration and parameter tuning are described in detail with the FLORIS and the WFSim model. A sensitivity study is performed using the FAST.Farm model analyzing the impact and uncertainty of different parameters. Then the validation with simulation and wind tunnel data is shown and furthermore, the validation of the reduced-order POD models are performed. In the last chapter several models are compared in a blind test with field-testing data to emphasize the predictability of the wake shape under realistic conditions of the wake models. Altogether various aspects of the models are stated and their capabilities are evaluated and compared.

2 MODEL CLASSIFICATION

2.1 Introduction

High-fidelity models, that couple wind turbine dynamics models with advanced computational fluid dynamics (CFD) flow models, usually play a key role in the development of control strategies for wind farm, since they allow testing the algorithms in a simulation environment that is quite well reproducing the physical phenomena that govern the interaction between wind turbines and their surrounding flow field. However, these models are generally computationally expensive, which means that they are generally not suitable to be used in support of the controls synthesis or even their tuning and quick verification.

This last consideration is therefore the motivation for the development of control-oriented models characterized by a much lower computational cost. These models could be based on:

- differential equations that solve simplified fluid dynamics and turbine dynamics governing equations
- analytical equations, derived from the fluid dynamics and turbine dynamics governing equations, that employ empirically-derived parameters
- compressing high-fidelity CFD data into reduced-order model obtained through a data-driven model identification procedure

Independently from the approach used for the control-oriented model synthesis, it is necessary to evaluate the models capabilities in terms of a proper prediction of the steady/unsteady flow field and the power/loads of the wind turbines within the wind farm for different inflow and operating conditions.

To this aim, the models developed within the WP1 and presented in deliverable D1.4 are first classified in terms of their capabilities, followed by their validation against high-fidelity simulations output, wind tunnel data or even full-scale data.

This chapter provides the general classification information of the models. It includes the general description and gives a model classification for each model. At the end of the chapter a classification spreadsheet is given which states the different aspects in model classification.

2.2 SOWFA

2.2.1 General model description

The Simulator for Wind Farm Applications (*SOWFA*), is an open-source numerical simulation system employed for the high-fidelity simulation of turbulent atmospheric flows together with the analysis of wind plant and wind turbine fluid physics and structural response.

The tool has been developed by the U.S. National Renewable Energy Laboratory (NREL) on top of the OpenFOAM Computational Fluid Dynamics (CFD) tool-kit [29] and the NREL's aeroelastic wind turbine simulation tool OpenFAST [21], that allows to include wind turbine controllers and a super-controller for the wind farm.

The turbulence closure for the wind flow solution is addressed through large-eddy simulation (LES) method, which directly resolves the larger, energy-containing turbulent scales, to simulate the atmospheric boundary layer and the turbulence contained within it [16].

Turbine blades - flow interaction is addressed by the Actuator Line (AL) method as proposed by [33] in which turbine models are placed in the flow to create wakes that interact with one another, and actuator lines are coupled with OpenFAST.

The flow is computed using an unstructured, collocated, variable, finite-volume formulation that is second-order accurate in time and space [16]. The Boussinesq approximation for incompressible flow is implented in OpenFOAM through the *buoyantBoussinesqPimpleFoam* solver, which introduces the PISO-SIMPLE algorithm to solve the pressure-velocity-temperature coupling. This algorithm does not solve the continuity equation; instead, it solves a pressure Poisson equation that enforces continuity. Coriolis force is added to the momentum equation as a volumetric force in order to account for the Earth's rotation. The ground surface boundary conditions based on Monin-Obuhkov similarity theory is used, whilst the upper boundary is a stress-free, rigid lid. Extensive details of the tool are given by Churchfield et al., [11, 10]

As for OpenFAST, the aeroelastic module of SOWFA, the model is two-way loosely coupled to the actuator line model. The LES model samples the velocity along the actuator line segments and returns those values to OpenFAST, which normally computes those velocities using blade element momentum theory. The blade forces computed with OpenFAST are returned to the LES solver and imposed as the body forces that enter the momentum equation so that Large-scale structures like the rotor wake and blade tip, root, and bound vortices are resolved [16].

The simulation procedure starts by generating a turbulent atmospheric boundary layer precursor, which is essentially a LES simulation that complies with horizontally homogeneous conditions. To this end, the case is run with periodic boundary conditions at the sides of a flat domain that do not include any turbines, and the model is run until the flow field reaches a quasi-equilibrium state.

The velocity field is afterward mapped (in space and time) as inflow conditions to the wind successor simulation which contains the wind turbine models and potentially terrain elements. Ground and upper boundary conditions are the same as in the precursor whereas downstream boundaries are configured as outflow.

2.2.1.1 General model classification

For the CL-Windcon project, the latest versions of SOWFA and OpenFAST (30/06/2018) were used together with the version 2.4.x of OpenFOAM. A set of seven precursors that covered three wind

speeds (4.5, 7.7 and 11.4m/s) and three levels of turbulence intensities (based on the Roughness length, z_0) were generated and recorded to use as inputs for the sucessor SOWFA computations as well as for the FAST.Farm simulations. Those computations were performed in a 5km x 5km x 1km domain with a flat terrain, and once the flow was stabilized, at least the final 75 minutes, with a resolution of 0.3 seconds, were recorded.

The work shown in this deliverable describes these precursors at great detail, as a base for SOWFA and FAST.Farm inputs, that have been and will be used for wind farm studies with several control strategies that takes into account one, three and nine wind turbines.

2.3 FLORIS

2.3.1 General model description

The FLOw Redirection In Steady-state (FLORIS) tool is a set of low-fidelity steady-state wind farm models developed by the Delft University of Technology and the US National Renewable Energy Laboratory (NREL). FLORIS has been developed for real-time online wind farm control and low fidelity offline wind farm analysis and layout optimization. Fundamentally, it is built in a modular way and includes a number of existing steady-state wake deficit and wake deflection models from the literature to provide a relatively accurate prediction of the time-averaged flow field and turbine power capture in the wind farm at a very low computational cost.

2.3.2 General model classification

The FLORIS model is continuously under development, however a full and stable version is available on github (Link). The stable version includes two turbine types, the NREL 5MW and scaled G1 turbine. The model is partially validated through simulations in different ABL stabilities, various TI levels, various yaw misalignment angles and axial induction factors. Validation through wind tunnel tests is not yet finished. FLORIS is an engineering model and its parameters (between 10 and 15) can be tuned based on a suitable set of measurements. The wake models are nonlinear and static. They do not include wake dynamics or propagation. However, the model predicts the time averaged flow, so it includes to some degree the time-averaged effects of wake meandering or wind direction fluctuations etc. The turbines are parametrized using wind speed dependent c_T (thrust coefficient) and c_P (power coefficient) curves, the turbine dynamics are not explicitly modeled. However, additional work exists, that couples FLORIS with CCBlade or FAST. FLORIS allows for axial induction control and wake redirection wind farm control. The model outputs include individual turbine power and optionally the wind farm flow field. The computational effort is low and real time operation possible. Uncertainty can be included in the method of optimization (control), rather than in the model itself. The model can be adapted to different ABL stabilities, wind speeds, wind directions. The model can be adapted to turbines on/off (off equals axial induction factor = 0). The main question in this model is how to find the right parameters for all these different configurations, and at the right time. Currently only flat terrain is modeled, but it is still to be seen how well the model can be fit to data for different topologies. The model can work with different rotor diameters and turbine types, but the hub heights have to be identical. Turbine operational constraints can only be taken into account by providing corresponding wind speed dependent c_T and c_P curves.

2.4 Model based on data reduction techniques

2.4.1 General description

The reduced-order models (ROMs) based on data reduction techniques developed by TUM for this WP1 (deliverable D1.2) enable the development of control strategies that could potentially increase the overall wind plant power output, as well as increase the wind turbines lifetime by reducing their loads, while allowing execution in real time at low computational costs. The models are able to predict the deflection experienced by the wake shed by a wind turbine that is rotated out of the wind, as well as the impact that such a technique has on the performance of downstream wind turbines. The implementation of these models requires the availability of detailed flow data, obtained here by means of CFD simulations performed with SOWFA (high-fidelity large-eddy simulation tool). Thus far, since the method used is based on system identification, ROMs are derived for particular configurations (wind farm layout, wind speed, TI, etc.). Further research will aim at enhancing the models in order to cover a broader range of realistic scenarios for a successful coordinated control of wind turbines within a farm.

2.4.2 General model classification

The model has been developed by TUM and can be considered under construction since further developments are continuously being studied. The model has been fully validated in terms of flow and power outputs with the simulation tool SOWFA for different yaw misalignments set points and under turbulent and non-turbulent conditions. For these comparisons, once the model was obtained, another subsequent CFD simulation was performed with a different yaw misalignment control law in order to validate the prediction capabilities of the previously obtained model. Additionally, it has been also partially validated against wind tunnel test data (in this case, from the wind tunnel at Politecnico di Milano) in terms of power outputs for different yaw misalignments set points and under turbulent conditions. As in the previous case, a yaw misalignment prescription was given to the wind tunnel turbine model and a comparison in terms of power outputs was performed a posteriori.

The ROMs are data-driven models, since they are obtained by a data-driven, equation-free, modeling procedure based on system identification. Models focus on modeling the flow evolution and power outputs considering yaw misalignment as degree of freedom. Hence, they are currently only intended for wake redirection control applications; so not yet for axial induction control or load mitigation, although the modeling procedure could, in principle, easily allow for loads estimation, for example. Models aim at reproducing accurately enough the dominant dynamics of wind turbine wakes, i.e. low order dynamics. They are able to reproduce a 3D flow including the 3 velocity components (streamwise, crosswise, and vertical velocities) for a previously-defined 3D spatial domain. Additionally, they also aim at reproducing wind turbines performance (essentially, power outputs), although other desired output quantities, such as rotor speed, torque, etc., can also be included. At the same time, models present low computational cost. The models do not only predict steady-state wakes for specific yaw angles, but they are dynamic models where transitions are taken into account

and modeled. Furthermore, during the model obtaining process, there is only the need of "tuning" one parameter, i.e. the choice of the order of the model (the number of POD modes chosen for the state projection).

Currently, since the method used is based on system identification, ROMs are derived for a particular configuration. As previously mentioned, the employed method is used to derive models from wind turbines performance and flow data for particular conditions, e.g. inflow conditions (wind speed, TI, wind direction, etc.). Also currently, both the specific wind farm layout and size and the wind turbine geometry are fixed. Therefore, these models could not be directly used do predict the flow within a wind farm characterized by configurations that considerably differ from the ones used to derive the models. Should that be the case, it would be necessary, in principle, to execute other CFD simulations and derive again reduced-order models using the new generated data and outputs. Continuing stressing the applicability of the model to different operating conditions, the reduced-order models have been currently derived for wind tunnel applications. Therefore, rigorously, they must be tested in full-scale conditions before considering their application in other ABL atmospheric conditions. Besides, model reliability on other types of terrain, different than flat one, have not been studied yet. In conclusion, the range of operating conditions is assumed as limited. To overcome these drawbacks, future research activities, focused on improving the model so as it could cover a broader range of realistic scenarios, are required.

Lastly, models can be enriched with state update techniques, i.e. state observers. The observers enable a proper model prediction even for slightly different scenarios like, for example, different wind direction and wind speed.

2.5 SimWindFarm

2.5.1 General description

The SimWindFarm (SWF) toolbox (http://www.ict-aeolus.eu/SimWindFarm/) is initially developed as part of the Aeolus FP7 project and is aimed at providing a fast wind farm simulation environment for development of wind farm control algorithms. Wind farm simulators range from simple static models with low computational cost to high fidelity dynamic models with high computational cost. The main idea with SimWindFarm is to fit in between these to extremes. The main purpose was to be used as a simulator for testing wind farm controllers. SWF is designed as a Simulink toolbox which can generate wind farm models based on the user's choice of layout and turbine.

2.5.2 General model classification

SWF has been under development since 2009 and a number of versions has been made available via the above web site. The toolbox is free and open to the user. Some users has made considerable adaptations to fit their purpose. During the development of SWF done by several researchers devel-

opers always tried to verify that the software behaved as intended. However, SWF has never been validated neither against high fidelity models like SOWFA nor against full scale data.

SWF is a engineering type of model. The ambient wind field is generated using a spectral model for the longitudinal and transverse wind speeds at point of interest in the farm. These points are concentrated at wind turbine (WT) positions. The WTs are modelled with few degrees of freedom: tower fore aft, two drive train inertias and pitch and torque actuator dynamics. The WT aerodynamics is modelled by Cp and Ct curves. The individual WT thrust coefficients are used in simple wake models for deficiency and added turbulence. The ambient wind field are then modified by the local wake deficiency and added turbulence and this is what is used as input to the WT. Two WT controllers are included namely the NREL5MW FAST type and the Open Discon. Also two WT types are included namely the NREL5MW and the DTU10MW. The farm control is only a simple version as this is supposed to be supplied by the user. Only neutral atmospheric stability is implemented so far. Some fatigue load estimation is included.

So far only induction based farm control is implemented in the web site versions. For the NREL5MW version this can currently only be done via controlling the specific WT power references. For the DTU10MW model also relative derating between 0 and 1 can be used. The tool can only handle flat terrain and one wind turbine type but the geometry of the wind farm is free.

In a development version wake redirection using active yaw has been included. The models needed for this is similar to [31]. Until now wake meandering and added turbulence has been understood as relating to different physical phenomena by the developers of SimWindFarm. Now we consider both to model the same increased turbulence in a farm. Therefore the added turbulence has been removed in the current development version.

For small farms e.g. 3 turbines the simulation is faster than real time. The intended use of the SWF is that the user supplies all the necessary parameters for ambient wind, turbines and farm control and then runs the simulation. To simulate using “internal signals” like turbine pitch, TSR or thrust is not possible out of the box. However, there are always the possibility to change and manipulate the Simulink model to serve special purposes.

The tool is only made for constant mean wind speed, direction and turbulence within one simulation.

2.6 WindFarmSimulator

2.6.1 General model description

The WindFarmSimulator (WFSim) model is a medium-fidelity dynamical wind farm model developed by the Delft University of Technology. It has been developed for real-time dynamic wind farm control to be used as a surrogate model inside the control algorithm. In short, WFSim solves a modified set of unsteady two-dimensional (2D) Navier-Stokes equations over a spatially discretized horizontal plane at the turbine hub height. This surrogate model has a total of 5 tuning parameters, much

fewer than the state of the art steady-state surrogate wind farm models from the literature. WFSim has shown success in reconstructing the flow field and turbine power signals of simulation data derived from high-fidelity LES wind farm models. This model is particularly suited for closed-loop wind farm control as it is dynamical, includes both yaw and axial induction control capabilities, handles temporally and spatially varying inflows, and yields a relatively high accuracy with a manageable computational cost.

2.6.2 General model classification

WFSim is fully developed and complete, available in the public domain at Github. It has been validated with high-fidelity simulation data from SOWFA, a large-eddy simulation package, through 2-turbine and 9-turbine wind farm simulations in a neutral ABL. Furthermore, it has been validated using the large-eddy simulation package PALM through 2-turbine and 6-turbine wind farm simulations. The model relies on the physical two-dimensional Navier-Stokes equations to capture local wind speeds and directions, modified to better represent three-dimensional flow dissipation. It is a dynamical, nonlinear model of medium fidelity. The turbines are represented using the actuator disk model (ADM), relying on aero-elastic tables to map the turbine control settings to the non-dimensional turbine thrust coefficient. These aero-elastic tables should model the turbine control algorithm, and can be, e.g., a 2D table with pitch and wind speed. The ADM does not allow the prediction of dynamical structural loads.

Due to its physical basis and the few number of tuning parameters, calibration is fairly straightforward. WFSim only includes 5 tuning parameters, of which only one or two are expected to require online tuning. Furthermore, implementation of a new turbine or topology is very easy, as can be read in the D1.2 deliverable. Since the model is nonlinear and typically includes several thousands of states, the computational cost is relatively high - and real-time-controller synthesis is challenging. Controller performance such as accuracy and robustness is still to be investigated.

The model has not yet been tested under different ABL stabilities. In a neutral ABL, it shows a good match with high-fidelity data under various wind speeds, turbulence intensities, derating strategies, and yaw misalignments. WFSim can be used for power optimization and/or active power control (APC), while research is ongoing towards combined power tracking (APC) and loads minimization.

2.7 FAST.Farm

2.7.1 General description

FAST.Farm is a medium-fidelity multi-physics engineering tool for predicting the power performance and structural loads of wind turbines within a wind farm developed by the US National Renewable Energy Laboratory (NREL).

FAST.Farm uses OpenFAST to solve the aero-hydro-servo-elastic dynamics of each individual turbine, but adds additional physics for wind farm: ambient wind in the atmospheric boundary layer; a wind farm super controller; and wake deficits, advection, deflection, meandering, and merging. FAST.Farm is based on some of the principles of the DWM model, but addresses many of the limitations of previous DWM implementations, includes the controls capability of FLORIS, and functions more similarly to SOWFA. Validation and parameter calibration of FAST.Farm is currently performed against SOWFA simulations with widely accepted conditions.

While a high-performance computer is required to model a complete wind farm, FAST.Farm maintains computational efficiency to support iterative and probabilistic design. Applications of FAST.Farm include reducing wind farm underperformance and loads uncertainty, developing wind farm controls to enhance operation, optimizing wind farm siting and topology, and innovating the design of wind turbines for the wind-farm environment.

2.7.2 General model classification

For the Cl-Windcon project a pre-release was made available by NREL to investigate and classify the tool. The expected first public release is expected in fall 2018. In first investigations validation are performed against SOWFA LES simulations. The simulation cases differ in settings for the atmospheric stability , various TI levels, different yaw misalignments, and on a small wind farm layout with three wind turbines.

The model consists of multiple submodels which interact with each other. Each module represents different physical domain of the wind farm:

- Each representing different physics domains of the wind farm:
  - FAST.Farm Driver.
  - Super Controller (Module SC).
  - OpenFAST (Module OF).
- Wake Dynamics (Module WD):
  - Wake Advection, Deflection, and Meandering.
  - Near Wake Correction.
  - Wake Deficit Increment.
- Ambient Wind Array Effects (Module AWAE):
  - Ambient Wind.
  - Wake Merging,

Characterizing the model, the system has the following properties: dynamic and nonlinear. Its model fidelity is high for the wake model and medium at the turbine level. The controller is included on the turbine as well as on the wind farm level.

2.8 FarmFlow

2.8.1 General model description

For the accurate calculation of wind turbine wake effects in (large) offshore wind farms, ECN has developed the software tool FarmFlow. FarmFlow uses a wake model based on the UPMWAKE code [13]. This model is a 3D parabolised Navier-Stokes code, using a k-ϵ turbulence model to account for turbulent processes in the wake. The ambient flow is modelled in accordance with the method of Panofsky and Dutton [30]. The free stream wind as a function of height is calculated for a prescribed ambient turbulence intensity and the Monin-Obukhov length, which takes the atmospheric stability into account. For the deceleration and expansion of wind turbine wakes, FarmFlow uses an axisymmetric vortex wake model to calculate the stream wise pressure gradients, which are prescribed as a source term in the flow equations. This hybrid method of wake modelling in the near wake region, including an adapted near wake turbulence model, gives very accurate results in a very acceptable amount of computational time.

2.8.2 General model classification

FarmFlow is ECN's in-house simulation tool for modeling wake effects in wind farms. It is based on simplified (parabolized) 3D CFD code, and includes an engineering model for describing the turbulence propagation in the wake. The model is tuned based on wind tunnel and full scale field measurements, and delivers high accuracy at a reasonable computational time (about 1 second per turbine wake on a single code, parallel computations are supported). The state of development is mature: the tool is fully operational and is being used in research and commercial projects for many years now. It has been validated in numerous full-scale measurement studies [7], and requires no further calibration. The rotor is modeled as an actuator disk through the rotor Cp and Ct coefficients. These are provided as input to the model as function of the wind speed. The model is flexible enough to model wind turbines with different hub heights and rotor types. The FarmFlow model has been specifically developed for the analysis and design of wind farm control algorithms, and supports modeling the effects from both induction control (realized by reduction of the rotor thrust coefficient, Ct) and wind redirection (by yaw misalignment). Induction control is implemented by interpolating between different modes of operation, each one being modeled by separate Cp-wind and Ct-wind curves (each for a separate pitch angle or tip-speed ration, for instance). Combinations of induction control and wake redirection are also possible. In its nature, the model is static. However in the CL-Windcon project a quasi-dynamic functionality was added by adding functionality to simulate a time realization of the upcoming wind speed and direction. The time propagation of the inflow through the farm is modeled using time-delays. This allows the simulation and analysis of

dynamic active wake control algorithms, and investigating the impact of wake meandering on their performance. Using the new quasi-dynamic functionality for time-domain simulations, however, significantly decreases the computational speed of the model because for each single time instant a whole batch of farm simulations needs to be performed to properly account for the inherent time delays. For providing loads predictions, a loads module has been developed which is based on a pre-computed database containing the results from a large number of aeroelastic load simulations under various conditions such as wind speeds, turbulence intensities, wake properties (wake center position, wake width and depth), yaw misalignment, and pitch angle offset). Using FarmFlow's output, the loads at each turbine are interpolated from the database. Furthermore, an advanced optimizer has been developed that allows to optimize the farm control strategy for power or loads for the complete range of wind conditions. The complete software package has been used already to analyze the impact from farm control on the annual power production and lifetime loads for several commercial wind farms. A typical optimization and analysis workflow, covering all wind speeds and directions (fine-gridded) takes up to several days on a computer cluster of 100 cores.

2.9 DNV GL model based on LongSim

2.9.1 Generel model description

This model is a development of a time-domain simulation model with the working name "LongSim", developed by DNV GL since 2012 to help tune supervisory control parameters of a single turbine in the context of site-specific long-term wind conditions, as reported in [6] . To capture the important turbine control dynamics it runs with a time step of around 1 second, and yet it can run very long simulations (several years if necessary), driven by site-specific met mast data, in order to capture the statistics of relatively infrequent supervisory control events which depend on low-frequency variations in meteorological conditions.

This combination of short timesteps and long simulation times is ideal for testing wind farm controllers over changing wind conditions. DNV GL has therefore extended this model to cover a whole wind farm, by generating a correlated wind field over the whole farm, adding a dynamic model for wake effects, extending the turbine controllers to respond to wind farm controller demands, and adding a wind farm controller to generate these demands. An illustration of the use of the model for testing wind farm controllers is reported in [5]. DNV GL investigations to date have used a generic 2MW turbine model.

2.9.2 General model classification

This model has been developed for internal use by DNV GL. Although it can be considered complete, documented, and ready to use, it remains under continuous development and improvement. DNV GL is willing to use it to carry out simulations within the CL-Windcon project if this is useful. Any of the wind farm controllers developed during the project could be evaluated by simulating their

performance using the appropriate wind farm definition, driven by 10-minute met mast data from any appropriate source.

The model assembles a number of different sub-models, which can be considered validated to varying degrees. Some aspects of the wake model were extensively validated in a static sense over many years using measurements from a number of wind farms, but some aspects are considered in need of further validation, for which the CL-Windcon project should be helpful. Validation is here considered to represent the process of increasing confidence in a model by means of an iterative process: comparison against measurements, use of measurements to calibrate any empirical parameters, and to inform improvements in the model assumptions and structure. Validation of such a model can never be considered complete: for example it has to give good results over a very wide range of combinations of different atmospheric conditions; and validating the finer details of the model requires measurements which are ever more difficult to acquire in a meaningful way. The wake model is the Ainslie model, as used in the WindFarmer code [18]. This has been validated (and calibrated and improved) over many years using measurements from number of wind farms. The added turbulence model of Quarton-Ainslie is entirely empirical, and since wind turbines and wind farms have changed in various ways since the model was calibrated, further development and validation of the way wake turbulence is modelled is considered desirable. Nevertheless, the WindFarmer validation referred to above includes the effect of the Quarton-Ainslie model of added turbulence, which significantly affects the wake development, and has resulted in satisfactory validation even for modern wind farms which differ greatly from those used in the original Quarton-Ainslie work. The dynamic wake meandering model is used, which has been validated by other authors, although specific validation of its implementation within the DNV GL model has not yet been done. By default, the wake deflection model due to Jimenez is used, but more sophisticated models can be plumbed in, such as the EPFL model which has been found to fit at least one field measurement campaign reasonably well. Further work on this is ongoing during the CL-Windcon project. The model has a choice of models for wake advection, for which very little information currently exists. Measurement campaigns are required in order to increase confidence. The same is true for wake superposition. Wind field coherence parameters are also somewhat uncertain. They are based on very limited numbers of measurement campaigns reported in the literature, but can be expected to vary significantly with meteorological and geographical effects. A choice of different wake models and variants is now available to be used in place of any of the default models for wake deficit, added turbulence, wake deflection, wake superposition and wake advection.

The turbine modelling is relatively well validated, but some uncertainties remain, for example on the effect of yaw misalignment on power production, and the detailed effect of discrete meandering wakes on downwind turbine fatigue loads.

The model would be classified as an “engineering” model. Although fundamentally physics-based in most respects, it uses various simplifications and empirical relationships to realise a practical model with low computational requirements. It is a dynamic time-domain simulation model and

there are no specific assumptions of linearity, like some aspects are definitely non-linear, e.g. rotor aerodynamics, turbine control.

The model fidelity is high on the wind turbine and control integration and the wake is considered with a lower complexity, however, this doesn't imply low fidelity. The model is not difficult to calibrate in principle, but the measurements required to calibrate it are not easy to achieve. Calibration does not yet cover a very wide range of conditions. More measurements are needed to build confidence for a wider range of conditions. Loads are estimated indirectly via external high-fidelity modelling. Further integration between wake details and fatigue loads is being pursued.

The model is completely applicable for wake redirection, axial induction control, load mitigation, etc. The wind farm controller is quite general and any other options are easily incorporated. It deals with any wind farm topology, but cannot be relied upon for complex terrain. Furthermore, it is easy to adapt for different wind turbines, as long as the relevant detailed information is available. The model can also use much simpler turbine descriptions, but fidelity is sacrificed.

A large wind farm can be simulated in real time on a single processor. As with any time-domain model, trade-offs are available between speed and accuracy of solution.

The model can handle local wind directions, moreover, the wind direction is constantly varying, and is modelled as such.

2.10 Wake Dissipation Model

2.10.1 General model description

The wake dissipation model is an engineering model that described several effects of a turbine wake. Mainly the wake deficit, the wake evolution and the wake redirection is included.. The computational costs are very low since engineering modelling techniques are used. The current source code can be downloaded on GitHub.

2.10.2 General model classification

The wake dissipation model was derived to support wake tracking for lidar-based wake applications. It is mainly application driven and follows the idea of providing a simple 3D wake model for wake tracking. It consists of different sub-models that describe aspects of the wake behavior or its evolution. The Jimenez wake redirection, e.g. is used to realize wake redirection. The power extraction is modeled with an actuator disk approach. The wake evolution is described with a 2D Gaussian filter that models the wake mixing. Altogether, the model hasn't been validated yet, since its main purpose is to provide a suitable wake shape approximation.

2.11 Summary

The final section of the chapter aims at summarizing the previously described models and comparing the different states of the models. The following table provides an overview on the current state of the models, their capabilities and complexities.

CL-WINDCON - MAP OF TOOLS			FLORIS	WFSim	FAST.Farm (DWM/FAST)	SimWindFarm	Model based on data reduction techniques	Wake Dissipation Model for Wake Tracking	FarmFlow	DNV GL
State of development	Under construction		Yes	Yes, at TU Delft	X	Further development considered (Inclusion of yaw wake redirection)	Developed at TUM. Further developments still under study.	Yes, at USTUTT.	No	Under continuous development & improvement
	Full version available		Yes, https://github.com/TUDelft-DataDrivenControl/FLORISSE_M	Yes, at TU Delft: https://github.com/Bartdoekemeijer/WFSim	Expected in 2018 (Spring).	Yes		Yes, at USTUTT: https://github.com/SWE-UniStuttgart/DynamicWakeDissipationModel	Yes	Yes, internally to DNV GL
State of validation	Not validated yet									Some aspects still need validation and/or calibration
	Partially validated	Through simulations (under which particular conditions and simulation tool?)	Yes, different ABL stabilities, various TI levels, various yaw misalignment angles and axial induction factors	Yes, for neutral ABL stability, various TI levels, axial induction and yaw misalignment	Expected in 2018 (Spring). Against SOWFA simulations. For different ABL stability, various TI levels, various mean wind speed, yaw misalignment, and a small wind farm (three NREL 5-MW).	Verified to behave as supposed/specified	-	No		Some comparisons against RANS; more in progress
		Through wind tunnel test (under which particular conditions?)	Unsure	No			Conditions: Below rated wind speed in turbulent conditions. Different yaw misalignments were used. Comparisons in terms of power outputs. Politecnico di Milano wind tunnel test data were used.	No		Historical validations of some model components; more in progress
		Through wind field test (under particular conditions?)	Unsure	No			No	Used in wake tracking analysis of historical data, more in progress.		Historical validations of some model components with data from many wind farms; more in progress
	Fully validated	Through simulations (under which particular conditions and simulation tool?)					Conditions: Below rated wind speed in turbulent and non-turbulent conditions. Different yaw misalignments were used. Comparisons in terms of flow and power outputs. SOWFA simulation tool was used.			No model can ever claim to be fully validated!
		Through wind tunnel test (under particular conditions?)					-		Yes	No model can ever claim to be fully validated!
		Through wind field test (under particular conditions?)					No		Yes	No model can ever claim to be fully validated!
Model Nature	Modelled physics		Engineering model, Only ADM for rotor modelling	ADM for rotor, Navier-Stokes for flow	Yes, both. For wind turbine model and for wake model. See D1.2.	Engeneering model (spectral wind representation, wake meandering, added turbulence)	Physics are not directly modeled.	Engineering model, ADM for rotor, 2D Gaussian filter for wake evolution.	Yes	Engineering model, semi-empirical, many aspects fundamentally physics-based
	Data Driven		Yes, for parameter tuning, rotor and flow modelling	Yes, tuning factors for force on flow, and turbulence modelling	Yes. Calibration (offline) of FAST.Farm wake dynamics parameters.		The ROMs are obtained by a data-driven equation-free modeling procedure. Models focus on modeling flow evolution and power outputs with yaw misalignment as degree of freedom. Models aim at reproducing accurately enough the dominant dynamics of the wind turbine wakes (are capable to reproduce 3D flows) and of the wind turbine performances (essentially power output), while having at the same time low computational cost. The models do not only predict steady-state wakes for specific yaw angles, but they are dynamic models were transitions are taken into account and modeled.	For the parameter.	Yes	
		Static	Yes	No			As a consequence of the model being dynamic	x	Yes	No, time-domain simulation
		Delay	No	Yes		Passive tracer wake meandering and delay.	-	x	Yes	?

CL-WINDCON - MAP OF TOOLS			FLORIS	WFSim	FAST.Farm (DWM/FAST)	SimWindFarm	Model based on data reduction techniques	Wake Dissipation Model for Wake Tracking	FarmFlow	DNV GL
Fidelity in the modelling	Wake models	Low order dynamics	The steady-state model predicts the time-averaged flow, so it includes to some degree the time-averaged effects of meandering, etc.	Yes		Wake meandering, added turbulence	The model is a reduced-order model focused on low order dynamics.	Included through the 2D filtering process + passive tracers	No	Wake meandering, wake advection, turbulence evolution and advection, wake added turbulence, turbine rotor speed with torque, pitch and yaw control, supervisory control, wind farm control
		Non-linear models	Yes	Yes			The model is capable of capturing some non-linearities, although the model itself is a linear model.		Yes	No specific assumptions of linearity; some aspects are definitely non-linear, e.g. rotor aerodynamics, turbine control.
		Navier Stokes 2D	No	Yes	Quasi-steady axisymmetric formulation of the thin shear layer approximation to Navier-Stokes and closes the system with an eddy-viscosity model.		-			Yes (option)
		Full Navier Stokes	No	Approximations made to model the vertical dimension			-		Yes	No
	WT Integration	Static Aero Charact.	Aero-elastic parametrization for CT and CP	Optionally: could be coupled to CCblade/FAST for rotor modelling.		Cp and Ct curves	No turbine is actually modeled explicitly.	x	Yes	Yes
		Loads integration	Optionally: work exists with FLORIS coupled to CCBlade and FLORIS coupled to FAST, see Powerpoint slides	See above		Tower and drive train	-		Yes	Loads database interpolation
		Full WT dynamic	See above	See above	OpenFAST. Blade Element Momentum.		-		No	Rotor speed, pitch, yaw, no structural dynamics
	Control integration	WT considered	Through look-up tables. No actual turbine dynamics modelled explicitly.	Currently not, but could be incorporated through look-up tables, just like FLORIS.	Yes. OpenFAST.	FAST type WT controller for NREL5MW and DTU10MW. Open Discon controller for DTU10MW.	Yes, for yaw misalignments	No	No	Full wind turbine control (excluding high frequency dynamics where not relevant), including supervisory control
		Wind Farm controller	Yes, for axial induction factors and yaw angles	Yes, for axial induction factors and yaw angles	Yes. SuperController.	Only very simple example.	Yes, for yaw misalignments	Yaw angles	No	Yes, induction control through delta set-points, wake steering through nacelle position set-points, but full flexibility to incorporate any wind farm controller.
Modelling effort	Number of parameters		Traditional FLORIS: in the order of 15 Gaussian FLORIS: in the order of 11	Around 4	18		One: the order of the reduced order model, i.e. the number of POD modes chosen for the state projection	6	>10	Very flexible, but default values provided for most flow-related aspects. Turbine model allows many parameters to provide realistic model of turbine and controller.
	Output variables		Output powers, flow fields (optional)	Output powers, flow fields	FAST.Farm: Wake deficit, wake center (at different planes), TI downwind turbines,... OpenFAST: loads, power,...	Time series for probably all interesting signals. Some fatigue analysis is also offered.	To be specified, since the modeling procedure is flexible. Currently, power output of all machines in the wind farm and SEWSs. However, other output quantities such as rotor speed, torque, etc. can also be included. Additionally, the model states can be converted to the three velocity components of the wind speed (u,v,w velocities) for a certain previously-defined 3D domain.	u,v,w velocities	>10	Time histories of wind farm power and individual turbine operational parameters such as incident wind and turbulence, rotor speed, pitch, yaw, power, control variables. Loads are also generated in a post-processing step. Numbers of supervisory events such as yaw manoeuvres, stops & starts if applicable, total yaw travel, etc. Wind farm totals also provided.

CL-WINDCON - MAP OF TOOLS			FLORIS	WFSim	FAST.Farm (DWM/FAST)	SimWindFarm	Model based on data reduction techniques	Wake Dissipation Model for Wake Tracking	FarmFlow	DNV GL
Controllability	Control DoF	Wake redirection	Yes	Yes	Yes. WT controller (bladed style dll interface).	Ongoing work to add this in a similar manner as reported in Raach et. Al. 2016.	Yes	x	Yes	Yes
		Induction control	Yes	Yes	Yes. WT controller (bladed style dll interface).	Yes. For NREL5MW controller the control handle is absolut power whereas it is relative derating for the Open Discon.	No (not yet)	x	Yes	Yes
Computational effort	Real time option	Low	Yes			Small computation effort compared to SOWFA.	Yes. Reasonably accurate models (in the form of state-space representation) can be obtained with around only 15 states (15x15 state matrix).	x		Yes
		Small		Between small and medium			-		Yes	
	Off-line use	Medium		Between small and medium	X		-			
		High					-			
Limitations wrt real-world application	Capability to deal with real wind conditions (changing wind speeds/direction/stability & related uncertainties; turbines cutting in and out; external curtailment due to grid demand)		Uncertainty can be included in the method of optimization (control), rather than in the model itself. The model can be adapted to different ABL stabilities, wind speeds, wind directions The model can be adapted to turbines on/off (off equals axial induction factor = 0). The main question in this model is how to find the right parameters for all these different configurations, and at the right time.	This model can deal with varying inflow directions. It is still to be investigated whether it is valid for different ABL stabilities and TI levels.	X	Constant wind mean, direction and turbulence intensity. Only neutral atmosphere. No cut in/out	Several models can be obtained for different specific wind farm layout and wind conditions (wind speed, TI). However, the use of state observers can enable a strong reduction of the number of required ROMs. No cut in/out limit.	Changing wind direction can be included in a limited fashion by changing the general orientation of the wind field coordinate system. Changes in wind speed are considered each time step, however, propagated with Taylor's assumption.	Yes	Changing wind speed, direction and turbulence, may be driven by measured data (e.g. met mast) over long periods, turbines can cut in/out and other supervisory control actions, external curtailment can be implemented
	Wind farm complexities: non-flat terrain, mix of turbine types (hub heights, rotor sizes, ratings,...)		Currently: flat terrain modelled, but it is still to be seen how well the model can be fit to data for different topologies. The model can work with different rotor diameters and turbine types, but the hub heights have to be identical.	Currently: flat terrain modelled, but it is still to be seen how well the model can be fit to data for different topologies. The model can work with different rotor diameters and turbine types, but the hub heights have to be identical.	X	Flat, one turbine type	Flat terrain and same turbine geometry.	At the moment only flat terrain is included.	Only flat terrain.	Any number of different turbine types, sizes, heights, etc. Terrain effects can be included via pre-calculated speed ups etc. Not suitable for very complex terrain.
	If applicable, capability to deal with turbine operational constraints in the farm control optimization: generator torque, thrust, stall margin...		Unsure. One can assume optimal torque controller operation, and then make a Cp-Ct table for blade pitch angles and incoming wind speed. Then, turbine operation is included in the model, indirectly.	Unsure. One can assume optimal torque controller operation, and then make a Cp-Ct table for blade pitch angles and incoming wind speed. Then, turbine operation is included in the model, indirectly.	X		No	No	No	Yes; but different software is used for optimisation.
Evolution options	Modelling improvement	Own development	Yes	Yes.		Yaw actuation. Including DTU10MW. Including Open Discon WT controller.	Yes, and also inspired by previous research publications.	Yes	Yes	Long to-do list!
		Exporting to	-	-			-			
		Merging with	-	-	Collaboration with NREL.		-			
	Concrete aspects of evolution: which limitations will be addressed?	Real wind conditions	First, assessment of weak points of model are to be investigated through high-fidelity simulations. From current simulations, it is expected that modelling for axial induction control will be much tougher than modelling for wake redirection control.	First, assessment of weak points of model are to be investigated through high-fidelity simulations. It is expected that modelling for axial induction control will be much tougher than modelling for wake redirection control.			Firstly, models have been currently conceived for wind tunnel application. Therefore, they should be first tested in full-scale conditions before other considerations. Besides, models can be enriched with state update techniques, i.e. state observers. The observers enable a proper model prediction even for different scenarios like, for example, different wind directions or wind farm layouts.	Dynamic wind propagation with Taylor's assumption.	Yes	Improved modelling of e.g. wake superposition, wake turbulence, effects of shear and veer etc. are sought.

CL-WINDCON - MAP OF TOOLS			FLORIS	WFSim	FAST.Farm (DWM/FAST)	SimWindFarm	Model based on data reduction techniques	Wake Dissipation Model for Wake Tracking	FarmFlow	DNV GL
		Wind farm complexities	See above	See above			Currently, wind farm layout and size are fixed. Future perspectives focus on enhancing the model in order to cover a broader range of realistic scenarios. Currently, since the method used is based on system identification, ROMs are derived for a particular configuration. If other conditions were desired, another CFD simulation would be, in principle, required for the new layout.			
		Turbine operational constraints in wind farm optimization	See above	See above	Desired.		-		Yes	
	Evolution plans: in-scope or out-of-scope of CL-Windcon?		Mainly in-scope	In-scope		Yaw redirestion. Validation against SOWFA and perhaps full scale.	in-scope	in-scope	in-scope	
Appropiate for	Possibilities of application under current state	Wake redirection	Yes	Yes	Yes. WT controller.		Yes	Yes	Yes	Evolution will occur in parallel with CL-Windcon
		Induction control	Yes	Yes	Yes. WT controller.	Yes	No		Yes	Yes
	Possible future usage	Wake redirection	Yes	Yes	Yes. SupercController.	Maybe	Yes		Yes	Yes
		Induction control	Yes	Yes	Yes. SupercController.	Yes	Medium-highly possible		Yes	Yes

3 SOWFA BASE REFERENCE SIMULATIONS

3.1 SOWFA precursor simulations

As described above, there are a couple of non-stationary models in the project capable of simulating the interaction between wind turbines and the fully turbulent atmospheric flow. Some examples are the high-fidelity LES model SOWFA (see section 2.2) and the FAST.Farm model, described in section 2.7.

One of the essential inputs for these type of models is the turbulent flow that serves as inflow and internal wind flow. There are several methods and tools available for generating turbulent inflows. These methods range from the simple generation of random velocity values (white noise) to methods based on stochastic techniques [34, 22]; technique based on the digital filter [24] to the more realistic model developed by [25, 26] which employs a modelled spectral tensor to create a turbulence field employing Fourier methods.

Since the accuracy of the models in depicting the proper wake dynamics, turbine-flow interaction and future control strategies will largely depend on how close are the inflow turbulent structures to the real atmospheric flows, the most consistent method is to generate these conditions from the same LES model that is used for the high-fidelity simulations which will serve to calibrate the lower-fidelity and less computationally expensive models, an approach that is already applied in the results presented in section 50).

Therefore, this section shows the numerical set-up and outcome of the precursor simulations carried out for different scenarios of mean wind speed and turbulence intensity defined in previous stages of the project. While all the possible scenarios were reported in the deliverable D1.2, only those chosen as high priority by the consortium were finally simulated and shown in the next sections. Their naming convention, characteristics and overall results are summarized in Table 3.1.

As can be also seen in Table 3.1, simulations were run during approximately 100×10^3 s to develop the flow and achieve convergence of second-order statistics.

Table 1. Overall conditions for the simulated scenarios. The total simulated time is the addition of the Initial precursor time and the Recorded precursor time.

Case name	z_0[m]	U_{hub} [m/s]	Initial prec. time [s]	Recorded prec. time [s]	Obtained TI_{hub}
A1	0.001	4.5	110000	4848	0.0536
A2	0.01	4.5	144000	5511	0.0691
A4	0.001	7.7	91000	4619	0.0539
A5	0.01	7.7	84000	4801	0.0706
A6	0.2	7.7	108000	4490	0.0866
A7	0.001	11.4	111000	4879	0.0580
A8	0.01	11.4	106000	5246	0.0623

For each case, the ground surface is set to a wall with the uniform aerodynamic roughness length specified in the Table 3.1. Since all the cases are configured for neutral atmospheric conditions, the turbulence level obtained at the end of the simulation is only modulated by the overall wind speed and the different roughness values. The resulting values of each scenario are listed in the last column of Table 3.1.

After ensuring convergence, the precursor simulations were run for at least another 4500 seconds (as shown the total simulation time shown in Table 3.1) in which all the information required for the future successors simulations, by SOWFA and other models, is stored at 3.33 Hz frequency, that is, a constant $\Delta t = 0.3$ s

In addition to the goal of ensuring that the simulation time is enough to develop the flow in the atmospheric surface layer, the analysis presented below aims at verifying the characteristics of the main wind speed statistics developed at each scenario.

Further analysis with the spectra and characteristics will be presented in the deliverable D3.5.

3.1.1 Numerical set-up

As discussed during previous phases of the project, all the simulated scenarios were carried out under the assumption of neutrally-stratified wind flow. SOWFA LES model is coupled with the *One Equation Eddy Viscosity Model* SGS model [36, 23] were ν_{SGS} is estimated from the subgrid turbulence kinetic energy k_{SGS} which is in turn computed from a transport equation. SOWFA employs the PISO algorithm for the solution of the pressure-velocity equations. A backward interpolation scheme is applied in the solution of the transient term and central differencing for the remaining terms.

The computational domain consists of a box of dimensions $\mathrm{L}_x \times \mathrm{L}_y \times \mathrm{L}_z = 5 \times 5 \times 1$ km, respectively, where axes describe directions aligned with the west-east, north-south and vertical directions of the domain. Since all the scenarios are based on flat terrain conditions, they all share the same mesh created with the OpenFOAM's basic grid generator*blockMesh* which produces a perfectly structured and fully orthogonal grid. Analogously, the number of grid point in every every direction is $500 \times 500 \times 100$ resulting in a uniform grid-spacing of 10 m in all directions with a size of 25 million cells. All lateral boundaries are set to periodic boundary conditions. Hence, the inlet flow is recycled from the outlet. The flow is driven by a uniform pressure gradient that is dynamically adjusted every time step so that the velocity magnitude at hub height (i.e. 119m above surface) reaches the target velocity of every case study listed in Table 3.1.

All lateral boundaries are set to periodic boundary conditions. Hence, the inlet flow is recycled from the outlet. The flow is driven by a uniform pressure gradient that is dynamically adjusted every time step so that the velocity magnitude at hub height (i.e. 119m above surface) reaches the target velocity of every case study as listed in Table 3.1.

The Coriolis force included in SOWFA allows the simulation of the complete Atmospheric Boundary Layer (ABL). This also avoids the parametrization of the components of the shear stress at the top of

the ABL as they become negligible at this altitude. The latitude set for the simulations is $\varphi = 41.3°$, which produces a Coriolis frequency of $f = 9.625596 \times 10^{-5}\ \mathrm{s}^{-1}$ defined as:

$$f = 2\Omega \sin \varphi \tag{3.1}$$

where $\Omega = 7.292 \times 10^{-5}$ rad/s is the Earth's rotation rate and φ the aforementioned latitude.

The wind direction is set to 45 degrees (from the north) at hub height. Therefore the west- and south-boundaries work always as inflow boundaries while the east and north lateral sides become always an outflow type of condition.

The Δt is configured as adaptive with a limiting of maximum Courant-Friedrichs-Lewy number of CFL $= 0.75$ over the whole domain.

3.1.2 Analysis of the A4 case

The results of the so-called A4 case are already being employed for the simulations and sensitivity analysis performed with the FAST.Farm model (see section 2.7), hence, this section deepens on the analysis of this case, while the results for the rest of cases are described in section 2.2 with lesser details as many of the findings and conclusions of A4 case are also shared with the rest of the simulated scenarios.

Overall results: first order statistics

As can be seen in the table 3.1, the case is configured with a target mean wind speed at hub height of 7.7 m/s and roughness length of $z_0 = 0.001$ m. Figure 5 illustrates the spacial fluctuations of the target velocity through an instantaneous snapshot at $t = 91000$ seconds (end of the precursor simulation), of the horizontal wind speed field in a x-y cross-section plane at hub height which is defined at 119 m above ground. That bottom panel of Figure 5 also shows the vertical y-z cross-section at the x-direction midpoint.

Despite all cases consider neutral atmospheric surface conditions, the vertical cross-section illustrates the capping inversion layer which defines the initial boundary layer height. The distance from the ground of capping layer was set-up to ≈ 700 m for all the cases. As seen in Figure 5 (b), this distance remains throughout the entire simulation due to the zero hear flux of the neutral conditions.

The next figures (Figure 2 and 3) show the evolution of precursor simulation in time. Figure 2 presents the wind speed output in a column located at center of the domain. The values of wind speed are averaged in time with a 1×10^{-3}Hz frequency, that is, in 1000 s intervals. The turbulence intensity, TI (Figure 2 right), is computed as ratio of standard deviation U_{std}, and mean wind speed $|U|$ for each interval.

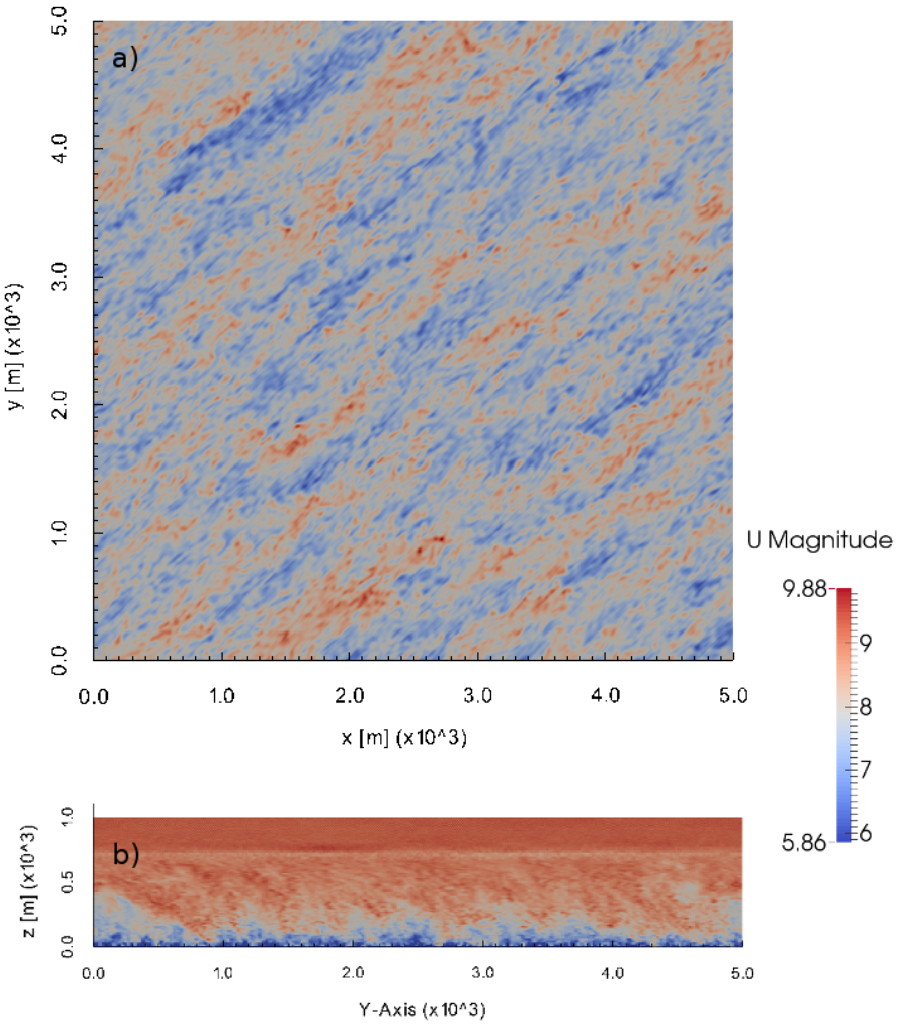

Figure 1. Instantaneous horizontal wind speed [ms^{-1}] in the first time step of the recorded precursor (t=91000s), from the A4 case study, at hub height, i.e. 119 m above the surface (a) and in a x-direction plane midway through the domain (b).

The sensitivity to the averaging window is addressed in Figure 3. The left panels show the variations in the convergence pattern between the original data at 0.2Hz and the temporal averages at 1×10^{-3}Hz, 2×10^{-4}Hz, that is, 1000s and 5000s respectively; both for the wind speed (top left) and turbulence intensity (bottom left). On the other hand, the right panels of Figure 3 depict the values of velocity and TI at 1000s and 5000s averaging times at different heights of the domain.

Note from both Figure 3 and Figure 2, the drastic oscillation, particularly the wind speed values, in the region of the inversion layer in the upper part of the domain. The amplitude and frequency of the oscillation is clearly observed in the evolution of the velocity at 795m (purple line) on 3 top right panel.

The Coriolis force and pressure gradient imposed to drive the flow are the dominant terms terms in the momentum budget equation in the upper part of the domain. In this region, the resulting system resembles a simple harmonic oscillator whose signal amplitude is related to the initial unbalance

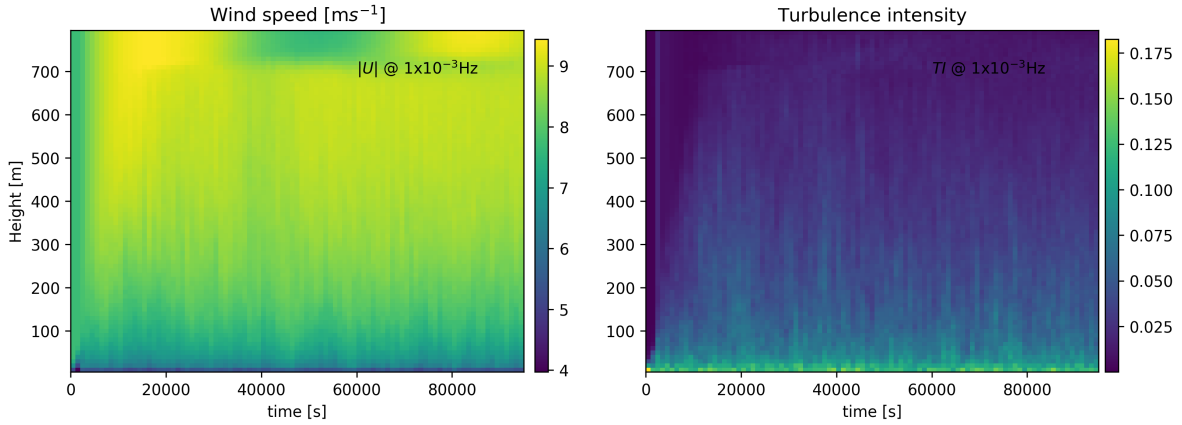

Figure 2. Evolution in time of the averaged wind speed (left) and turbulence intensity (right) of the A4 case study. The averaged values are based on 1000s intervals.

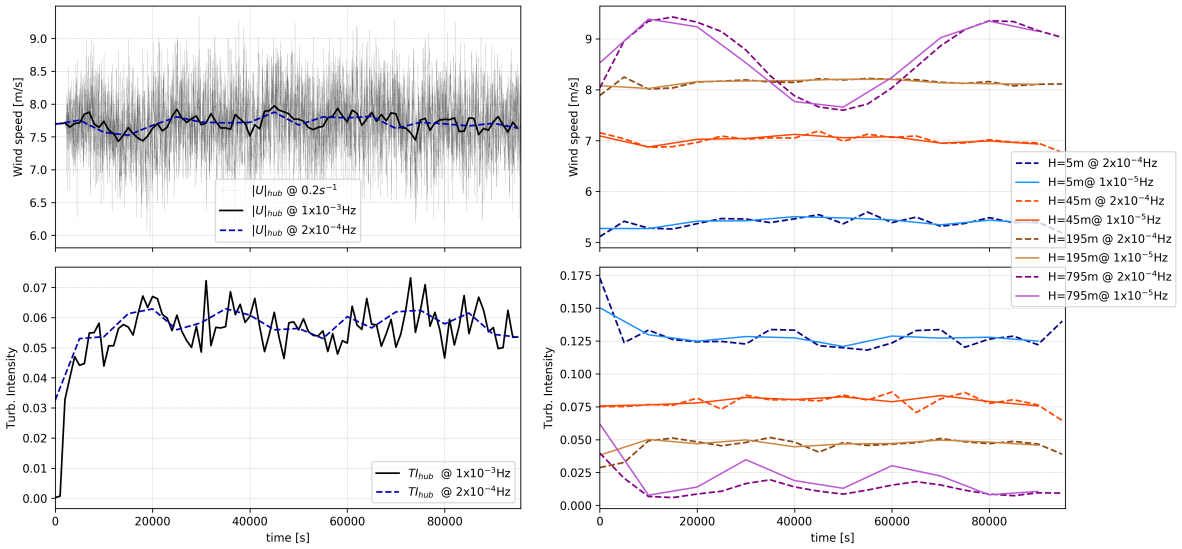

Figure 3. Evolution in time of the averaged wind speed (top panels) and turbulence intensity (bottom panels) of the A4 case study. Comparison among different averaging windows are shown for the wind speed and derived turbulence intensity values at hub height (left panels), and for other relevant heights (5m, 45m, 195m and 795m) on the right panels.

between the wind speed prescribed at the initial conditions and the wind speed value that satisfies the geostrophic balance. Acordingly, the frequency of the oscillation is also strongly related to the Coriolis frequency as defined in equation 3.1, as it is observed in the previous Figure 3 and Figure 2. This finding is identical in the rest of the cases, which for the sake of simplicity is not shown, with small variations due to differences in the mean wind speed.

On the other hand, the prescence of the Coriolis term causes the well known effect of the turning of the wind with height. This feature, also related to the latitude and Coriolis coefficient, can be clearly seen in Figure 4 that shows the resulting vertical profile of wind direction averaged on the last 1×10^4 seconds.

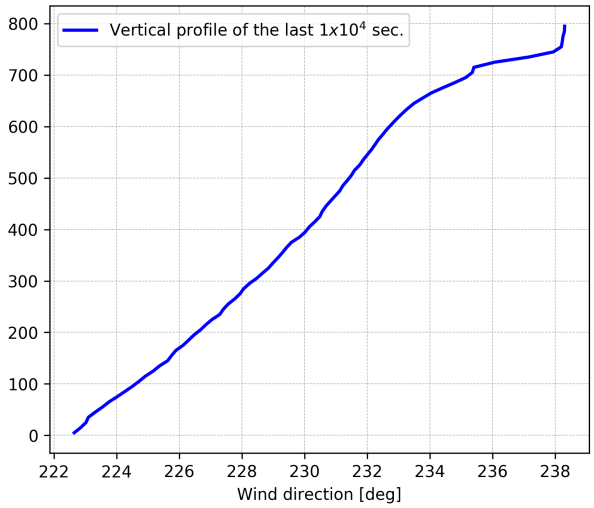

Figure 4. Vertical profile of the wind direction averaged on the last 1×10^4 seconds of the precursor A4 simulation.

Turbulence parameters

Appart from the first-order statistics of mean wind speed and turbulence intensity, the following statistics were analized to verify the proper convergency of the SOWFA precursors.

The first one is the friction velocity , u^* defined as: $u^* = \left[(\overline{u'w'})^2 + (\overline{v'w'})^2\right]^{1/4}$. The second one is the resolved turbulent kinetic energy , k defined as: $k = \frac{1}{2}\overline{u_i' u_i'}$

Figure 5 shows the evolution of these paremeters, where a proper convergence to a stationary value can be seen in the different vertical levels of the domain.

The proper spatial resolution of the simulation of essential for the reliable LES simulations. Figure 5 shows the comparison between the resolved turbulent kinetic energy k, and its evolution in time, versus the estimated subgrid turbulent kinetic energy k_{SGS}. The difference between them in at least two orders of magnitude indicates a proper resolution to solve the important scales of the atmospheric surface layer.

Finally, Figure 7 show the vertical profiles obteined at different times in the precursor simulation. They all correspond to the wind speed time series and turbulence intensity obtanied from the 5000 s averaging periods. This figure shows that the values and profiles of velocity and turbulence in the surface layer (first 200 m) are not severely influenced by the problems of the the oscillations generated in the upper region of the domain. Nevertheless, some damping methods, and procedures such as artificial numerical diffussion on the top of the domain are being investigated to mitigate these oscillations.

3.1.3 Results for the rest of scenarios

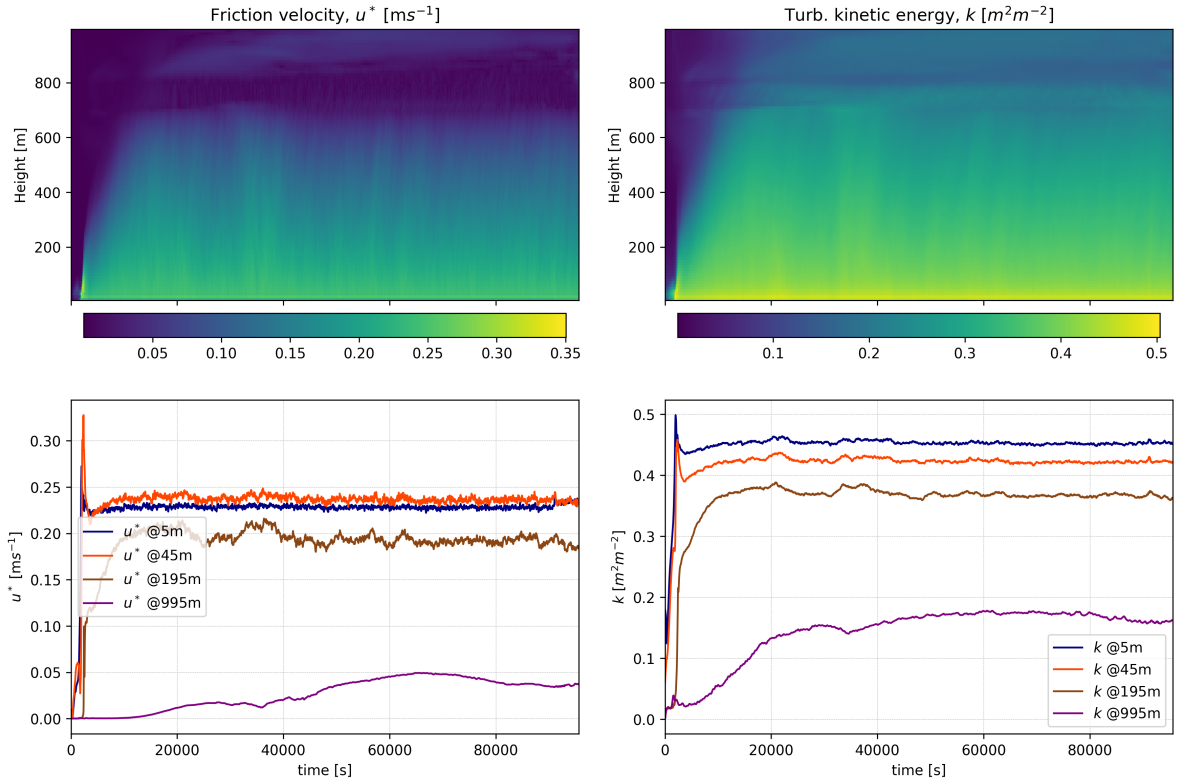

Figure 5. Evolution in time of the friction velocity (left) and resolved turbulent kinetic energy (right) throughout all the domain height (top panels) and at specifically certain heights above ground (bottom panels).

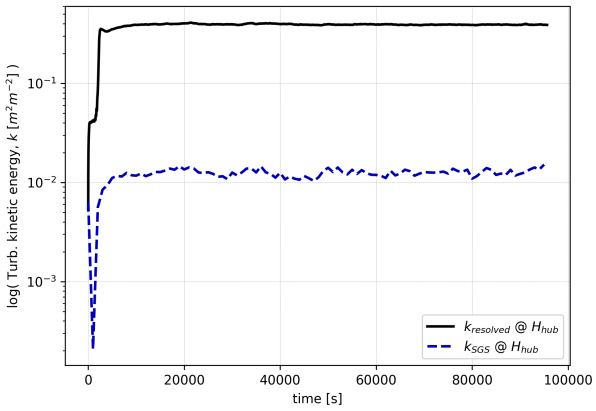

Figure 6. Evolution in time of the resolved turbulent kinetic energy (solid line) and the subgrid tke accounted by the model (dashed line) in the A4 case study.

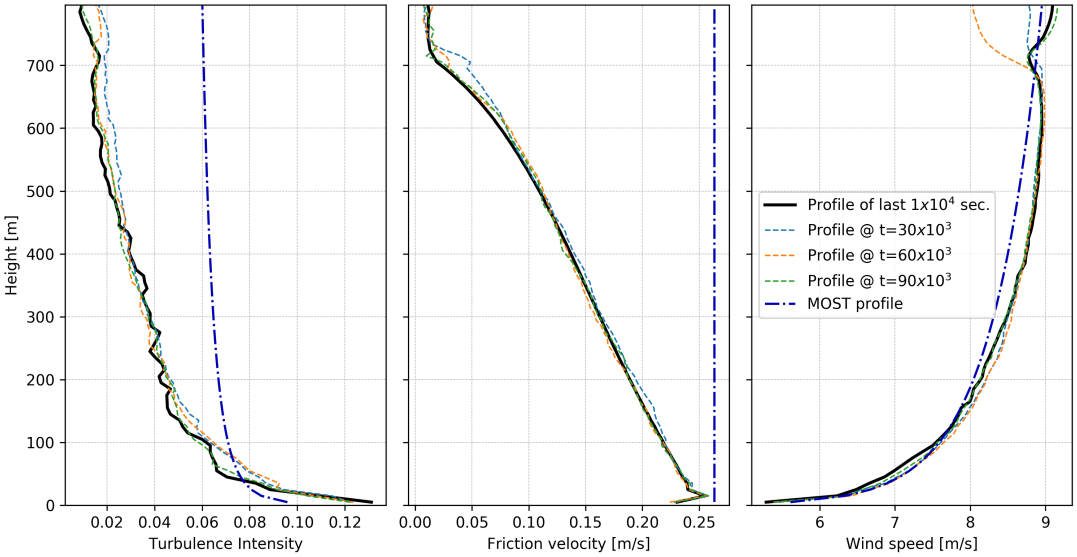

Figure 7. Vertical profiles of turbulence intensity (left) friction velocity (center) and wind speed (right) for the A4 case study. The profiles correspond to different periods of the evolution of the precursor simulation (i.e. at the 30, 60 and 90×10^3-th seconds) from the simulated velocity averaged every 5000 seconds. Additionally, the vertical profiles obtained with the Monin-Obukhov Similarity Theory (MOST) are shown for reference.

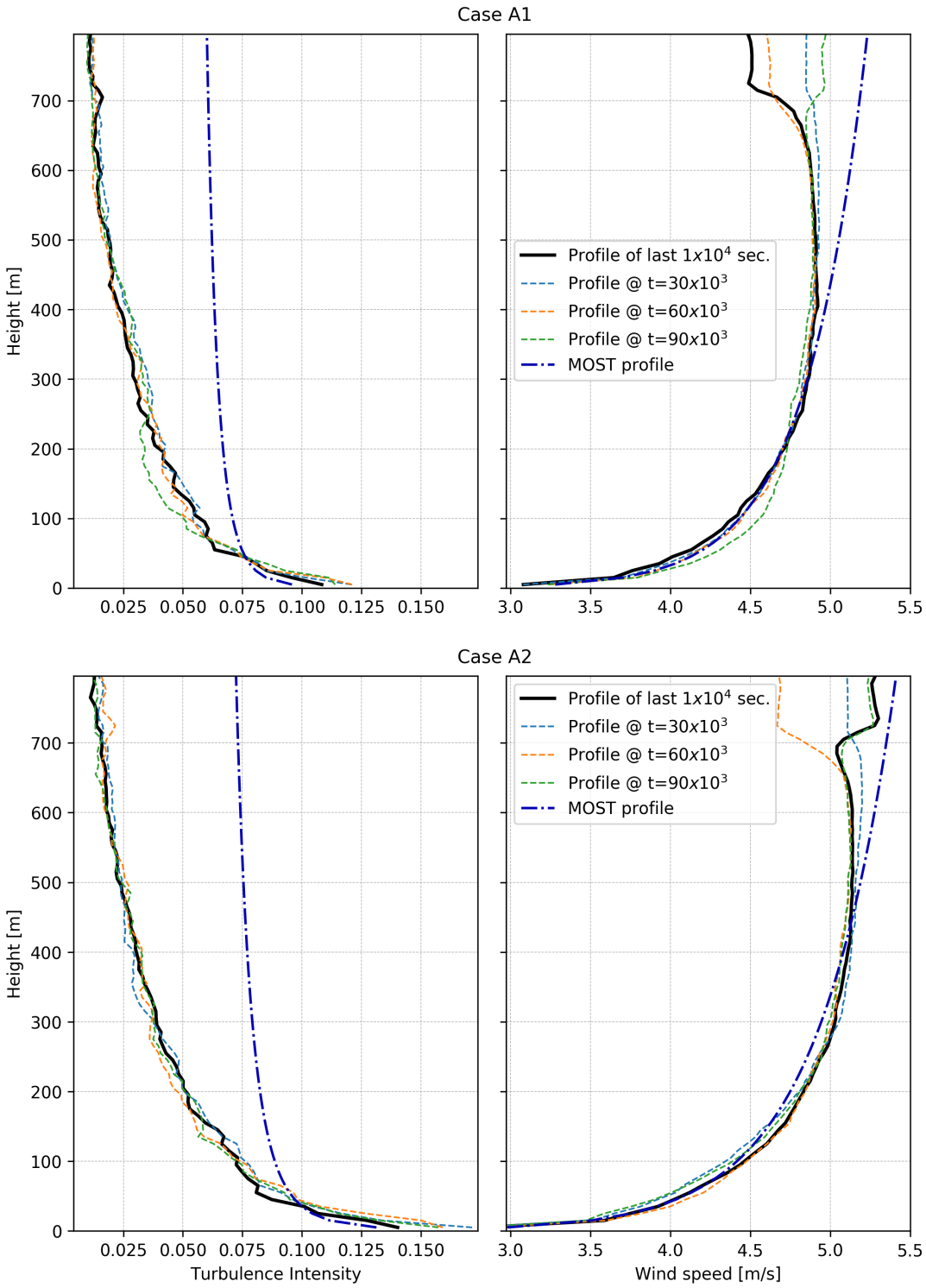

Figure 8. Vertical profiles of turbulence intensity (left) and wind speed (right) for the A1 and A2 cases. These cases share the same 4.5 m/s target velocity at hub height. Similar to Figure 7, the profiles correspond to different periods of the evolution of the precursor simulation (i.e. at the 30, 60 and 90×10^3-th seconds) from the simulated velocity averaged every 5000 seconds. Additionally, the vertical profiles obtained with the Monin-Obukhov Similarity Theory (MOST) are shown for reference.

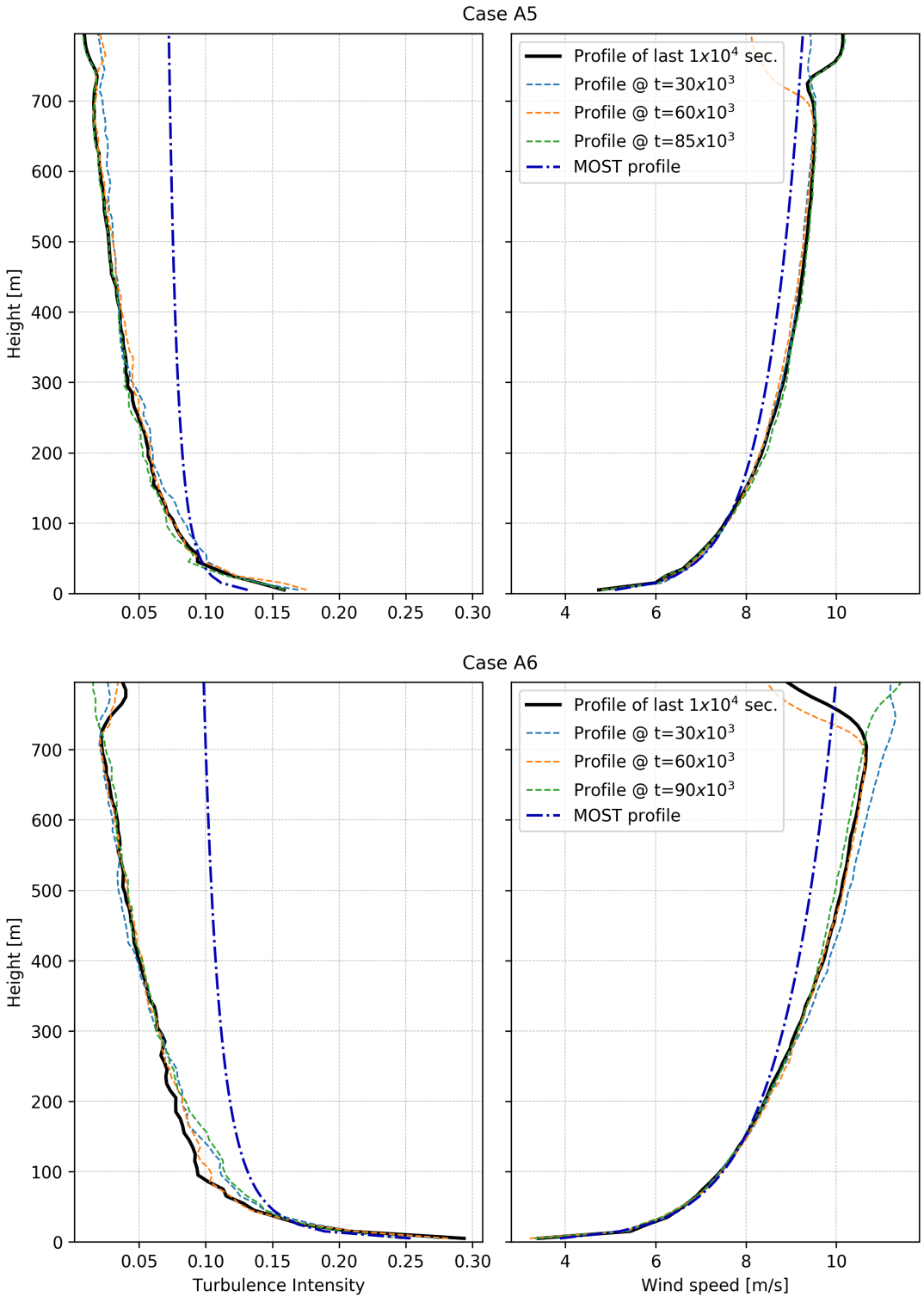

Figure 9. Vertical profiles of turbulence intensity (left) and wind speed for the A5 and A6 cases. These cases share the same 7.7 m/s target velocity at hub height. Similar to Figure 7, the profiles correspond to different periods of the evolution of the precursor simulation (i.e. at the 30, 60 and 90×10^3-th seconds) from the simulated velocity averaged every 5000 seconds. Additionally, the vertical profiles obtained with the Monin-Obukhov Similarity Theory (MOST) are shown for reference.

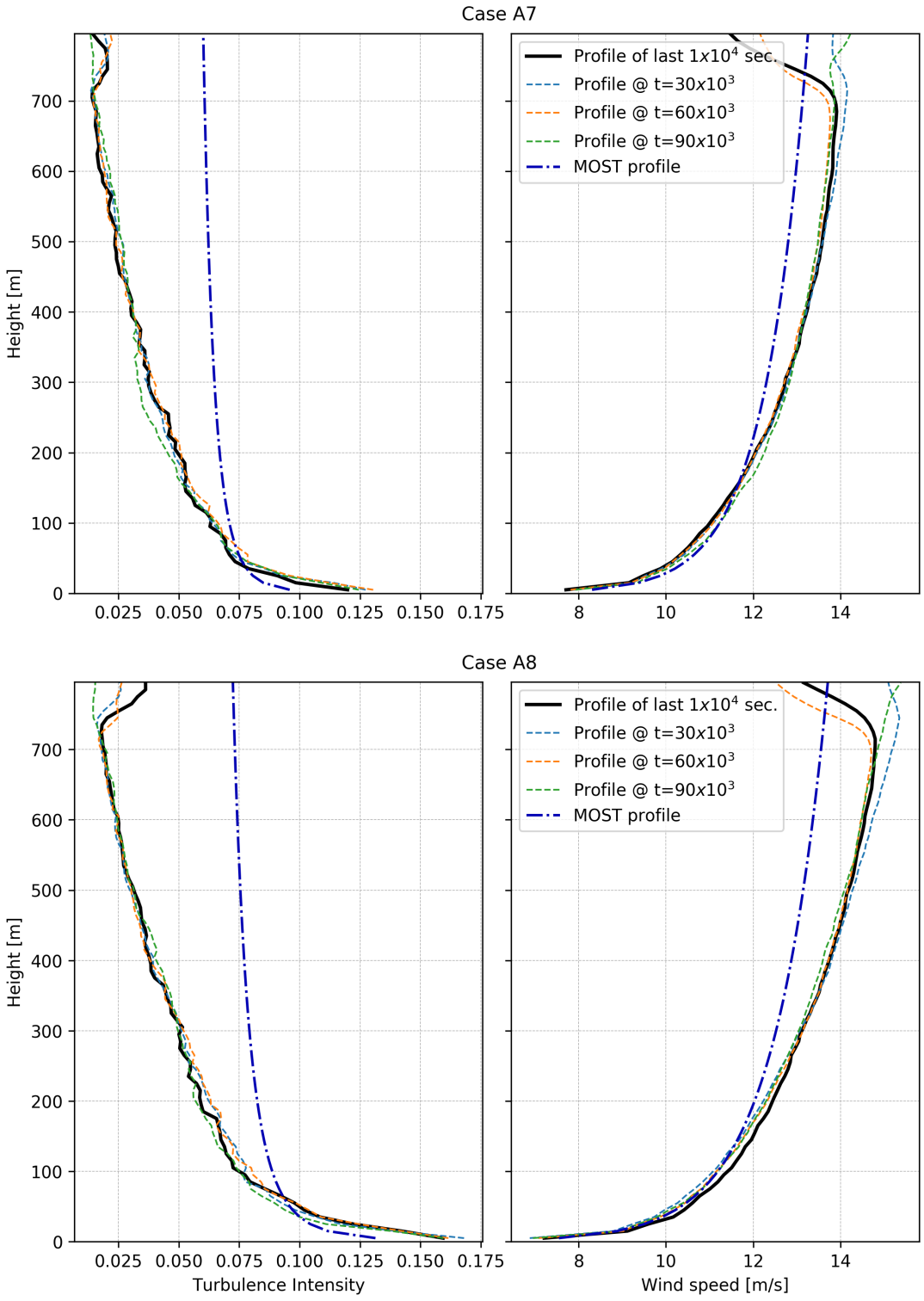

Figure 10. Vertical profiles of turbulence intensity (left) and wind speed for the A7 and A8 cases. These cases share the same 11.4 m/s target velocity at hub height. Similar to Figure 7, the profiles correspond to different periods of the evolution of the precursor simulation (i.e. at the 30, 60 and 90×10^3-th seconds) from the simulated velocity averaged every 5000 seconds. Additionally, the vertical profiles obtained with the Monin-Obukhov Similarity Theory (MOST) are shown for reference.

4 CALIBRATION AND PARAMETER TUNING OF FLORIS AND WFSIM

The work presented here is going to be published in the near future at an upcoming conference, the American Control Conference 2019, as part of an annually recurring series on the topic of wind energy control [14].

4.1 FLORIS

The surrogate model "FLORIS" has a number of tuning parameters that may vary with, e.g., the wind farm topology and wind turbine types. Specifically, some of the literature of these models is based on wind tunnel experiments, in which flow behavior is known the deviate from the actual large-scale wind farms. For this reason, the parameters α, β, k_a, k_b, a_b and b_d are tuned to high-fidelity, true-scale wind farm simulation data in this section, prior to controller synthesis.

We perform a set of single-turbine simulations in SOWFA to calibrate the surrogate model with. This set contains:

- Two types of inflow: one set with uniform inflow and one set with turbulent inflow,
  - each consisting of a set of simulations with yaw angles ranging from -30° to 30° with collective blade pitch angles 0°,
  - and another set of simulations with yaw angle 0° and the collective blade pitch angle varying from 1° to 4°.

This covers both wake deflection and turbine derating for typical turbine operation. Using this data, the model is now calibrated offline as follows.

4.1.1 Calibration methodology

1. A spatially and temporally averaged vertical inflow profile is extracted from the high-fidelity dataset. The same inflow profile is used in the surrogate model through a linear spline interpolation. An example is given in Figure 11.
2. The flow field from the high-fidelity simulation is time-averaged over a 10-minute window to average local fluctuations. This fits the scope of what the surrogate model intends to reproduce.
3. This time-averaged flow field is sliced at $3D$, $5D$, $7D$ and $10D$ downstream, and measurements are sampled over a rectangular grid at each downstream location. An example is shown in Figure 12 for one of the simulations with uniform inflow.

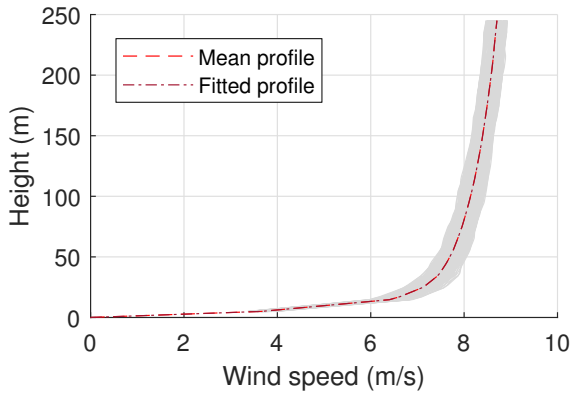

Figure 11. Inflow comparison. In gray are all vertical profiles along the spatial domain, upon which a single mean profile is fit using spline interpolation.

4. A cost function is set-up, where the root-mean-squared error between the flow measurements from SOWFA and that predicted by the surrogate model is minimized for arguments $\Psi = \begin{bmatrix} \alpha & \beta & k_a & k_b & a_d & b_d \end{bmatrix}$, as:

$$\Psi_{\text{opt}} = \arg\min_{\Psi} \sum_{i} \left(U^i_{\text{SOWFA}} - U_{\text{FLORIS}}(\Psi) \right), \tag{4.1}$$

where i covers the full set of single-turbine simulations. The control settings and ambient conditions varying with i are neglected in notation here.

An important remark is that, in a more elaborate study, one would have to include the combined effect of turbine derating and wake redirection. Furthermore, a wider range of turbulent inflows should be considered, at various turbulence intensities and various wind speeds. Also, it is important to consider the interaction for multiple turbine wakes. However, this is outside of the scope of this work.

4.1.2 Calibration results

The surrogate model has been implemented in MATLAB, and made available to the public [15]. A constrained genetic algorithm optimization approach is used to solve the problem of Eq. 4.1 in an efficient, parallelized manner, taking approximately 20 CPU-hours. The optimized parameters Ψ_{opt} are displayed in Table 2. The lower and upper bounds on the parameter optimization space are chosen as to stay within the same order of magnitude as the nominal values presented in the literature [2], in order to limit overfitting and parameter divergence.

Inspecting Table 2, it is seen that most of the optimized values lay between their lower and upper bound. This is a good sign, as the opposite situation may indicate overfitting and parameter divergence.

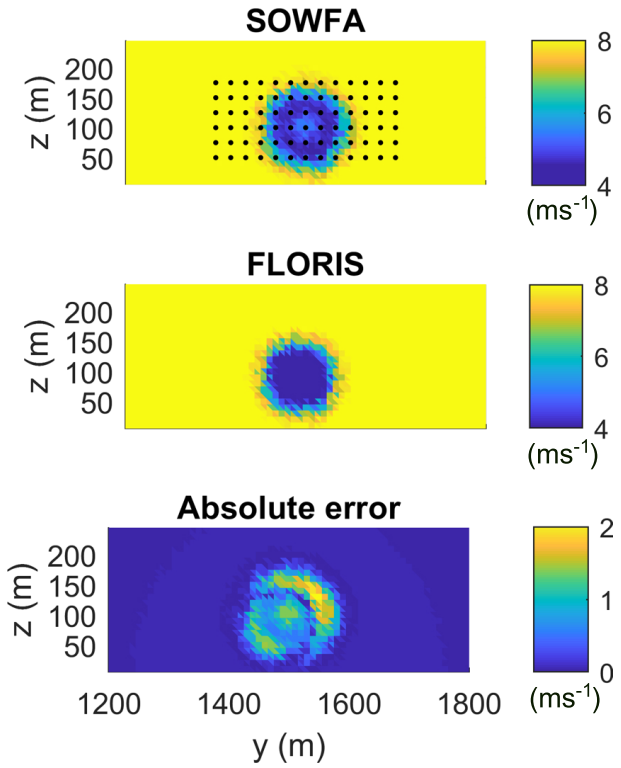

Figure 12. Wake comparison at 5D downstream. The black dots in the top subplot show the locations of the measurements that will be used to calibrate the surrogate model with SOWFA.

4.1.3 Validation results

To ensure that the model calibration procedure was successful, the calibrated model is compared with a high-fidelity simulation dataset of a 9-turbine wind farm in which arbitrary yaw angles are applied to the turbines. The model has not been fit for wake interaction, and hence this is an interesting case to inspect. The yaw angles are derived from a Gaussian distribution, yielding

$$\vec{\gamma} = [2.9^\circ,\ 32.1^\circ,\ 12.6^\circ,\ -20.3^\circ,\ 16.1^\circ,\\ -14.4^\circ,\ -1.9^\circ,\ -21.6^\circ,\ 29.4^\circ].$$

Note that the pitch angles are kept constant at 0° in this validation case, since it is in unlikely they will be exploited for power maximization [1]. The time-averaged horizontal plane is shown in Figure 13. Furthermore, the time-averaged wake deficits at different distance downstream are displayed in Figure 14. From these Figures, a good fit can be seen in the far-wake regions and in the single-turbine wakes. As more wakes interact, the fit gets worse, as the model has not been calibrated for this situation. Furthermore, the calibrated model parameters Ψ_{opt} has improved the model compared to the nominal model parameters from the literature Ψ_0, especially for the near-wake and far-downstream region.

The power predicted from the surrogate model is compared to the power from SOWFA in Figure 15. One can see that the trends are adequately captured in the surrogate model. Though, the surrogate

Table 2. Optimal parameters Ψ_{opt} for the surrogate model after calibration using high-fidelity simulation data

Variable	Lower bound	Upper bound	Optimal value
α	1.16	4.64	3.94
β	$7.70 \cdot 10^{-2}$	$3.08 \cdot 10^{-1}$	$3.05 \cdot 10^{-1}$
k_a	$1.92 \cdot 10^{-1}$	$7.67 \cdot 10^{-1}$	$1.95 \cdot 10^{-1}$
k_b	$1.90 \cdot 10^{-3}$	$7.40 \cdot 10^{-3}$	$2.92 \cdot 10^{-3}$
a_d	$-7.12 \cdot 10^{-2}$	$-1.78 \cdot 10^{-2}$	$-1.79 \cdot 10^{-2}$
b_d	$-2.00 \cdot 10^{-2}$	$-5.00 \cdot 10^{-3}$	$-5.17 \cdot 10^{-3}$

model slightly underestimates the power capture in most situations. Furthermore, the calibrated parameters Ψ_{opt} show improved performance compared to Ψ_0.

In conclusion, the surrogate model can accurately capture the wake and power of this 9-turbine wind farm. However, it is still to be checked whether the surrogate model can capture more difficult situations such as deep-wake effects and partial overlap situations such as described in [27]. This should be addressed in future work.

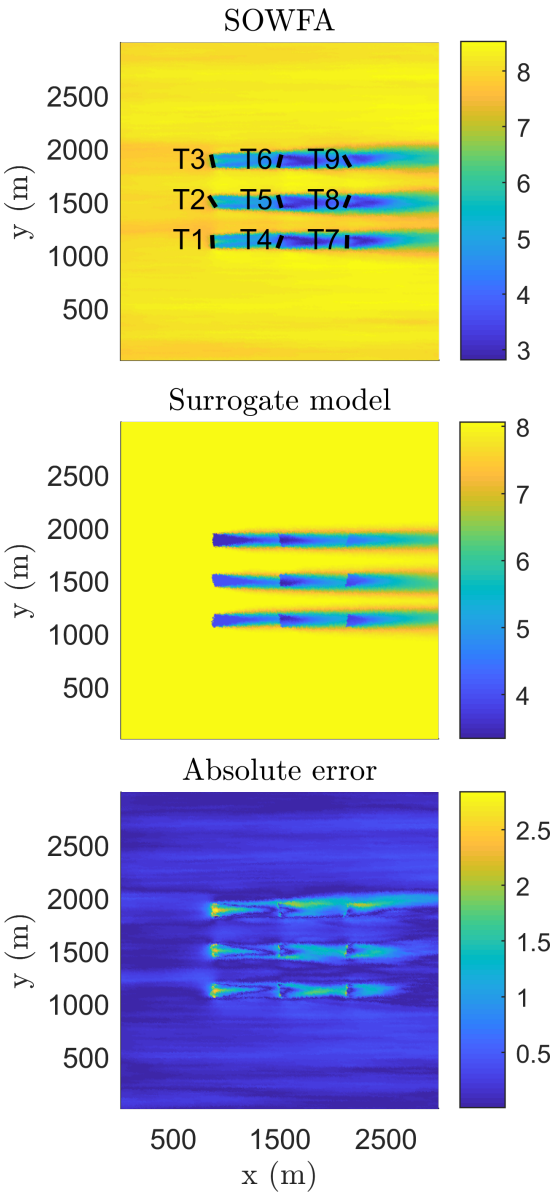

Figure 13. Validation of the surrogate model with SOWFA: time-averaged flow field at turbine hub height. Units are ms^{-1}.

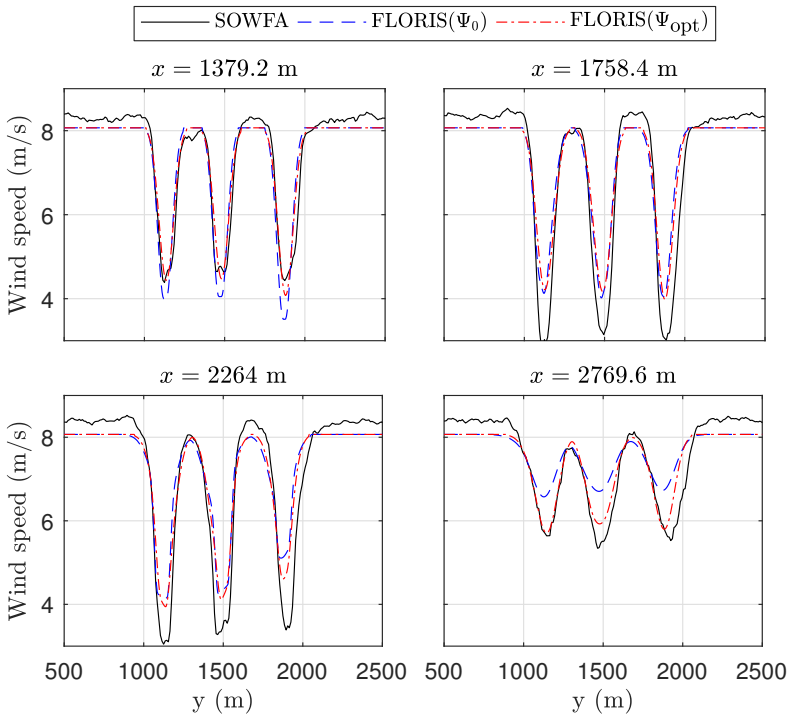

Figure 14. Validation of the surrogate model with SOWFA: wind speed at hub height at different distances downstream

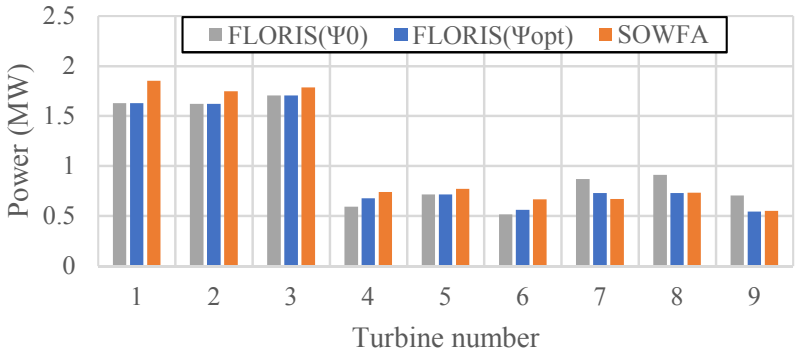

Figure 15. Validation of the surrogate model with SOWFA: time-averaged power capture per turbine

4.2 WFSim

This section presents validation results of the WindFarmSimulator (WFSim) model [4] with high-fidelity simulation data. The nomenclature used throughout this section is presented in Table 3.

Table 3. Nomenclature.

$L_x \times L_y$,	domain size wind farm	D	turbine rotor diameter
$N_x \times N_y$,	number of cells	$\Delta x \times \Delta y$	cell size
U^c,	flow centreline velocity	u_b, v_b,	upstream flow velocities
Δt,	sample period	k,	time index
u_k, v_k, p_k,	longitudinal and lateral flow velocities and pressure	$C'_{T,k}, \gamma_k$,	control variables
z_h	turbine's hub-height	TI	turbulence intensity

4.2.1 Tuning parameters in the WFSim model

The surrogate model "WFSim" is a dynamical wind farm model that is based on the Navier-Stokes equations. In order to obtain a computationally efficient, control-oriented model, modeling assumptions have to be made, which consequently lead to modeling errors compared to higher-fidelity models. In order to compensate for these errors, tuning parameters have been introduced in WFSim. These tuning parameters are used to fit the WFSim model to data from field experiments, wind tunnel data and/or high-fidelity simulation data.

The WFSim model has a total of five tuning parameters as described in Table 4. The interested reader can find a specific description on these parameters in [4].

Table 4. Tuning parameters of the WFSim model.

c_f	force scaling
c_p	power scaling
d'	start point local mixing length
d	total length local mixing length
ℓ_s	slope local mixing length

4.2.2 Validation of the WFSim model with SOWFA

This section presents validation results of WFSim with the large-eddy simulation package "SOWFA", which is a high-fidelity wind farm model. First, an overview of the specifications of the specific case study will be presented. Furthermore, the turbines' actuation signals, the wind farm's power output, and the flow field predicted by either mode, SOWFA and WFSim, is shown.

4.2.2.1 Case study specifications

Table 5 presents the specifications of the high-fidelity SOWFA simulation, and Table 6 presents the corresponding specifications of the surrogate model WFSim. The tuning parameters of WFSim were

found by manual tuning, minimizing a weighted cost function including the horizontal flow field at hub height, and the power predicted by each turbine in the farm.

Table 5. Summary of the SOWFA simulation set-up.

Domain size $L_x \times L_y \times L_z$	$3 \times 3 \times 1$ [km^3]	Turbine dimensions	D =126.4 [m], z_h =90 [m]
Grid size $N_x \times N_y \times N_z$	$500 \times 500 \times 166$	Turbine arrangement	3×3
Cell size $\Delta x \times \Delta y \times \Delta z$	$6 \times 6 \times 6$ [m^3]	Turbine spacing	$5D \times 3D$
Sample period Δt	0.02 [s]	Atmospheric conditions	$u_b = 12, v_b = 0, w_b = 0$ [m/s], $\rho = 1.2$ [kg/m^3]
Simulation time t	900 [s]	Inflow	turbulent (TI=5%)

Table 6. Summary of the WFSim simulation set-up.

Domain size $L_x \times L_y$	2.5×1.5 [km^2]	Turbine rotor diameter D	126.4 [m]
Grid size $N_x \times N_y$	100×42	Turbine arrangement	3×3
Cell size $\Delta x \times \Delta y$	25×15 [m^2]	Turbine spacing	$5D \times 3D$
Sample period	$\Delta t = 1$ [s]	Atmospheric conditions	$u_b = 12, v_b = 0$ [m/s], $\rho = 1.2$ [kg/m^3]
Force and power scaling	$c_f = \frac{5}{2}, c_p = 1.1$	Turbulence model	$d = 635, d' = 76.2$ [m] $\ell_s = 0.17$

4.2.2.2 Control signals

Figure 16 presents the thrust coefficients of all the nine turbines in the farm. Variations in the thrust coefficients result in an excitation of wake dynamics. It is important to excite these wake dynamics because these are the dynamics we want to capture with the control-oriented model WFSim. In this case study, all yaw angles are set to zero.

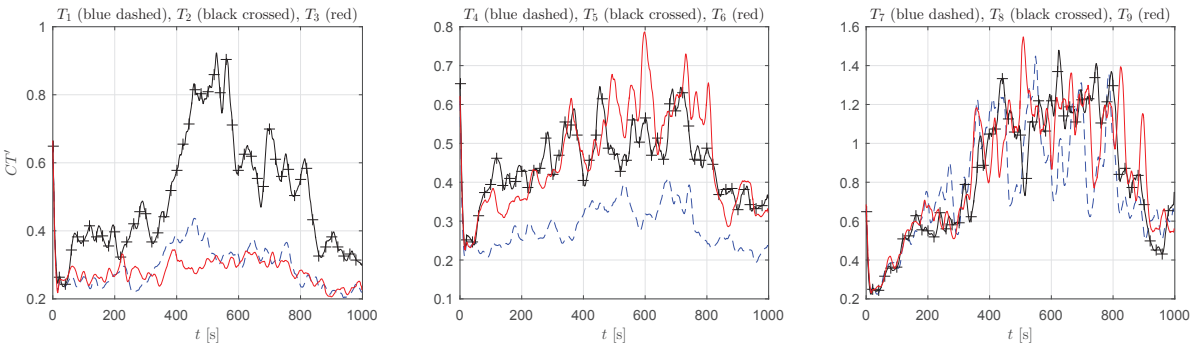

Figure 16. Time series of the thrust coefficients.

4.2.2.3 Power signal validation

Figure 17 depicts the wind farm power signals of SOWFA (blue dashed) and WFSim (black). It can be observed that WFSim is able to estimate the power data of SOWFA. This increases the confidence in the potential of WFSim as a model that can be utilized in a controller.

4.2.2.4 Flow velocity validation

Figure 18(a) presents the wind farm's topology. Figure 18(b) and Figure 19 depict the mean flow velocity centreline. This is the mean flow velocity across the rotor along the x-axis. Furthermore, Figure 20 depict the longitudinal flow velocity components at hug-height from SOWFA and WFSim.

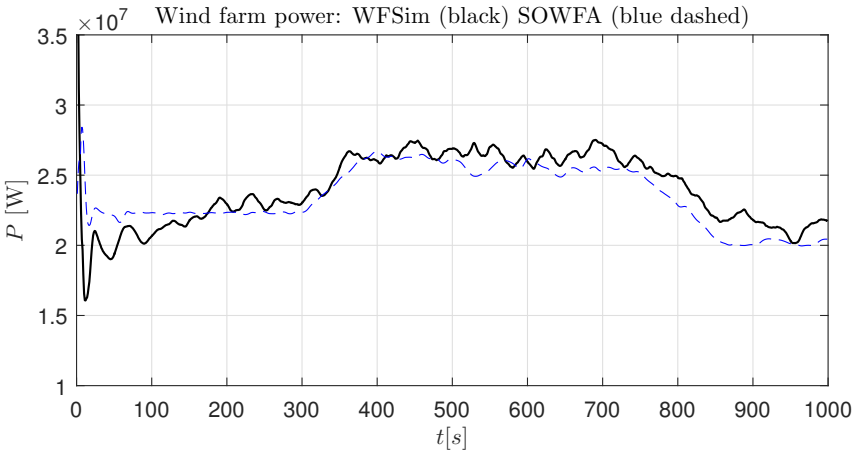

Figure 17. Wind farm power from SOWFA (blue dashed) and WFSim (black).

All these Figures illustrate that WFSim is capable of estimating SOWFA data. In the following section, WFSim will be validated with PALM data.

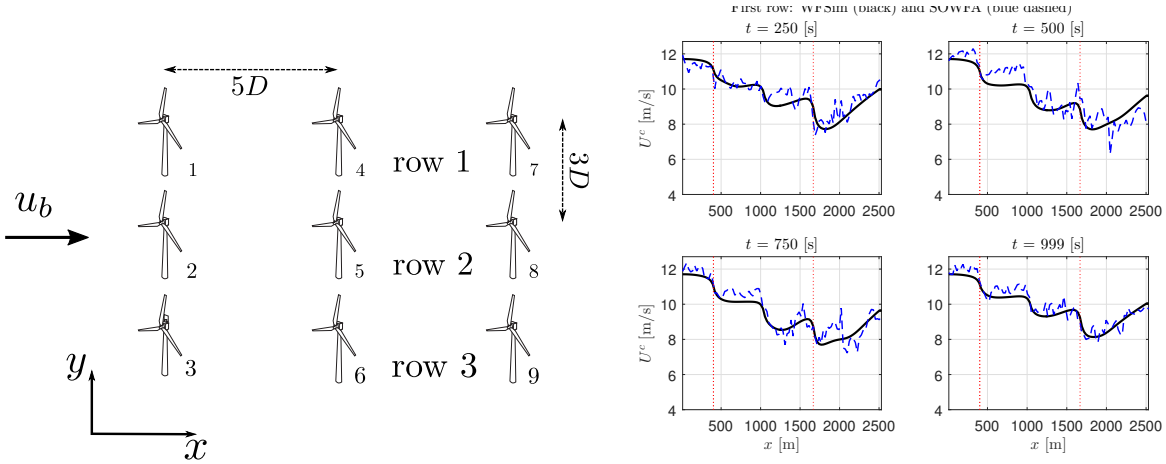

Figure 18. Topology simulated wind farm (a) and mean flow centreline at four time instances through the first row (b).

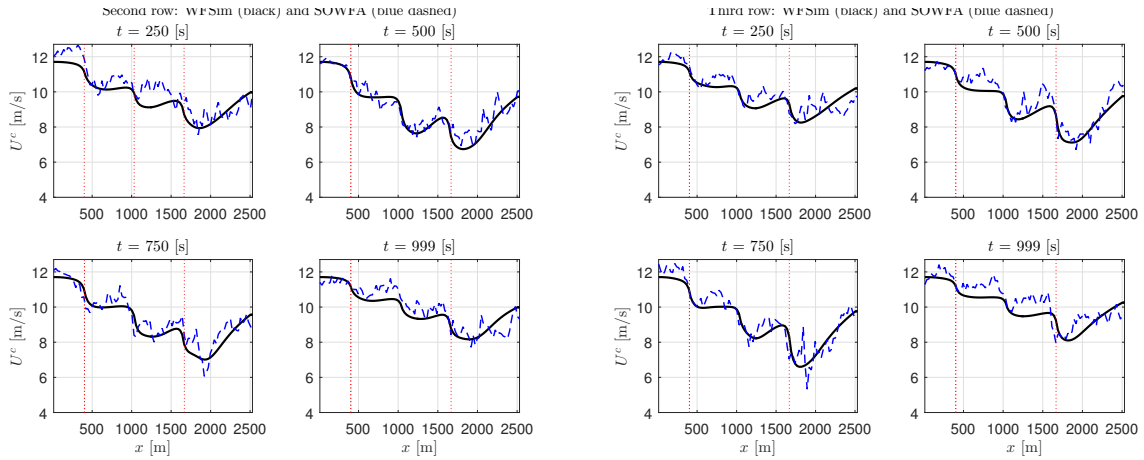

Figure 19. Mean flow centreline at four time instances through the second row (a) and third row (b) of turbines. The vertical red dashed lines indicate the positions of the turbines.

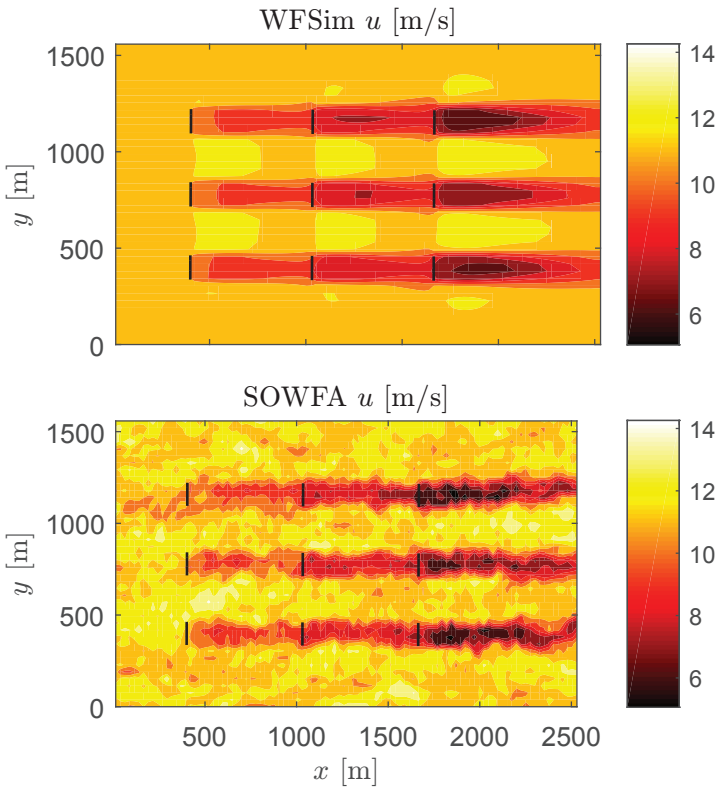

Figure 20. Longitudinal flow fields at hub height from SOWFA (below) and WFSim (above) at arbitrarily time step.

4.2.3 Validation of the WFSim model with PALM

This section presents validation results of WFSim with a second high-fidelity software simulation package, named "PALM". PALM is, just like SOWFA, a high-fidelity wind farm model that simulations the three-dimensional Navier-Stokes equations employing a large-eddy simulation (LES) approach. First, the specifications of the respective case study will be presented. Secondly, the actuation signals, the turbine power signals, and the flow field predicted by each model will be compared.

4.2.3.1 Case study specifications

Table 7 presents specifications of the PALM simulation, and Table 8 presents the specifications of the corresponding WFSim model. The WFSim parameters are again found through an iterative tuning process, minimizing the error in turbine power signals and flow fields predicted. Note that the slope of the mixing length ℓ_s is significantly smaller with respect to the ℓ_s value presented in Table 6. This is due to the fact that the simulation case study presented in this section has a laminar inflow, and hence less wake recovery occurs in the wake.

Table 7. Summary of the PALM simulation set-up.

Domain size $L_x \times L_y \times L_z$	$19.2 \times 2.56 \times 1.28$ [km^3]	Turbine dimensions	D =126 [m], z_h =90 [m]
Grid size $N_x \times N_y \times N_z$	$1920 \times 256 \times 85$	Turbine arrangement	2×1
Cell size $\Delta x \times \Delta y$	$10 \times 10 \times 15$ [m^3]	Turbine spacing	$6D$
Sample period Δt	1 [s]	Atmospheric conditions	$u_b = 8, v_b = 0, w_b = 0$ [m/s], $\rho = 1.2$ [kg/m^3]
Simulation time t	1750 [s]	Inflow	uniform (TI=0%)

Table 8. Summary of the WFSim simulation set-up.

Domain size $L_x \times L_y$	2×0.63 [km^2]	Turbine rotor diameter D	126.4 [m]
Grid size $N_x \times N_y$	50×25	Turbine arrangement	2×1
Cell size $\Delta x \times \Delta y$	40×23 [m^2]	Turbine spacing	$5D$
Sample period Δt	1 [s]	Atmospheric conditions	$u_b = 8, v_b = 0$ [m/s], $\rho = 1.2$ [kg/m^3]
Force and power scaling	$c_f = 1.7, c_p = 0.95$	Turbulence model	$d = 530, d' = 122$ [m] $\ell_s = 0.06$

4.2.3.2 Control signals

The control signal that are applied in this case study can be seen in Figure 21. As before, persistent excitation is imposed to excite the dynamics we would like to model with WFSim. Similar as before, the yaw angles are set to zero.

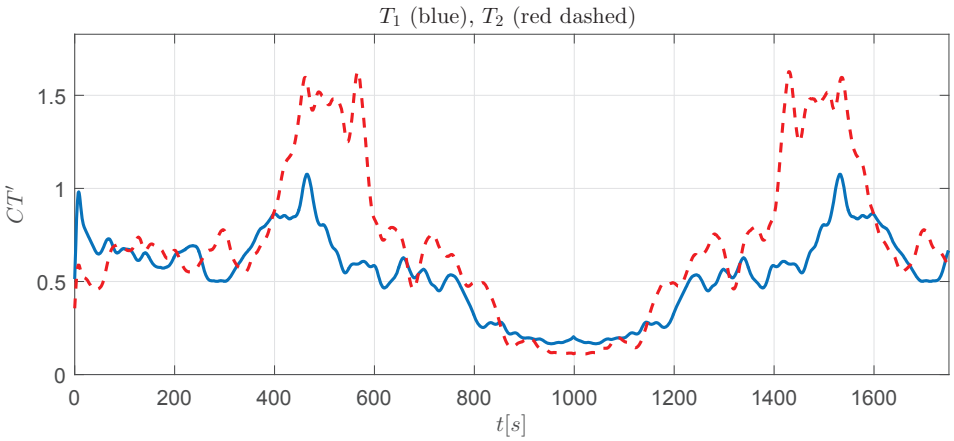

Figure 21. Time series of the thrust coefficients.

4.2.3.3 Power signal validation

Figure 22 depicts the wind farm power signals of PALM (blue dashed) and WFSim (black). It can be observed that WFSim is able to estimate the power data of PALM very accurately. Even though

the simulation is with a uniform inflow, it shows that the simplified surrogate model can accurately predict the turbine power signal of a three-dimensional large-eddy simulation model, which has a computational cost that is multiple orders of magnitude higher than the surrogate model.

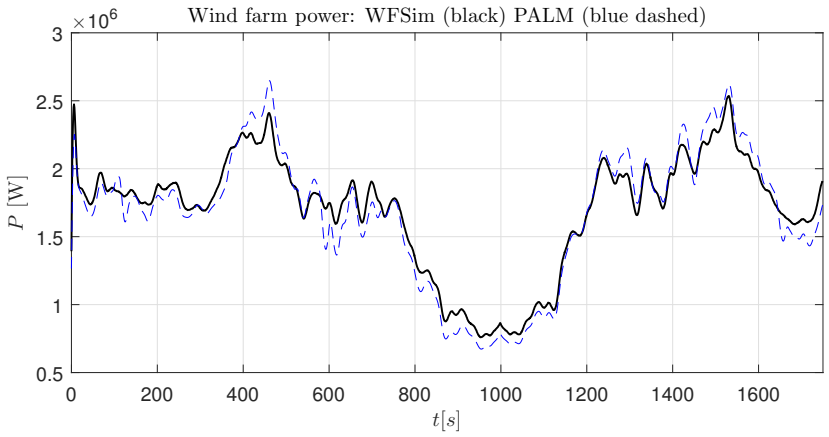

Figure 22. Wind farm power from PALM (blue dashed) and WFSim (black).

4.2.3.4 Flow velocity validation

Similar as in the previous validation results, the flow predicted by WFSim is compared with horizontal flow slice at hub-height from PALM. The mean flow velocity (across the rotor) at various up- and downstream distances along the x-axis is depicted in Figure 23. It can be observed that, behind the rotor, less wake recovery takes place due to the fact that the inflow in PALM is laminar. Nevertheless, also in this case, WFSim is capable of estimating the flow velocity components in PALM. Figure 24 also indicates that the longitudinal flow velocity component from PALM can be estimated with WFSim.

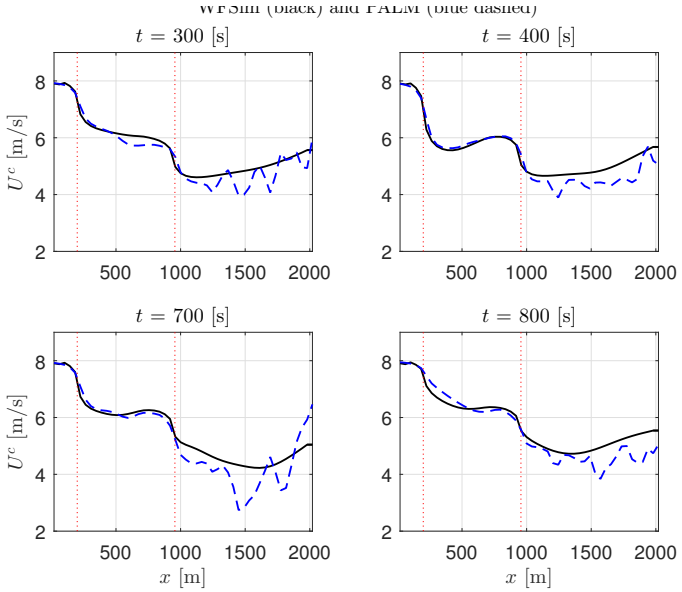

Figure 23. Mean flow centreline at four time instances through the farm. The vertical red dashed lines indicate the positions of the turbines.

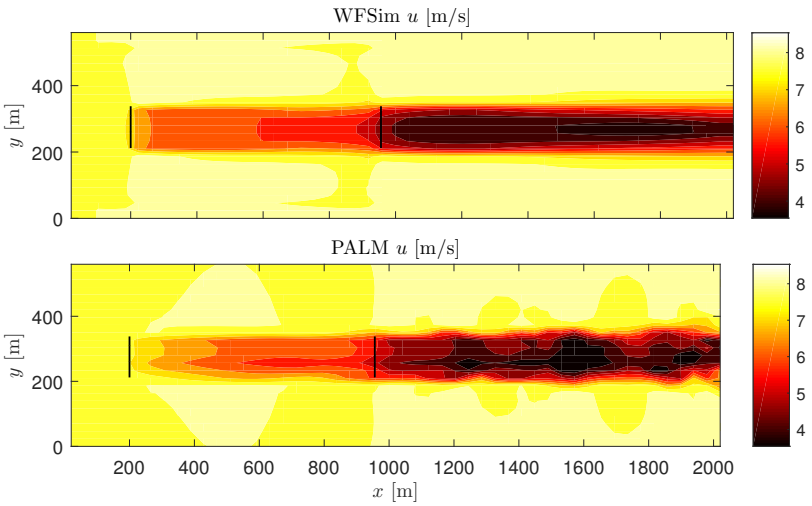

Figure 24. Longitudinal flow fields at hub height from PALM (below) and WF-Sim (above) at arbitrarily time step. Flow is flowing from left to right in this picture, with two turbines: one at $x = 200$ m, and one around $x = 950$ m.

5 SENSITIVITY ANALYSIS WITH FAST.FARM

5.1 Introduction

This section presents a FAST.Farm sensitivity analysis with the 10 MW INNWIND.EU wind turbine. A parametric study has been defined in order to study the effect of FAST.Farm parameters. The objective of this work should be the calibration of these values in order to obtain similar results to SOWFA. This section will show the methodology for the calibration and also some Figures that will be used directly for the selection of the calibrated parameters.

The current analyses show the individual study of the parameters (or set of parameters), including the effect on the wake center and the wake profiles in planes of the wake (0D, 3D, 5D, 7D and 10D) behind the wind turbine. The selected cases for the calibration of this model include one case without yaw and another case with yaw (yaw=20^o), because some of the parameters require the effect of the yaw and the rest of the analysis is simpler for a case without this interference. The wind data for the analysis is the precursor obtained with SOWFA for A4 case (it was selected because it had the highest priority). For these cases, the yaw degree of freedom of the wind turbine is disabled and remains constant during the simulations.

The parameters included in the definition of the cases for FAST.Farm have been defined in Table 9. The last two parameters of this table have not been studied here, because the selected cases for this analysis do not include significant changes in the wind or in the motion of the turbine, and the effect of the meandering parameters are not expected to be important.

The analyzed values in the parametric study are presented in Table 10. For all cases, the parameters not included in the investigation are set to their default values.

The reference system used in the sensitivity analysis is plotted in Figure 25 (x' and y'). X' axis is defined by the main direction of the wind and Y' is perpendicular (for yaw=0, y'=0 is coincident with the rotor plane). The reference system was selected for simplicity in the comparison with FLORIS and because the parallel planes to the rotor are practically defined by the x' coordinate (it will be used for the comparisons of wake center positions and the y' positions for the Figures with profile of the wakes). The inertial reference system will be used only for the comparison of the general profile of the velocities at the hub height (wake map).

The study of the parameters has been made step by step, and the calibration with SOWFA should be done in a similar way.

- parameters related with the position in the plane of the turbine (CHWkDlO and CHWkDlOY).
- parameters related with the profile in the near wake (CNearWake)
- parameters related with the position of the wake center in different planes (CHWkDfx and CHWkDfxY)

parameter	meaning	default value
$CHWkDflO$	correction for wake deflection defining the horizontal offset at the rotor	0.0
$CHWkDflOY$	correction for wake deflection defining the horizontal offset at the rotor scaled with yaw error	0.3
$CHWkDflx$	correction for wake deflection defining the horizontal offset scaled with downstream distance	0.0
$CHWkDflxY$	correction for wake deflection defining the horizontal offset scaled with downstream distance and yaw error	0.004
$CNearWake$	near-wake correction	1.8
$kvShr$	influence of wake shear layer in the eddy viscosity	0.016
$CvShrDMin$	transitional diameter fraction between the minimum and exponential regions (filter function for shear turbulence)	3.0
$CvShrDMax$	transitional diameter fraction between the exponential and maximum regions (filter function for shear turbulence)	25.0
$CvShrFMin$	value in the minimum region (filter function for shear turbulence)	0.2
$CvShrExp$	exponent in the exponential region (filter function for shear turbulence)	0.1
$kvAmb$	influence of ambient turbulence in the eddy viscosity	0.05
$CvAmbDMin$	transitional diameter fraction between the minimum and exponential regions (filter function for ambient turbulence)	0.0
$CvAmbDMax$	transitional diameter fraction between the exponential and maximum regions (filter function for ambient turbulence)	1.0
$CvAmbFMin$	value in the minimum region (filter function for ambient turbulence)	1.0
$CvAmbExp$	exponent in the exponential region (filter function for ambient turbulence)	0.01
f_c	cut-off (corner) frequency (in Hz) of the low-pass time-filter for wake meandering	0.0007
$CMeander$	wake meandering	1.9

Table 9. Parameters for FAST.Farm

Case Name	parameter/set values
Baseline	Default values
$HWkDflO1$	$CHWkDflO = -4$
$HWkDflO2$	$CHWkDflO = 2$
$HWkDflOY1$	$CHWkDflOY = -0.7$
$HWkDflOY2$	$CHWkDflOY = 1.3$
$HWkDflx1$	$CHWkDflx = -0.01$
$HWkDflx2$	$CHWkDflx = 0.01$
$HWkDflxY1$	$CHWkDflxY = 0.0$
$HWkDflxY2$	$CHWkDflxY = 0.004$
$NearWake1$	$CNearWake = 1.3$
$NearWake2$	$CNearWake = 2.0$
$vShr1$	$kvShr = 0.0$,$CvShrDmin = 0$, $CvShrDMax = 1$, $CvShrFmin = 1$, $CvShrExp = 0.01$
$vShr2$	$kvShr = 0.016$,$CvShrDmin = 0$, $CvShrDMax = 1$, $CvShrFmin = 1$, $CvShrExp = 0.01$
$vAmb1$	$kvAmb = 0.1$,$CvAmbDmin = 4$, $CvAmbDMax = 4.3$, $CvAmbFmin = 0 - 5$, $CvAmbExp = 0.5$
$vAmb2$	$kvAmb = 0.05$,$CvAmbDmin = 4$, $CvAmbDMax = 4.3$, $CvAmbFmin = 0.0$, $CvAmbExp = 0.5$

Table 10. Definition of the cases for calibration

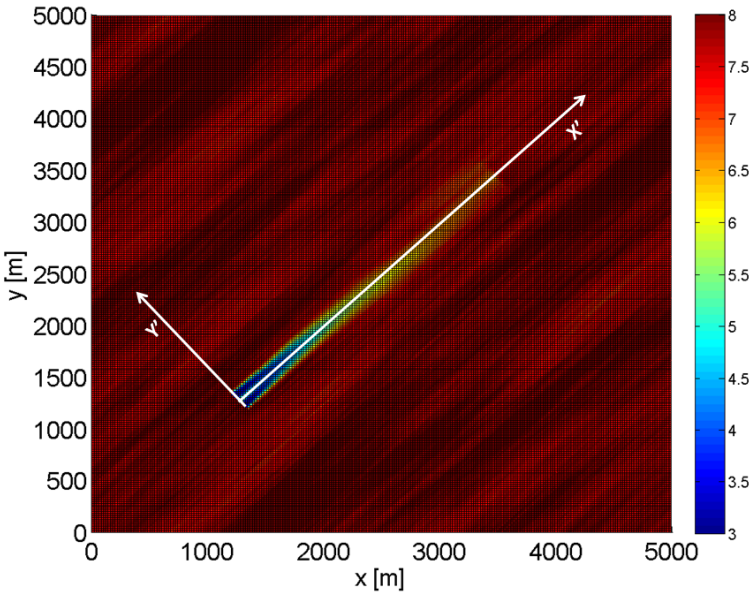

Figure 25. Reference Systems for the sensitivity analysis

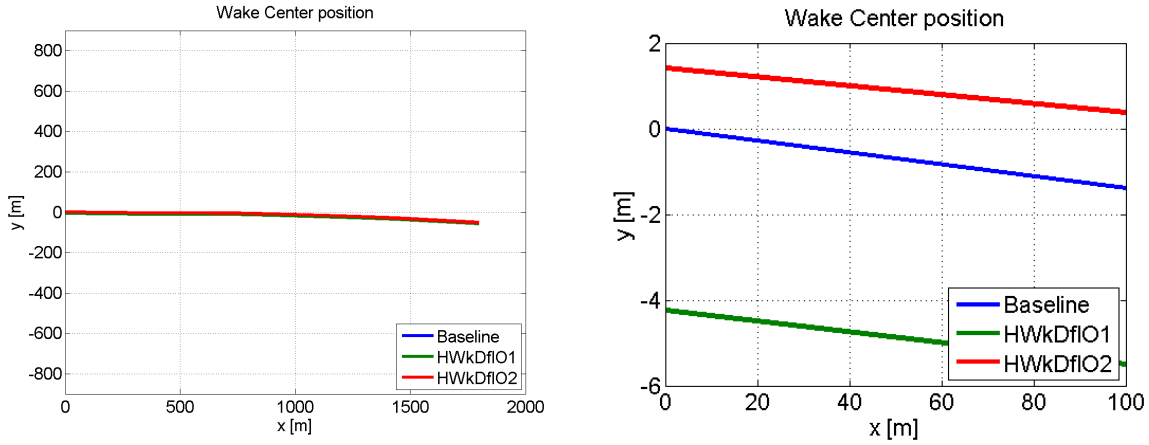

Figure 26. Wake Center position for different values of HWkDflO (case yaw=0^o)

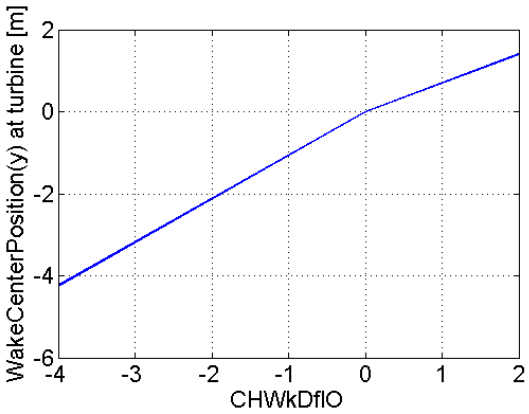

Figure 27. Wake center position at turbine for different values of HWkDflO (case yaw=0^o)

- set of parameters related with the evolution of the wake profile in different planes (vShr and vAmb)

5.1.1 HWkDflO analysis

The effect of this parameter is evident in the position of the wake center (Figure 26). The distance between the centers obtained in the simulations remains constant along the x position, so this parameter can be set using the SOWFA position of the Wake Center at the turbine (x=0), using the results shown in figure 27.

The variation of this parameter does not modify the results the wake profile at different wake locations (except for the effect of the wake center modification), as can be observed at figure 28.

5.1.2 HWkDflOY analysis

Since the yaw$= 0$ case does not present variation of the results when this parameter is modified, so the analysis has been made using the case with yaw =20^o. The effect of this parameter is evident

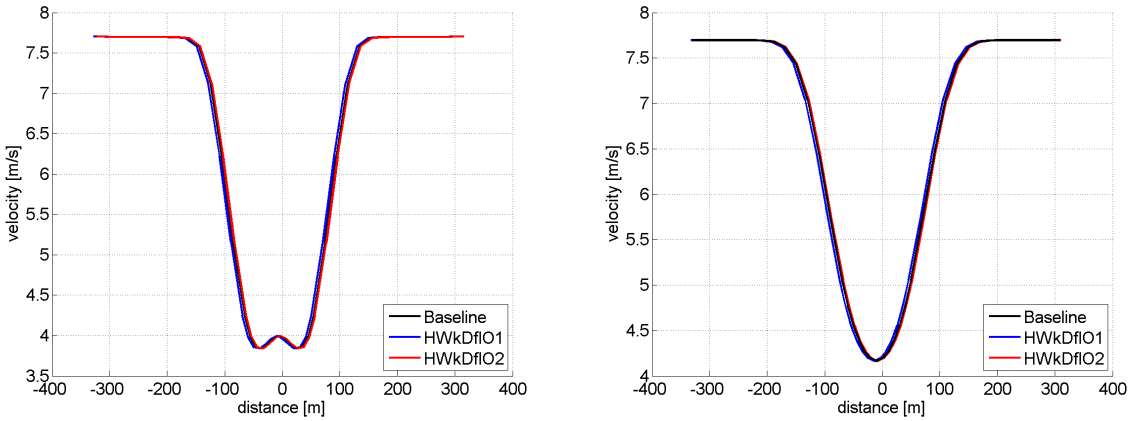

Figure 28. Wake profile at 3D (left) and 5D (right) for different values of HWkDflO (case yaw=0^o)

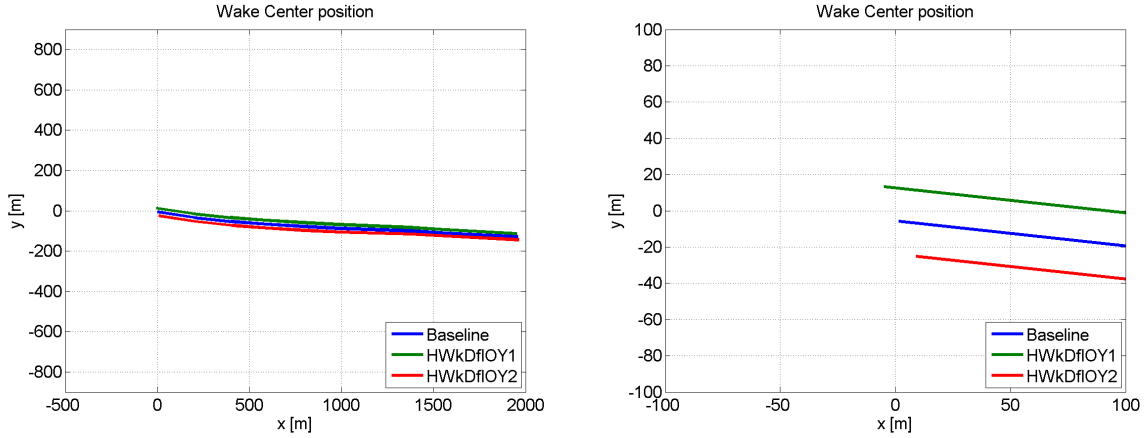

Figure 29. Wake Center position for different values of HWkDflOY (case yaw=20^o)

in the position of the wake center (Figure 29). The distance between the centers obtained in the simulations remains constant along the x position, so this parameter can be set using the SOWFA results for this conditions of the Wake Center at the turbine (x=0), using the linear approach observed in Figure 30.

The variation of this parameter shows a slight variation of the results of the wake profile at different positions of the wake (without the effect of the wake center modification), as can be observed in Figure 31. This effect is negligible, thus the calibration of this parameter is independent of the parameters related with the evolution of the wake profile.

5.1.3 CNearWake analysis

The effect of this parameter should be studied at the near wake (between 0D-1D), comparing the profile of the velocities in this region. There is also a slight effect on the evolution wake center positions that can be observed in Figure 32, but the most important change on the wake is observed in the profiles (Figure 33). The combination of two magnitudes can be used in order to calibrate this

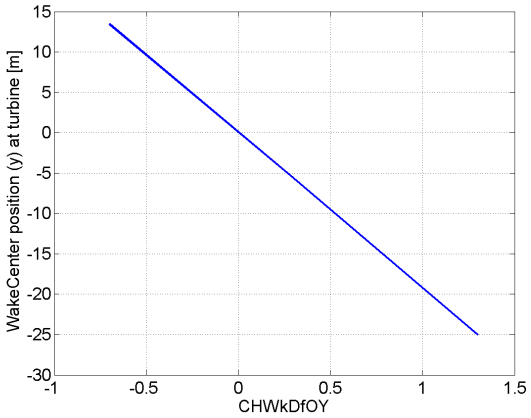

Figure 30. Wake center position (y) at turbine for different values of HWkDflOY (case yaw=20^o)

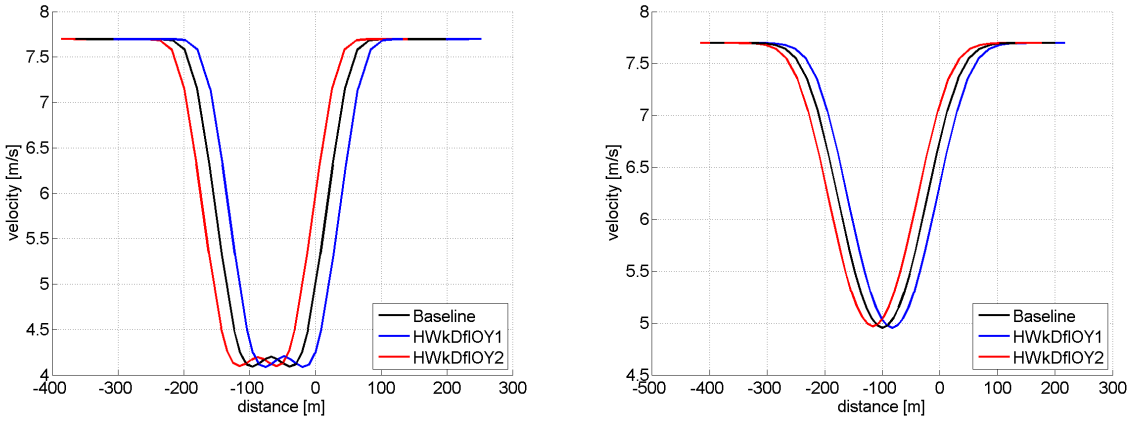

Figure 31. Wake profile at 3D (left) and 7D (right) for different values of HWkDflOY (case yaw=20^o)

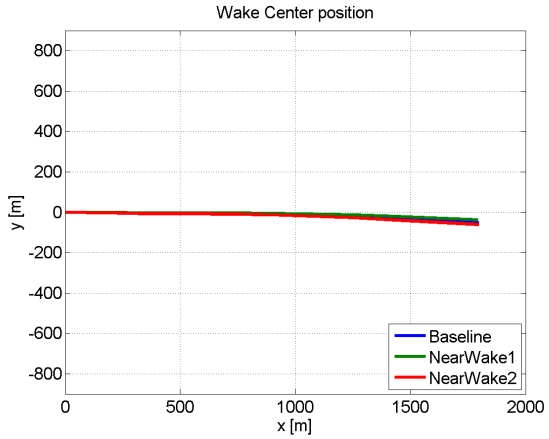

Figure 32. Wake Center position for different values of CNearWake (case yaw=0^o)

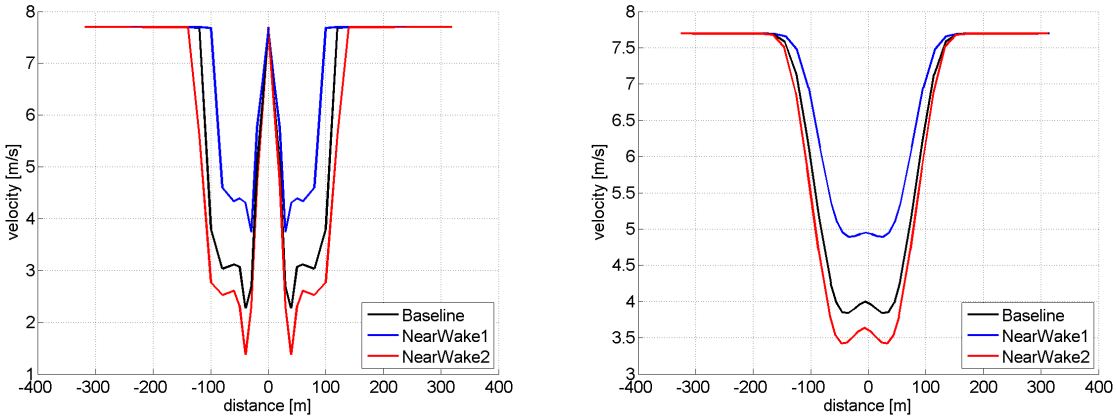

Figure 33. Wake profile at 0D (left) and 3D (right) for different values of CNearWake (case yaw=0^o)

parameter: the mean velocity observed in the near wake and the wake diameter in this plane. The objective of the calibration of this parameter is to obtain similar wake profile to SOWFA close to the turbine.

The change of the profile in the near wake region also affects the far wake (Figure 34), so it is important to calibrate this parameter before the set of parameters related with the turbulence and the recovery of the wake. The 3 different wake results can be seen in Figure 35 (velocities of the wake at z=HubHeight, FAST.Farm reference system), where the differences are clearly visible when velocity deficits are compared close to the turbine.

5.1.4 HWkDflx analysis

This parameter affects the position of the wake center as can be seen in Figure 36. The distance between the wake centers obtained in the simulations is increasing with the x position (at x=0, the difference is zero). The calibrated value for this parameter can be set using the SOWFA position of

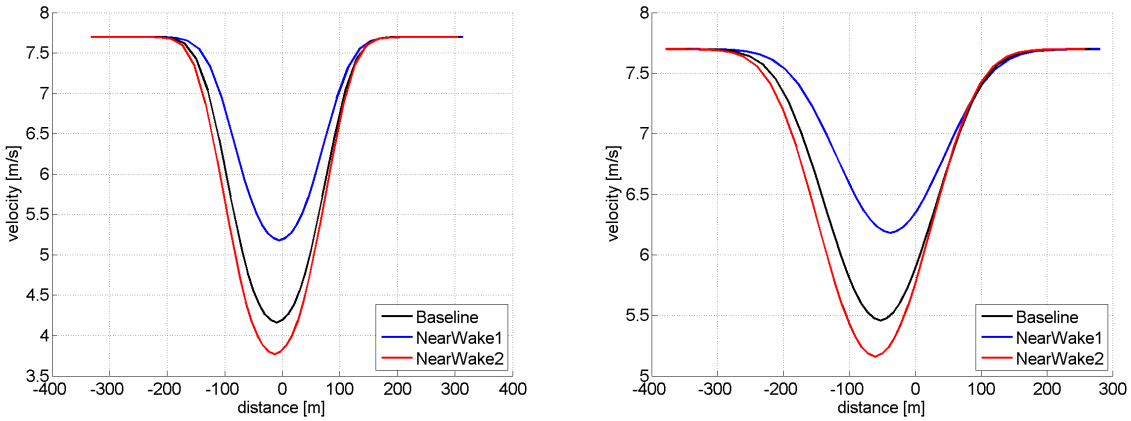

Figure 34. Wake profile at 5D (left) and 10D (right) for different values of CNearWake (case yaw=0^o)

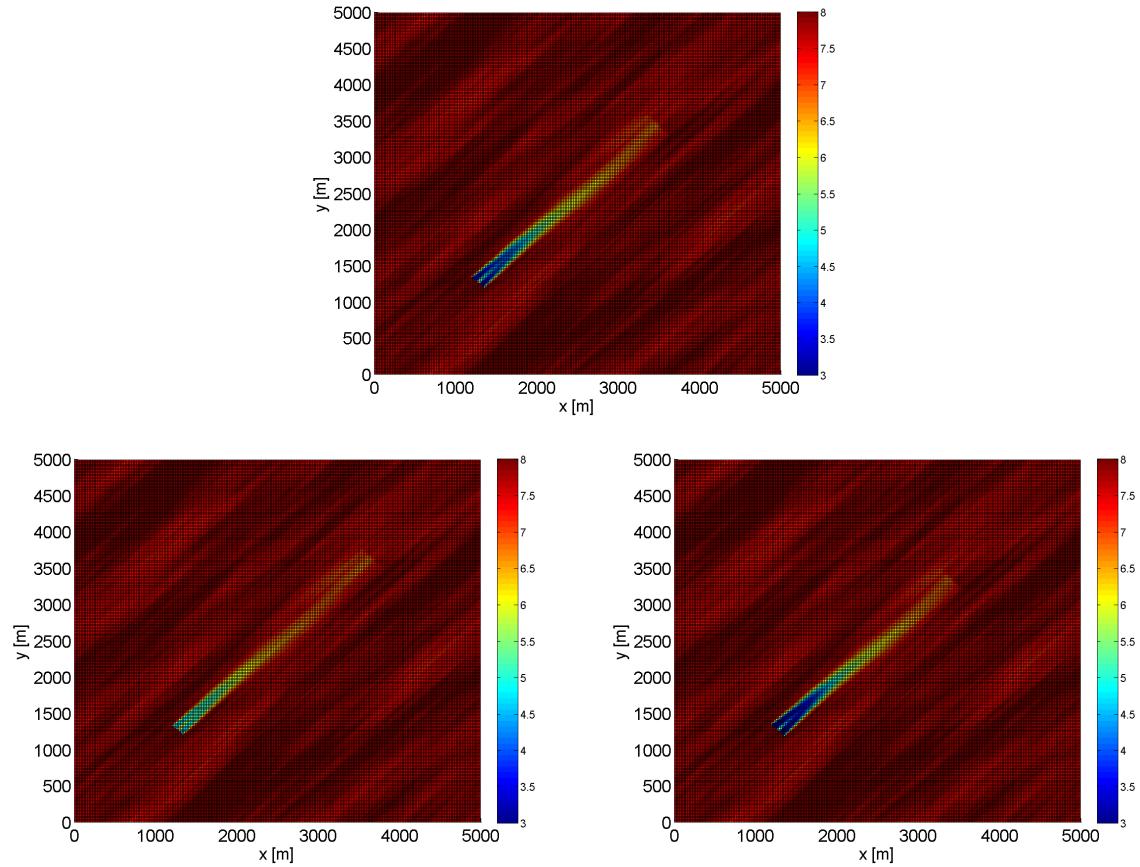

Figure 35. Wake map of velocities for baseline (up), Near-Wake1 (left) and NearWake2 (right)(FAST.Farm reference system)

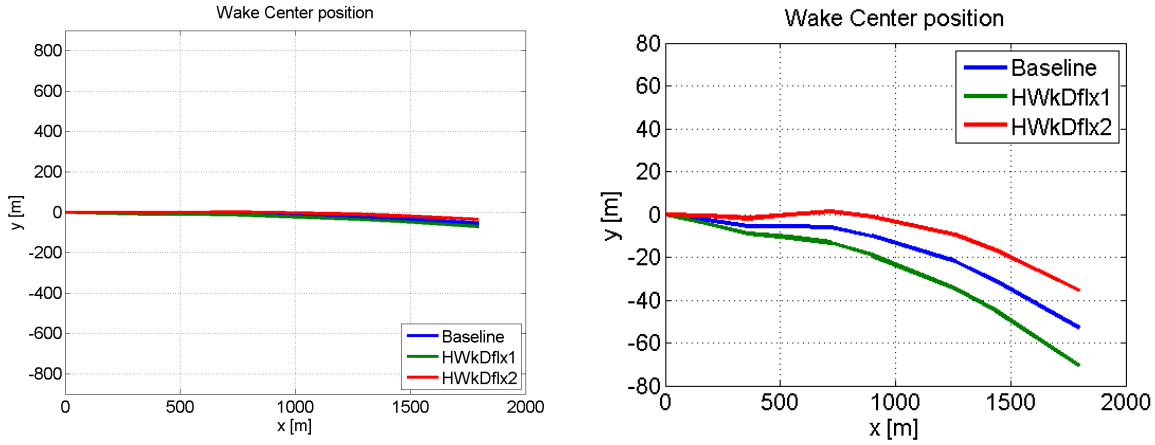

Figure 36. Wake Center position for different values of HWkDflx (case yaw=0^o)

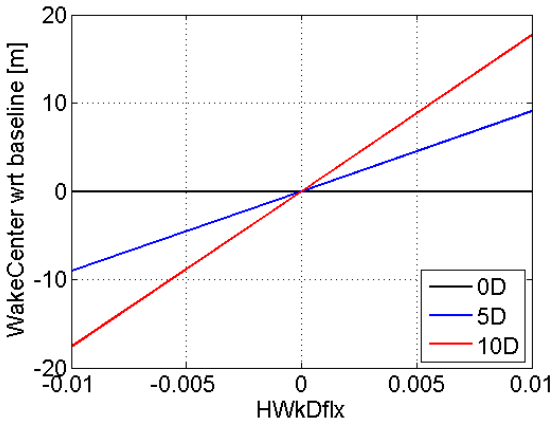

Figure 37. Wake center position with respect to baseline for different values of HWkDflx (0D, 5D, 10D, case yaw=0^o)

the Wake Center at plane 5D or 10D with respect to the baseline case, using the linear approach of Figure 37.

The variation of this parameter does not modify the results of the wake profile at different positions of the wake (without the effect of the wake center modification), as can be observed at Figure 38, similarly to parameter HWkDflO.

5.1.5 HWkDflxY analysis

The case without yaw does not present significant variation of the results when this parameter is modified. However, the effect of the parameter is clearly observed for the case with yaw (yaw=20^o). In Figure 39 (left), the wake center positions present different trend to the baseline case, the distance between the positions increase with the x position of the planes. The calibrated value for this parameter can be set using the SOWFA position of the Wake Center at plane 5D or 10D with respect to the baseline case, using the linear approach of Figure 39(right), similarly to the previous parameter.

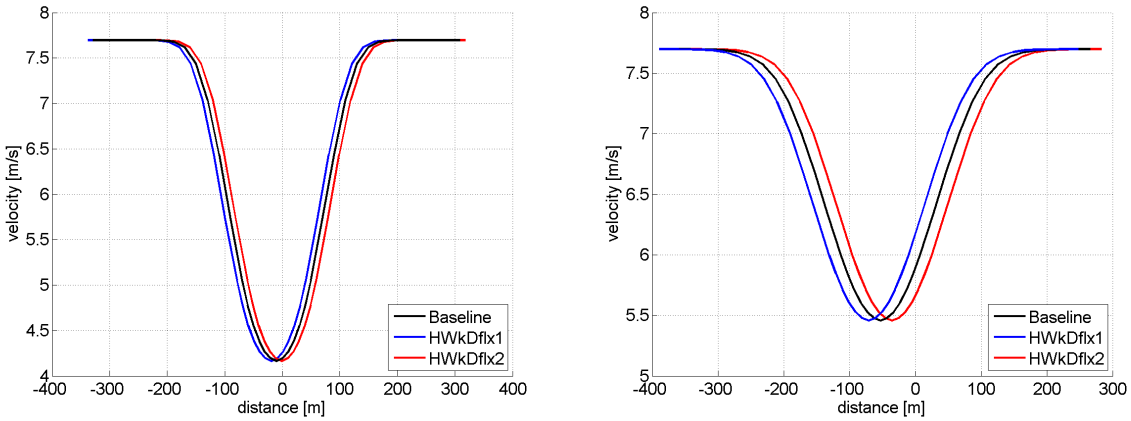

Figure 38. Wake profile at 5D (left) and 10D (right) for different values of HWkDfx (case yaw=0^o)

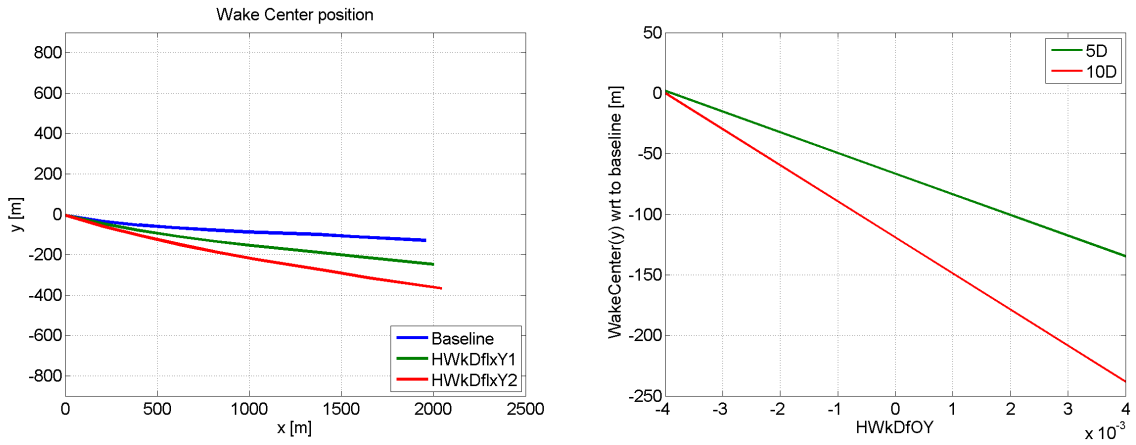

Figure 39. Wake Center position for different values of HWkDflxY (left) and positions with respect to baseline for 5D and 10D (right) (case yaw=20^o)

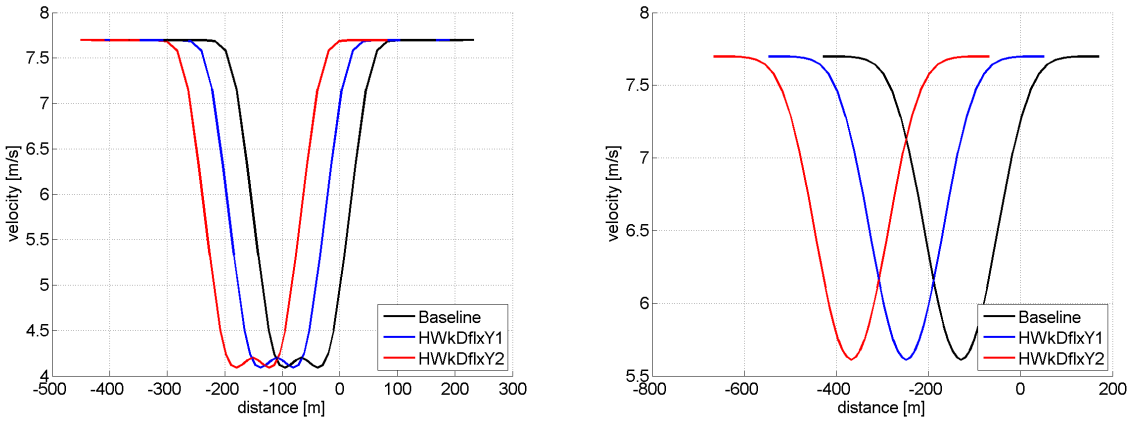

Figure 40. Wake profile at 3D (left) and 10D (right) for different values of HWkDfxY (case yaw=0^o)

The variation of this parameter does not modify the results the wake profile at different positions of the wake (without the effect of the wake center modification), as can be observed at right on Figure 40, similarly to parameter HWkDflx.

5.1.6 vShr analysis

The set of values used for this parametric study has been selected in order to simulate cases with a higher (vShr2) and lower (vShr1) contribution of the shear to the turbulence than the baseline case. This set of parameters defines the eddy viscosity filter function for wake shear layer, and the evolution of the mixing along the x positions of the wake.

The variation of this set of parameters can also modify the evolution of the wake center. However, the difference between the positions obtained in the parametric study is low and this distance is negligible compared to the distance that must be approximated with the previous parameters.

The main effect of this set of values can be observed in the profile of the wake for different planes, in Figures 43 and 44. The simulation with higher contribution to the turbulence (vShr2) shows faster recovery of the wake velocity at planes 3D and 5D, while for the planes located further the recovery of the baseline case is similar to vShr2.

The calibration of this set must be done after the CNearWake, and the approach of the values must be done comparing plane by plane, starting from the planes closer to the turbine. The selection of the values will be more difficult than the previous parameters and the objective is to obtain a similar representation of the evolution of the wake profiles than at SOWFA results.

The evolution of the wake can be also observed in FAST.Farm reference system (similar to SOWFA reference system) for the different sets of parameters in Figure 45. A similar Figure with results obtained by SOWFA could be extracted from the data in order to give a general view of the wake.

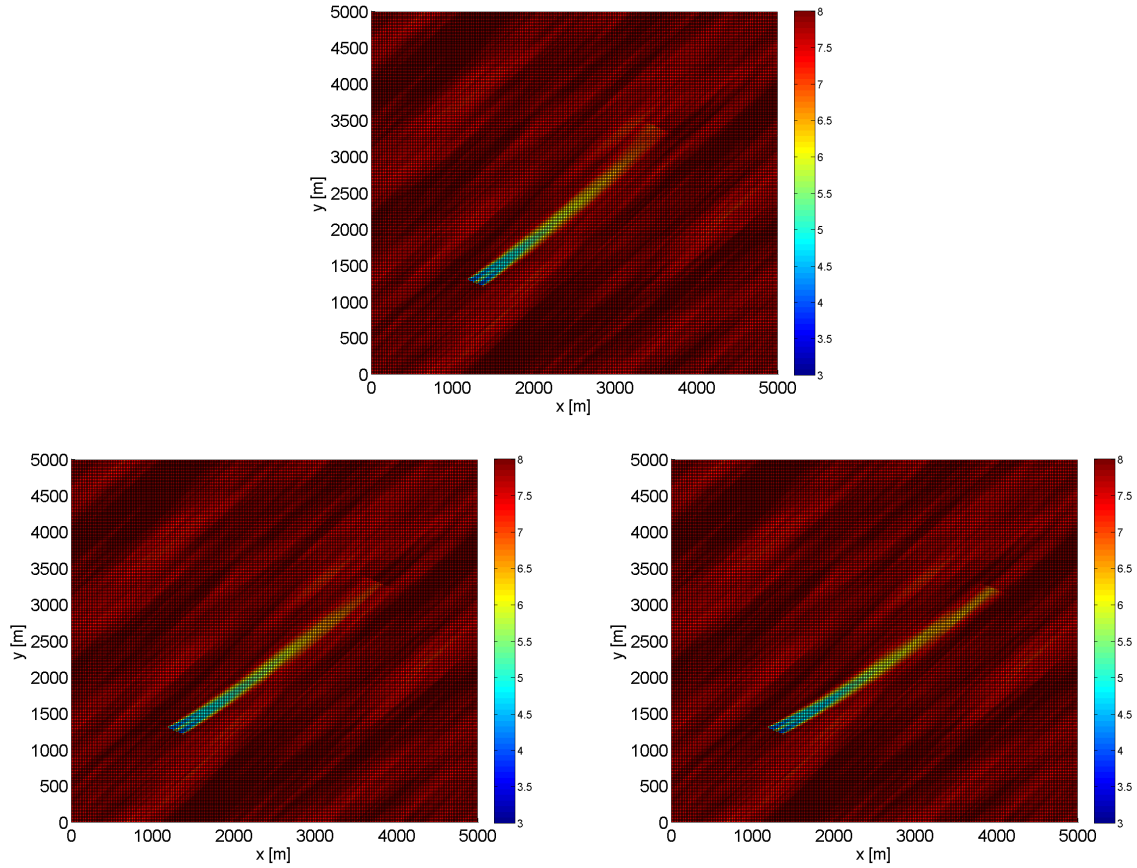

Figure 41. Wake map of velocities for baseline (up), HWkDflxY1 (left) and HWkDflxY2 (right), case yaw = 20^o (FAST.Farm reference system)

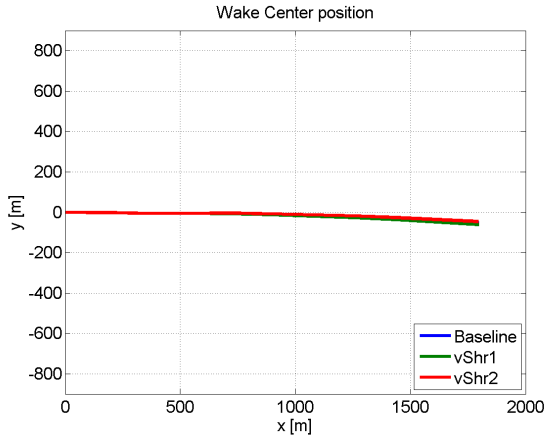

Figure 42. Wake Center position for different sets of vShr (case yaw=0^o)

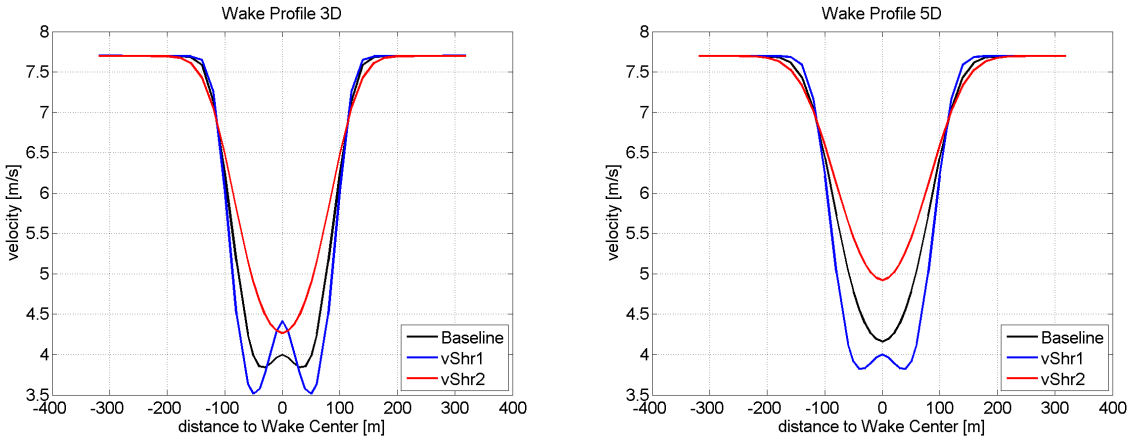

Figure 43. Wake profile at 3D (left) and 5D (right) for different sets of vShr (case yaw=0^o) at Wake Centers

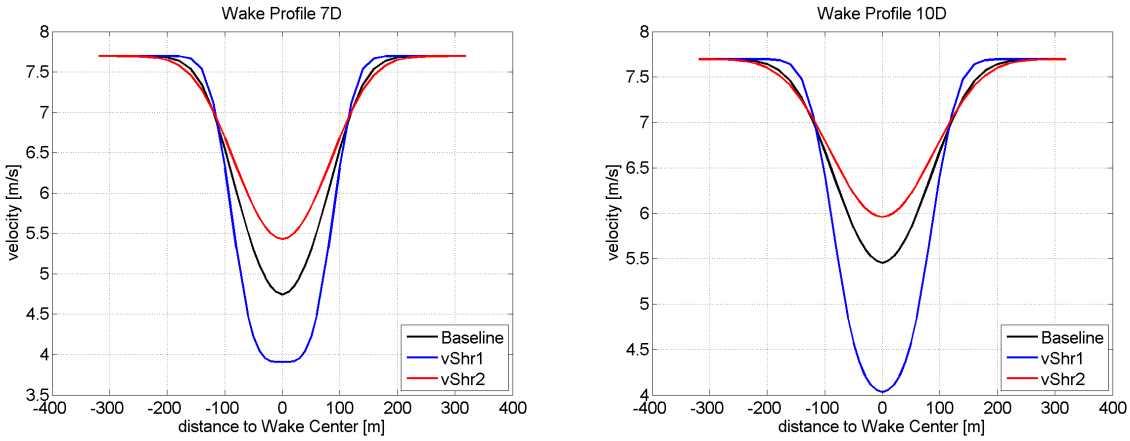

Figure 44. Wake profile at 7D (left) and 10D (right) for different sets of vShr (case yaw=0^o) at Wake Centers

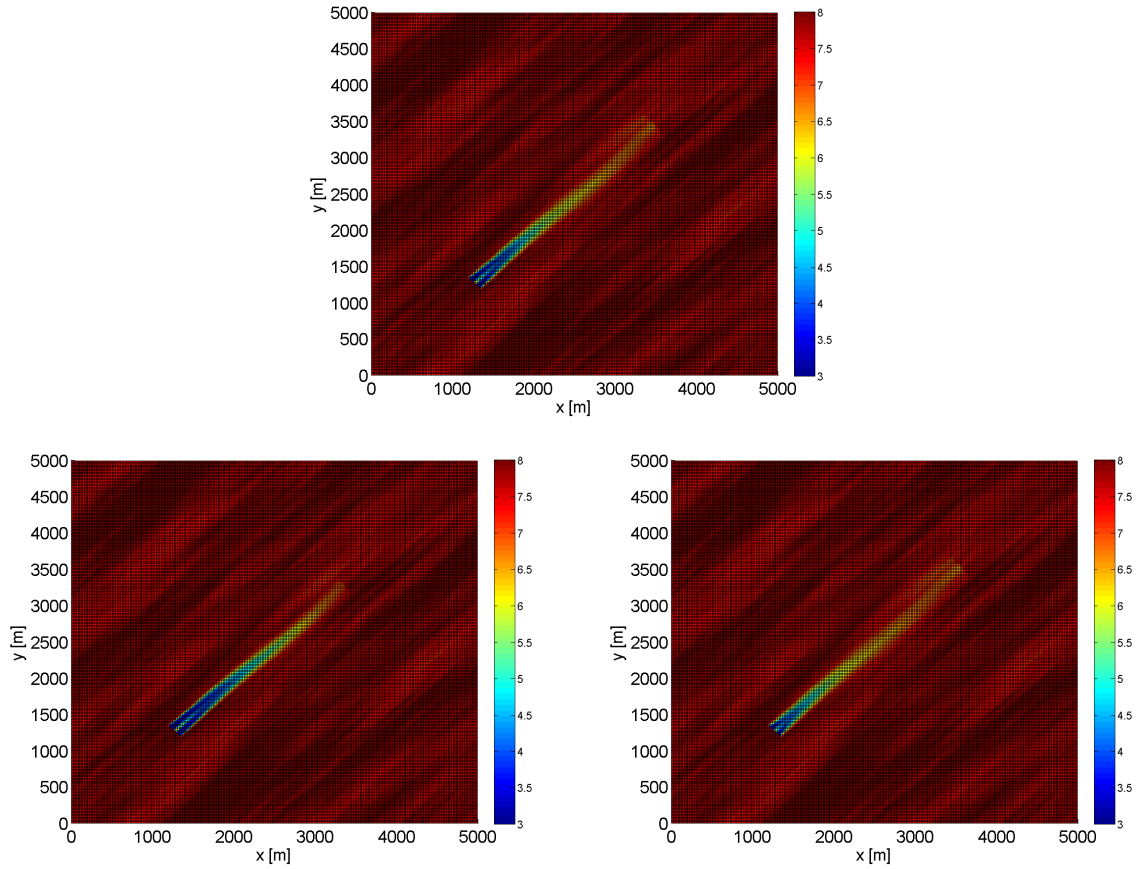

Figure 45. Wake map of velocities for baseline (up), vShr1 (left) and vShr2 (right)(FAST.Farm reference system)

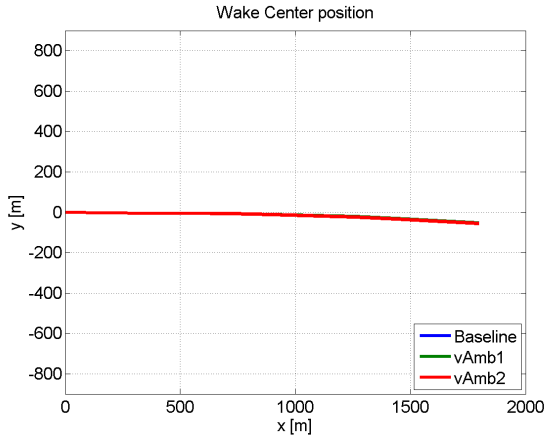

Figure 46. Wake Center position for different sets of vAmb (case yaw=0^o)

5.1.7 vAmb analysis

The set of values used for this parametric study has been selected in order to simulate cases with a higher (vAmb1) and lower (vAmb2) contribution of the shear to the turbulence than the baseline case. Case vAmb1 should present similar behavior to the baseline case until x=4D, because the filter is similar in that region, This set of parameters defines the eddy viscosity filter function for wake shear layer. For the rest of the planes, the filter of the vAmb1 case presents more contribution to the recovery.

The variation of the evolution of the wake center due to the modification of this set of parameters is negligible as can be observed in Figure 46.

The main effect of this set of values can be observed in the profile of the wake for different planes, in Figure 47. In the profile at 3D, the result obtained in the baseline case and for vAmb1 are similar (as it was expected due to the filter definition). For the rest of the planes the profiles are consistent with the values selected for the filters. The simulation with higher contribution to the turbulence (vAmb1) shows faster recovery of the wake velocity from plane 5D, and the vAmb2 case shows a slow recovery of the profile, while the baseline case presents an intermediate behavior.

The calibration of this set must be done after the CNearWake, and in parallel to vShr, and the approach of the values must be done comparing plane by plane. The definition of the filter is based in 2 different levels of contributions and the positions where the increment starts and ends. The selection of the calibrated set of parameters will be done comparing with SOWFA results.

The evolution of the wake can be also observed in FAST.Farm reference system for different set of parameters as can be seen in Figure 49. The effect on the profiles is evident, the size of the region limited by blue color is clearly different for the 3 cases.

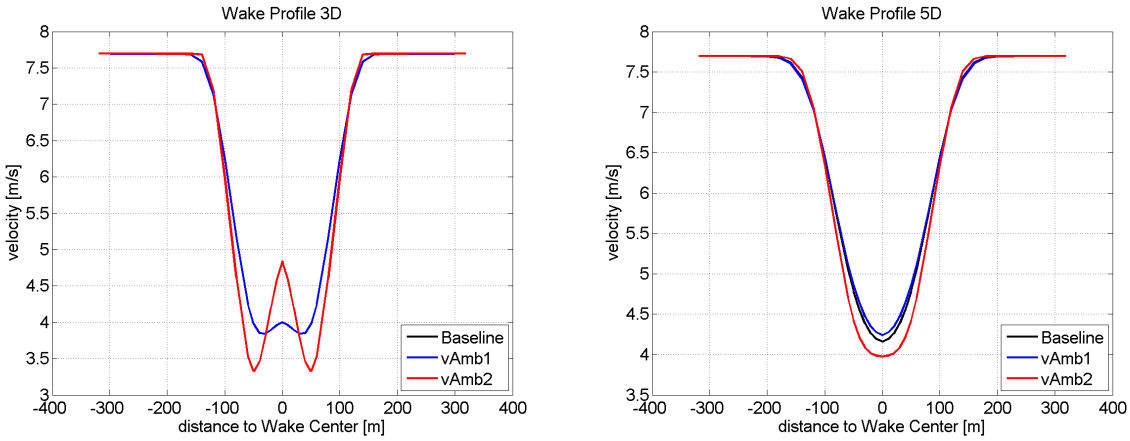

Figure 47. Wake profile at 3D (left) and 5D (right) for different sets of vShr (case yaw=0^o) at Wake Centers

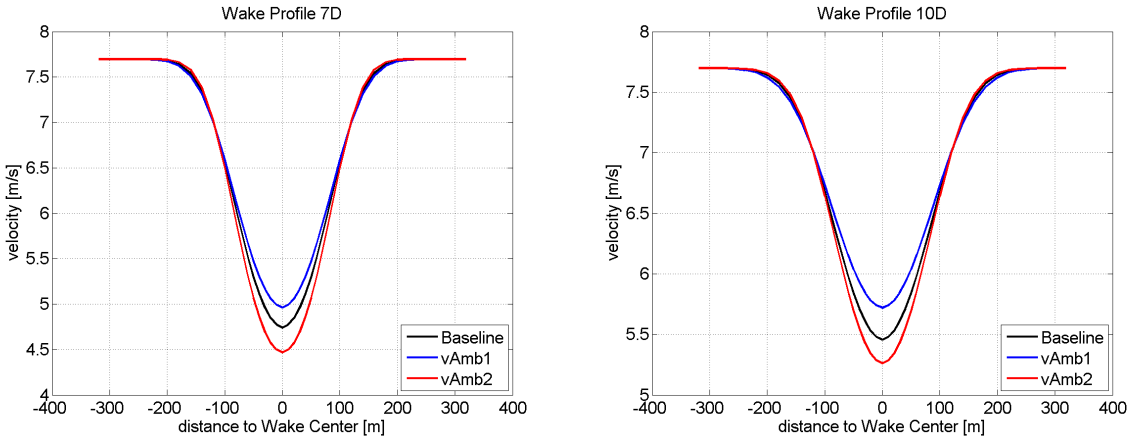

Figure 48. Wake profile at 7D (left) and 10D (right) for different sets of vShr (case yaw=0^o) at Wake Centers

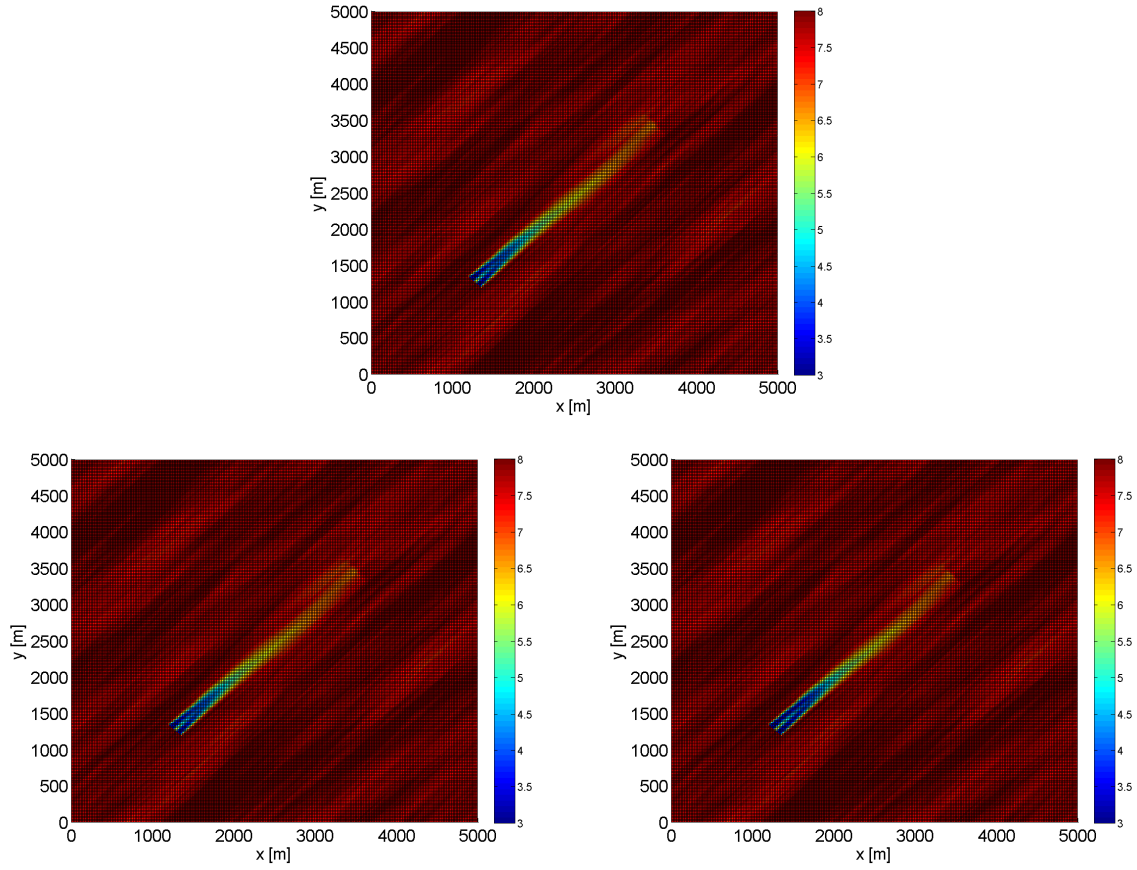

Figure 49. Wake map of velocities for baseline (up), vAmb1 (left) and vAmb2 (right)(FAST.Farm reference system)

5.1.8 Conclusions

The sensitivity of the parameters included in FAST.Farm has been analysed in previous sections, in terms of mean velocities (mean values obtained between 800s and 1000s of the simulations).

The individual effect of each parameter (or set of parameters) has been analysed in this section, and some Figures were shown in order to directly select the calibration with the values extracted from SOWFA results (Figures 27, 30, 37 and 39 for parameters HWkDflO, HWkDflOY, HWkDflx and HWkDflxY respectively).

The selection of the rest of the parameters will be more complex and the objective is to represent the behavior of the wake of SOWFA simulations. A comparison of the results obtained for both codes in terms of power, deflections and loads of the wind turbine is also important and must be taken into account.

After the calibration, the comparison of results of SOWFA and FAST.Farm for different turbine conditions (yaw/derating) will be conducted in the future, in order to evaluate the level of agreement once the parameters are fixed.

5.2 Comparison FLORIS/FAST.Farm

In this section, the results obtained with FLORIS wake model *Jensen* and the baseline case of FAST.Farm are compared in order to check the level of agreement between the codes without specific calibration. The case selected for this comparison has a yaw$= 0$ and the precursor used for FAST.Farm was "A4", while FLORIS uses a steady wind speed of $7.7 m/s$.

5.2.1 FLORIS configuration

The Jensen wake model was chosen instead of the Porté Agel model because at the moment there isn't a finished calibration for the 10MW wind turbine. Since the Jensen model has fewer configurable parameters, it is relatively easier to setup and the lack of proper calibration is not that significant as in the Porté Agel model. Although, we believe that once the Porté Agel model (see [2]) is fully calibrated for the 10MW wind turbine, the results obtained from the FLORIS model would have a higher accuracy when compared with models such as FAST.Farm.
The parameter configuration for the Floris *Jensen* model was:

- modelData.adjustInitialWakeDiamToYaw = false
- modelData.ad = -4.5/RotorDiameter
- modelData.bd = -0.01
- modelData.at = 0.0
- modelData.bt = 0.0
- modelData.KdY = 0.17
- modelData.useWakeAngle = true
- modelData.kd = deg2rad(1.5)
- modelData.Ke = 0.075
- modelData.KeCorrCT = 0.0
- modelData.baselineCT = 4.0*(1.0/3.0)*(1.0-(1.0/3.0))
- inputData.airDensity = 1.1716;

For this particular case, the wind speed was 7.7 m/s, with an uniform vertical profile and an atmospheric turbulence intensity of 5%.

5.2.2 Results comparison

Figure 50 shows the wind speed field at hub height for the analyzed case.

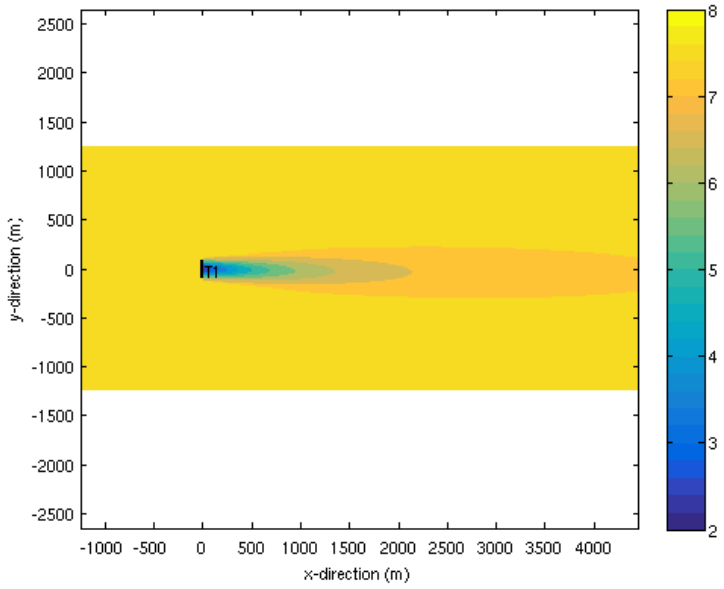

Figure 50. Floris (Jensen) wind map for (case yaw=0^o; v=7.7m/s and TI=5%)

The wake center positions are compared in Figure 51. The position of the wake for x=0 depends on parameters of calibration, that should be selected in order to present similar results to SOWFA. The evolution of the wake for higher values of x is similar, both codes presents negative values for y. However, the trend obtained with FLORIS is smooth (due to the steady calculation), while the positions observed for FAST.Farm depend on the turbulent wind.

The following comparisons of the profile of the wake are centered at the wake center of the different planes, in order to compare the profile without the effect of the deviation of the wake center. The profiles studied are calculated at 0D, 3D, 5D, 7D and 10D.

The result obtained at the first plane (0D, Figure 52 left) show similar minimum velocity and wake diameter. However, the shape of the velocity profile is clearly different. While the velocity for FLORIS is minimum at the wake center and then increases with the distance to the wake center, the result obtained for FAST.Farm presents values of the velocity related to the axial induction of every section of the blade. It is evident that at the wake center (hub) there is no blade effect and the velocity of the wake is similar to the wind for FAST.Farm, and the effects of the tower and nacelle are not included in this code. In general, the deficit observed from FAST.Farm is higher than the one obtained in FLORIS, in the rotor diameter region. In order to adapt the results of FAST.Farm to the FLORIS profile, the parameter *CNearWake* can be modified. However, the shape of the profile can not be modified since the effect would be observed in the wake diameter and the magnitude of the wake deficit.

For the rest of the planes (from 3D), the trend of the recovery is clearly different, as can be observed in Figures 52 (right), 53 and 54. The velocities observed for FLORIS are higher than for FAST.Farm and the wake diameter is wider. The shape of the profile is smooth for both codes, but FLORIS

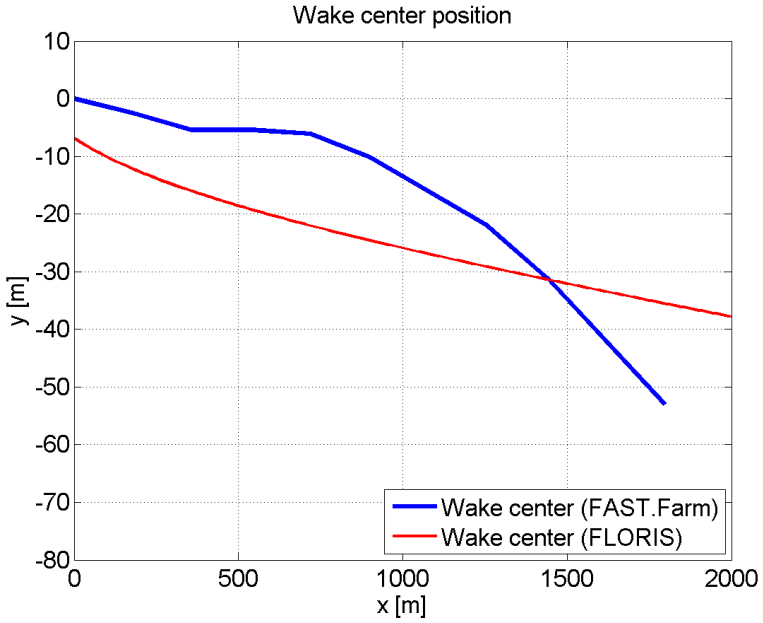

Figure 51. Wake Center position comparison (case yaw=0^o)

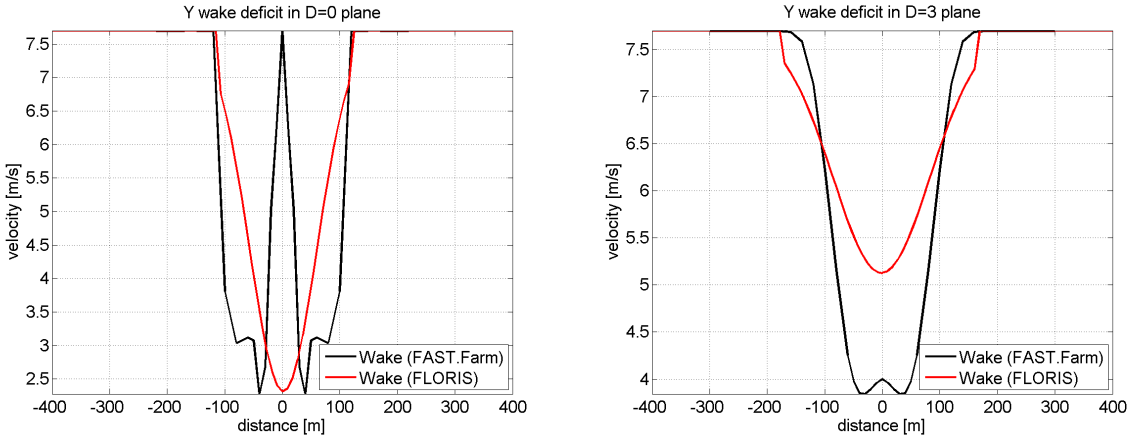

Figure 52. Comparison of wake profiles at 0D and 3D for FLORIS and FAST.Farm

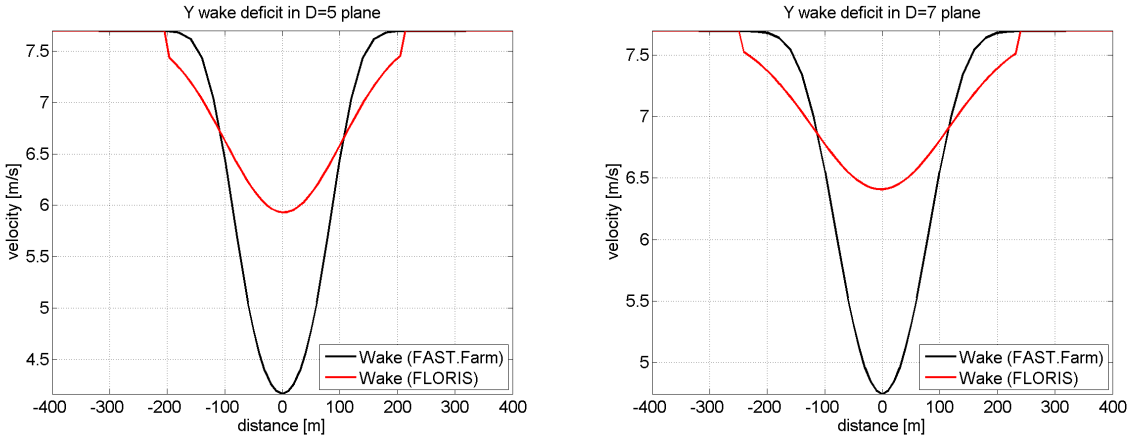

Figure 53. Comparison of wake profiles at 5D and 7D for FLORIS and FAST.Farm

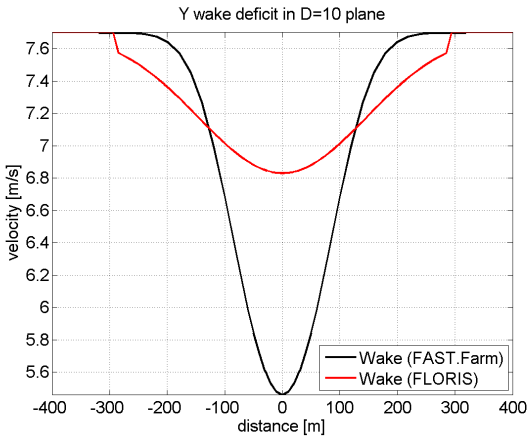

Figure 54. Comparison of wake profiles at 10D for FLORIS and FAST.Farm

present an abrupt change in the velocity at the wake diameter (for all planes) while FAST.Farm shows a smoother transition between these regions.

The change of the values for parameters of FAST.Farm related to *vAmb* and *vShr* could modify the results in order to have similar results to FLORIS. The parameter *modelData.Ke* in Floris could also be tuned in order to decrease the wake expansion. It would be necessary to increase the effect of the turbulence in order to accelerate the recovery of the wake velocities. The mean velocities of the wake can be approximated, but the abrupt change of velocity in the wake diameter of FLORIS can not be obtained using FAST.Farm.

5.3 Conclusions

The first comparison of results between FLORIS and FAST.Farm has shown that the wake center position differs at the turbine and the evolution of the wake for both codes presents different behavior. The modification of the parameters necessary to get similar results, from FAST.Farm's point of view has been explained. The FLORIS wake model used is an engineering model and has its limitations

as it can be seen from this comparison. By using a more advanced model like Porté Agel it would be possible to better adjust the wake's shape and recovery factor, which it is not possible with the wake model used. The next step, would be the calibration of the parameters in both codes to better emulate the real behavior of the wake. Using SOWFA results as reference, the calibration of the parameters for FLORIS and FAST.Farm will allow the realistic simulation of different cases. Despite a clear difference between both models, this test was able to provide an initial comparison that might be useful to define the next stages of development to achieve the goal defined in the beginning of the project.

6 VALIDATION OF THE FLORIS STEADY-STATE WIND FARM MODEL

6.1 Introduction

The FLORIS (FLOw Redirection In Steady-state) model is a set of low-fidelity steady-state wind farm models developed for real-time online wind farm control and low- fidelity offline wind farm analysis and layout optimization, whose governing equations are given in deliverable D1.2. The goal of this chapter is to assess the ability of the FLORIS model in properly predicting, under different operating conditions, the speed, position and turbulence intensity of the flow within a wake shed by a single wind turbine.

To this aim, at first a short description of the FLORIS model main features is given, with highlights on the required parametrization of the engineering wake models. Subsequently, the CFD simulation environment, used to generate the comparison data, is introduced, followed by a description of the performed simulations and the adopted tuning process of the models parameters. Finally, a comparison between high-fidelity CFD-SOWFA simulations and predictions obtained using the FLORIS model is given.

6.2 Model description

The FLORIS model has been conceived to provide accurate predictions of the time-averaged flow field and power capture of each turbine inside a wind farm. All this can be achieved at a very low computational cost, thus enabling the use of FLORIS for the optimization of the turbine control settings that aim at maximizing the overall plant energy production.

The analytical wake model used within FLORIS has been firstly proposed in [3], and it will be referred as Porté-Agel model in the following. This model assumes a Gaussian distribution of the wake velocity deficit. Differing from the previous model, the Porté-Agel model is based on an advanced manipulation of the mass and momentum conservation fluid dynamic equations, which led to a reliable analytical wind farm model capable of predicting the evolution of the wake velocity deficit, of the wake deflection due to yaw effects, as well as of the amount of turbine-induced turbulence added to the flow.

The analytical model consists of various equations, presented in Deliverable D1.2, as well as of parameters whose values should be tuned based on experimental/wind tunnel/CFD data. Specifically, the parameters to be tuned are determined according to the following equations.

The wind velocity in the far wake is expressed with Eq. 6.1, where U_∞ refers to inflow wind velocity, γ denotes the yaw misalignment, σ_y and σ_z indicate the wake widths in lateral and vertical dimensions. Additionally δ stands for the deflection in lateral direction and d is the diameter of the wind turbine.

$$\frac{\Delta U}{U_\infty} = \left(1 - \sqrt{1 - \frac{C_T \cos\gamma}{8(\sigma_y \sigma_z / d^2)}}\right) \exp\left(-0.5\left(\frac{y-\delta}{\sigma_y}\right)^2\right) \exp\left(-0.5\left(\frac{z-z_h}{\sigma_z}\right)^2\right) \tag{6.1}$$

The wake widths σ_y and σ_z, calculated as following

$$\frac{\sigma_y}{d} = k_y \frac{(x - x_0)}{d} + \frac{\cos\gamma}{\sqrt{8}} \tag{6.2}$$

$$\frac{\sigma_z}{d} = k_z \frac{(x - x_0)}{d} + \frac{1}{\sqrt{8}}, \tag{6.3}$$

make use of the wake decay coefficients k_y and k_z that apply to the lateral and vertical directions, respectively. In this work, it is assumed that the wake decay coefficients are equal in both directions, hence the equation for the wake decay coefficients can be expressed as:

$$k_y = k_z = k_a I + k_b, \tag{6.4}$$

where I stands for the inflow turbulence intensity, while k_a and k_b are two of the four parameters whose required tuning is discussed further in section 6.3.3. Since the wake decay coefficient is a function of the inflow turbulence intensity, it is expected that the model is capable of predicting the wake evolution for various inflow turbulence intensity conditions.

The two remaining tuning parameters are α^* and β^* included in the following equation

$$\frac{x_0}{d} = \frac{\cos\gamma\left(1 + \sqrt{1 - C_T}\right)}{\sqrt{2}\left[\alpha^* I + \beta^*\left(1 - \sqrt{1 - C_T}\right)\right]}, \tag{6.5}$$

and which govern the effect of atmospheric turbulence and turbine-induced turbulence on the near-wake core length.

Additionally, the Porté-Agel model is capable of calculating the amount of turbine-induced turbulence (I_+) added in the wake. To this aim, the model from [12] is used:

$$I_+ = TI_a a^{TI_b} I_0^{TI_c} (x/d)^{TI_d}, \tag{6.6}$$

where a denotes the axial induction factor, I_0 refers to the inflow turbulence intensity and TI_a, TI_b, TI_c and TI_d are parameters whose tuning is again discussed in the following. Finally, the derivation of the turbulence intensity in the wake is defined as:

$$I_{wake}^2 = \sqrt{I_0^2 + I_+^2}. \tag{6.7}$$

6.3 Validation of FLORIS with respect to CFD data.

6.3.1 Simulation environment

The numerical simulation environment is based on the open-source code `Foam-extend-4.0`. The model is based on a finite-volume LES formulation, implemented in the code `SOWFA` [17], coupled with a lifting line model of the blades, whose implementation is based on `FAST v8` [19]. The turbine nacelle and tower are modeled by an immersed boundary method [28].

The wind turbine used within the simulation framework is the scaled G1, described in Deliverable 3.1. Therefore, the simulation model aims at digitally reproducing the experimental facility described in Deliverable 3.1. To this aim, the simulation model includes the wind tunnel walls and the passive generation of turbulence obtained by the use of spires placed at the tunnel inlet. The simulation of the flow around the spires is particularly expensive, as it must faithfully represent the breakdown of the spire-shed vortices into a sheared and turbulent flow. In fact, a high-quality dense mesh — obtained by the mesh generator `ANSYS/ICEM`— is used to resolve the flow around the spires. Since the same turbulent flow can be used for several simulations characterized by different operating conditions of the wind turbines, the overall wind tunnel chamber is split into two separate computational domains. One models the tunnel inlet, the spires and the development of the turbulent flow, up to a distance of 36 m downstream of the inlet. The outflow of this first "precursor" simulation is then used as inflow of a second computational domain, which models the wind turbines and their wake interactions all the way to the tunnel outlet.

Iso-vorticity surfaces of the precursor and of a wind turbine cluster simulations are visualized together in Fig. 55. The figure shows the generation of large vortical structures by the spires placed at the tunnel inlet. Such structures break down into a sheared and turbulent flow that becomes the inflow of the downstream turbines.

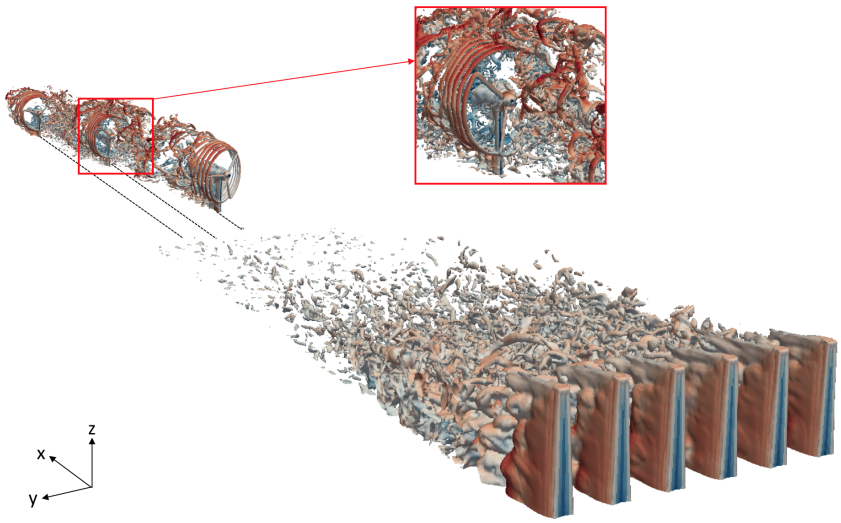

Figure 55. Visualization of iso-vorticity field for the precursor and turbine cluster simulations.

6.3.2 Performed simulations

CFD simulations were conducted with a single wind turbine and for two different inflow conditions: below-rated mid-turbulent inflow (mid-TI) , characterized by an average wind speed of 4.8 m/s and a turbulence intensity of 5.5%, and above-rated high-turbulent inflow (high-TI), characterized by an average wind speed of 6.9 m/s and a turbulence intensity of 14.1%. With the aim of simulating the impact produced by different thrust coefficients C_T on the wake behavior, two simulations were carried out with different setting of the rotor speed Ω and blade pitch β. Moreover, in order to address the effect of different yaw misalignment on the wake characteristics, various simulations were performed with yaw misalignment γ varying from -30° to +30°, where a positive misalignment corresponds to a counter-clockwise rotation from the wind to the rotor axis looking down onto the terrain. The wind turbine operating conditions, for each of the 13 simulated cases, are shown in Table 11.

Table 11. Overview of performed CFD simulations with mid-TI and high-TI inflow conditions.

	$\Omega[rpm]$	$\beta[°]$	$\gamma[°]$	$C_T[-]$
mid-TI V = 4.8 m/s	706.1	0.42	0	0.902
	700.2	1.54	0	0.789
	640.6	0.42	−30	0.741
	681.5	0.42	−20	0.834
	701.0	0.42	10	0.894
	682.3	0.42	20	0.836
	639.8	0.42	30	0.738
high-TI V = 6.9 m/s	693.4	0.42	0	0.718
	691.5	1.33	0	0.686
	623.6	0.42	−30	0.580
	659.3	0.42	−20	0.656
	682.3	0.42	−10	0.702
	686.6	0.42	10	0.701

For each scenario, CFD flow velocity and turbulence intensity data were sampled at several points at hub height and for 6 downwind distances ($x/d = 4 : 1 : 9$), thus resulting in 78 set of flow data. The post-processed data therefore consists of normalized flow velocity and turbulence intensity measured at each sample point, as well as key-parameters like the yaw misalignment value and the thrust coefficient/axial induction factor.

6.3.3 Model parameters tuning

In this section, the focus is on the model parameters tuning that has been performed by solving an optimization problem. At first, the CFD data were linearly interpolated to get over 1000 measurement points per each operating condition and downwind distance. An optimization problem, that seeks for the model parameters that provide the best match between model predictions and CFD data, is than solved using MATLAB's `fminsearch` function and considering, as cost function, the sum

of the root mean squared error (RMSE) associated to several data set, where the j^{th} RMSE is defined as:

$$\mathrm{RMSE} = \sqrt{\frac{1}{N}\sum_{i=1}^{N}(x_{i,CFD} - x_{i,FLORIS})^2}, \tag{6.8}$$

with *i* and *N* indicating a single measurement point and the total number of points within a data set, respectively, while *x* stands for either the CFD or FLORIS-predicted normalized flow velocity or turbulence intensity.

As highlighted in Eqs. 6.4 and 6.5, the wake velocity deficit and the wake deflection depend both on the potential core length and the wake decay, which enforces the need of a simultaneous tuning of k_a, k_b, α^* and β^*. As initial guess to the optimization problem, the parameters reported in Table 12 were used, with these letter derived by means of a dedicated experimental campaign conducted within the project and discussed in Deliverable 3.4. The adopted cost function was instead the sum of the RMSE associated to all 78 data set.

Table 12. Initial guess for the parameters of the Porté-Agel wake decay and potential core length sub-models.

Wake Decay		Potential Core	
k_a	k_b	α^*	β^*
0.1177	0.0194	1.2973	0.2375

The parameters of the Porté-Agel turbulence intensity sub-model, reported in Eq. 6.9, were than tuned by solving a similar optimization problem, but using, as cost function, the sum of the RMSE associated to the 24 data set related to simulations performed with the not-yawed wind turbine ($\gamma = 0°$). As initial guess, the values for TI_a, TI_b, TI_c and TI_d reported in Table 13 were used, with these letter presented in Deliverable 1.2, while the values of the axial induction factor have been computed as

$$a = \frac{1}{2\cos\gamma}\left(1 - \sqrt{1 - C_T\cos\gamma}\right), \tag{6.9}$$

using the yaw misalignment and thrust coefficient reported in Table 11.

Table 13. Initial guess for the parameters of the Porté-Agel turbulence sub-model.

Turbulence Intensity			
TI_a	TI_b	TI_c	TI_d
0.73	0.8325	0.0325	−0.32

6.3.4 Comparison between CFD and FLORIS-predicted wake flow.

Table 14 reports the output of the tuning process for parameters of the wake decay and potential core length sub-models.

Table 14. Tuned parameters of the Porté-Agel wake decay and potential core length sub-models

Wake Decay		Potential Core	
k_a	k_b	α^*	β^*
0.1702	0.0150	1.5950	0.3415

The FLORIS flow model predictions with the initial and tuned parameters, as well as the CFD data, are shown in Fig. 56-64 separately for each wind turbine operating condition, where each subplot refers to one downwind distance, denoted by the title above, while the normalized velocity are reported on the x-axis as function of the lateral distance from the rotor center. $FLORIS_E$ and $FLORIS_C$ refer to the model predictions with the initial and tuned parameters, respectively.

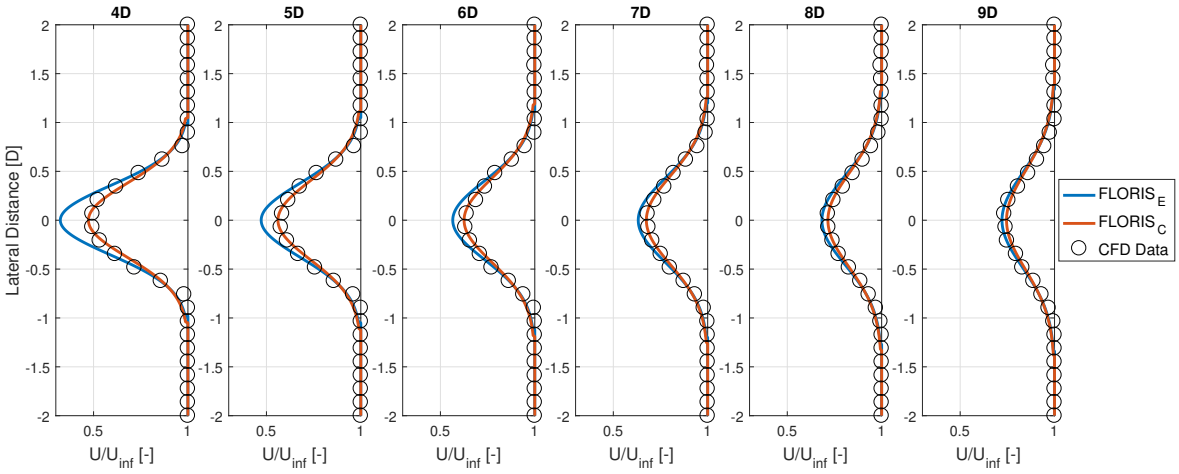

Figure 56. Porté-Agel flow velocity predictions and CFD data for mid-TI, $\gamma = 0°$, $C_T = 0.902$.

As it can be seen from the figures, the model predictions with the $FLORIS_E$ set of tuning parameters are already quite satisfactory, for both considered turbulence intensity, as well as for aligned or yawed wind turbines. However, an overestimation of the wake velocity deficit is observed, especially for downwind distances close to rotor disk.

The average of the RMSE associated to all 78 cases is equal to 0.034 and 0.0202, respectively with the $FLORIS_E$ and $FLORIS_C$ parameters. This highlights that a consistent improvement is achieved through parameter tuning, which led to an excellent model predictions for yaw angles between -$20°$ and $20°$angles. For yaw misalignment exceeding this range, the model predictions are satisfactory, yet not perfect.

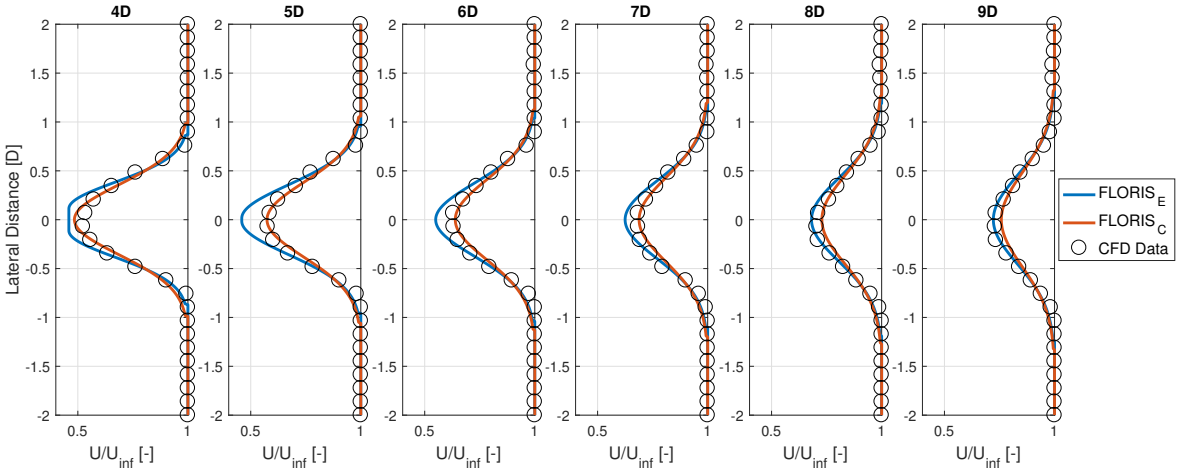

Figure 57. Porté-Agel flow velocity predictions and CFD data for mid-TI, $\gamma = 0°$, $C_T = 0.789$.

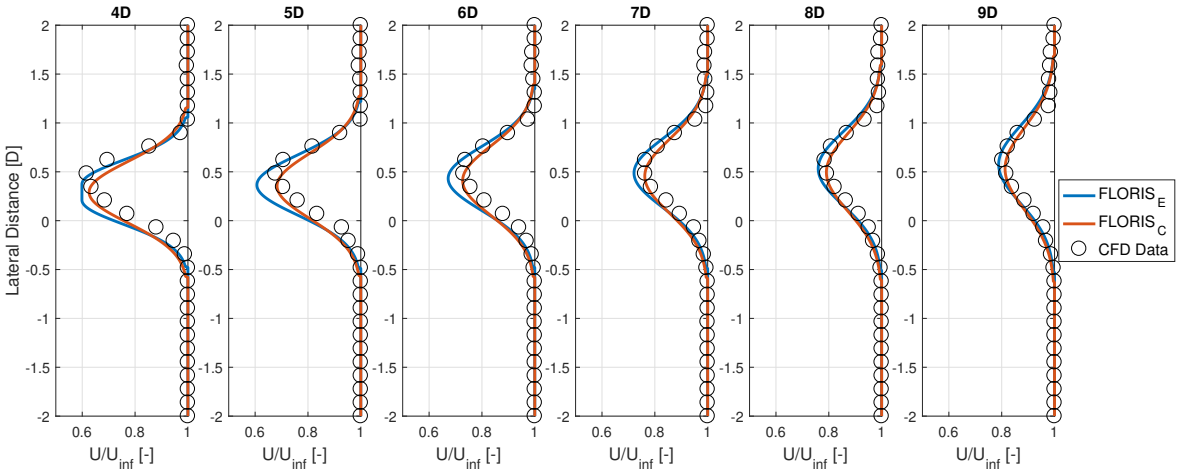

Figure 58. Porté-Agel flow velocity predictions and CFD data for mid-TI, $\gamma = -30°$.

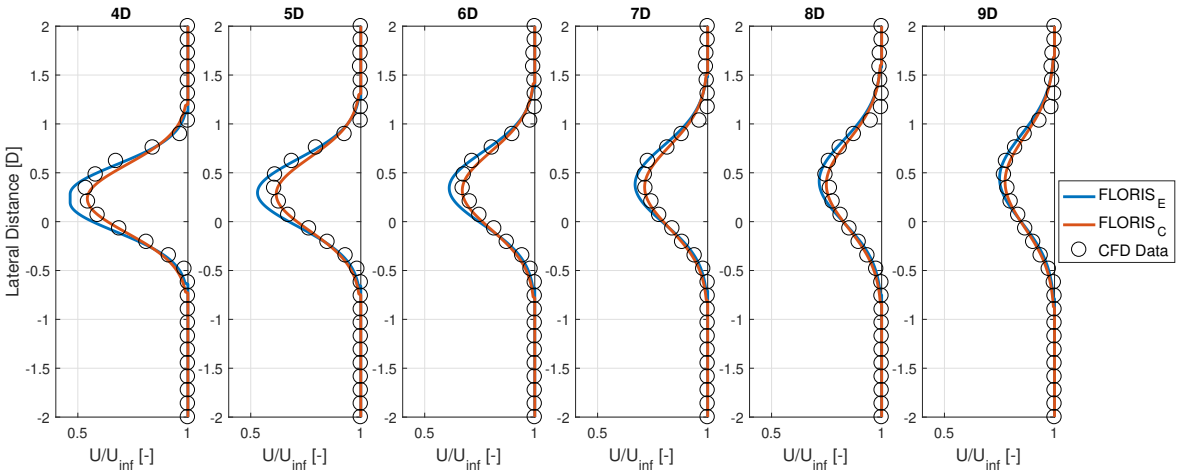

Figure 59. Porté-Agel flow velocity predictions and CFD data for mid-TI, $\gamma = -20°$.

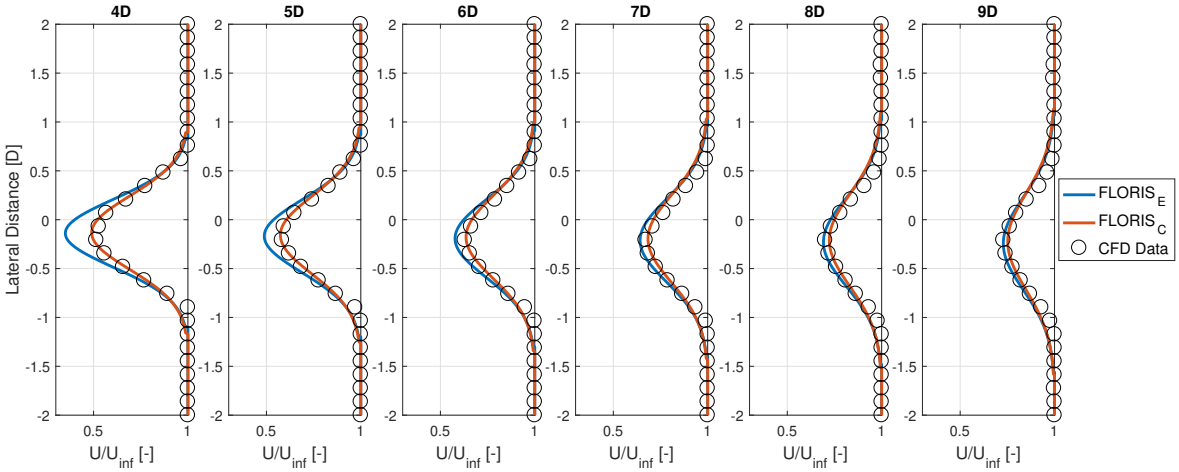

Figure 60. Porté-Agel flow velocity predictions and CFD data for mid-TI, $\gamma = 10°$.

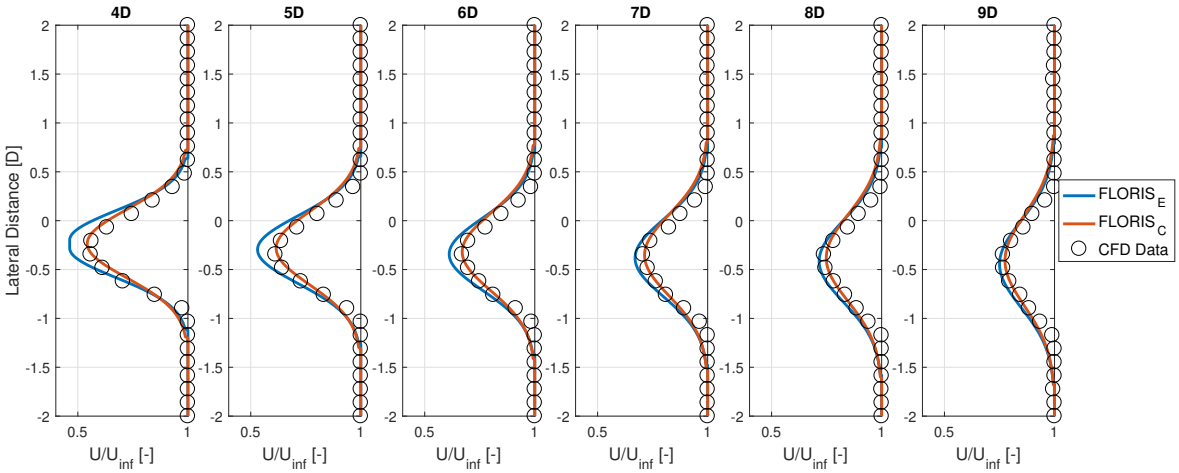

Figure 61. Porté-Agel flow velocity predictions and CFD data for mid-TI, $\gamma = 20°$.

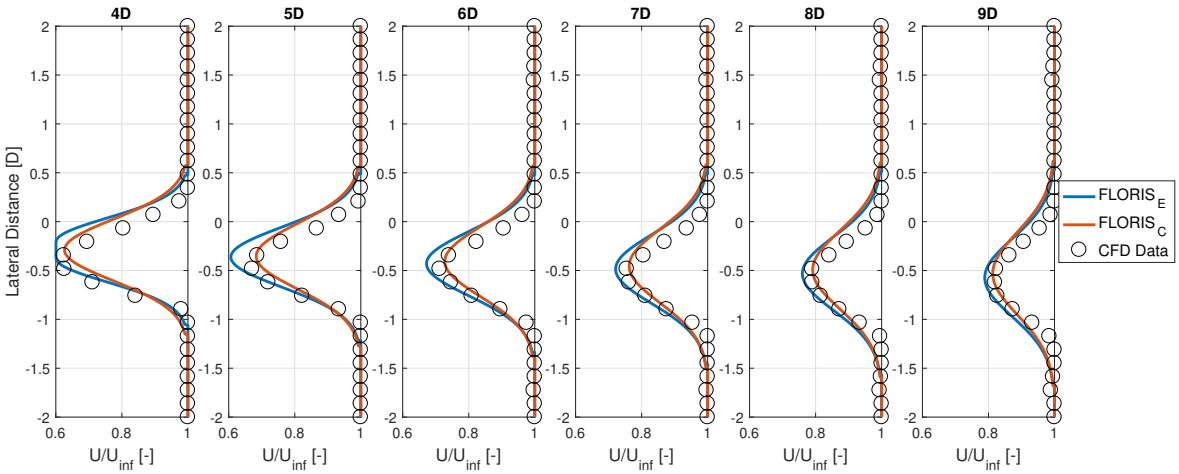

Figure 62. Porté-Agel flow velocity predictions and CFD data for mid-TI, $\gamma = 30°$.

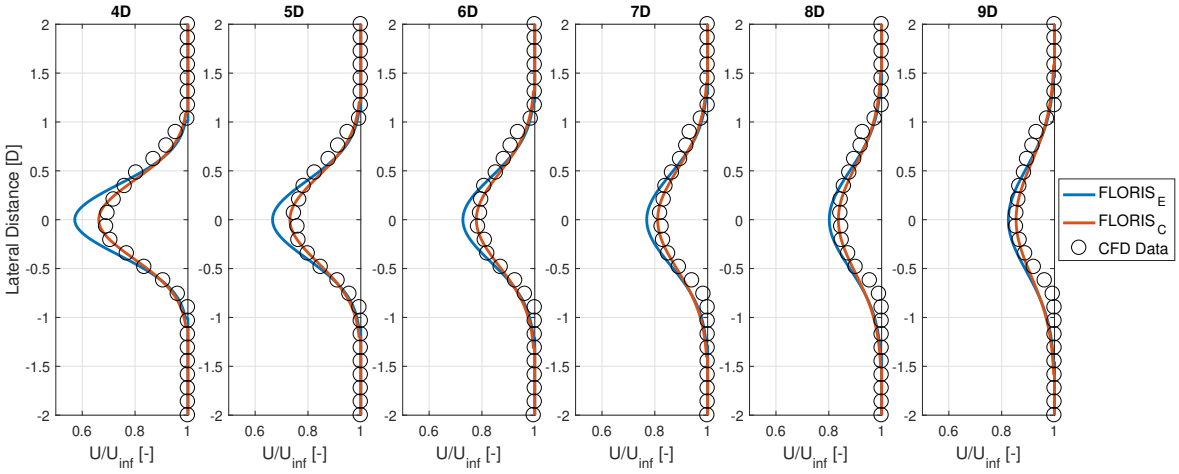

Figure 63. Porté-Agel flow velocity predictions and CFD data for high-TI, $\gamma = 0°$, $C_T = 0.718$.

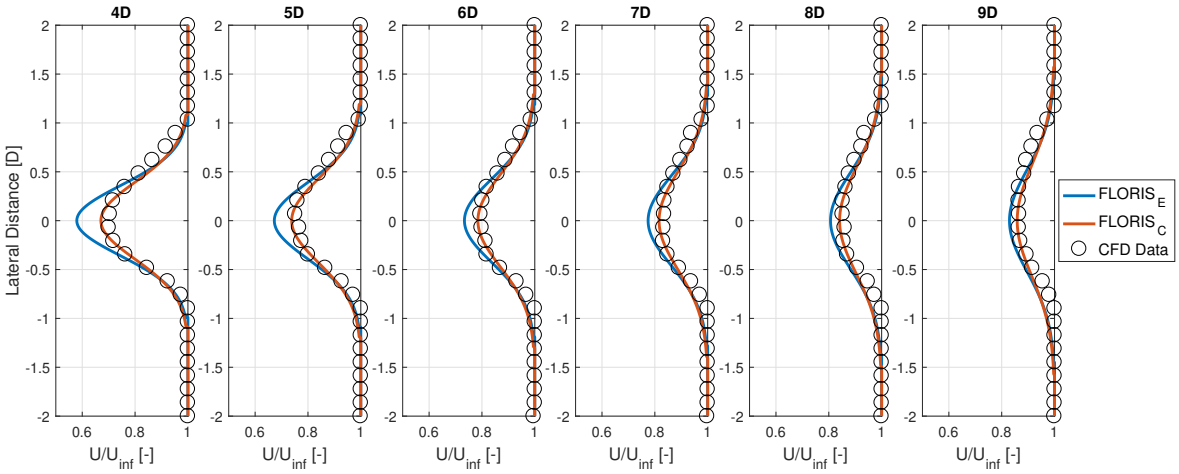

Figure 64. Porté-Agel flow velocity predictions and CFD data for high-TI, $\gamma = 0°$, $C_T = 0.686$.

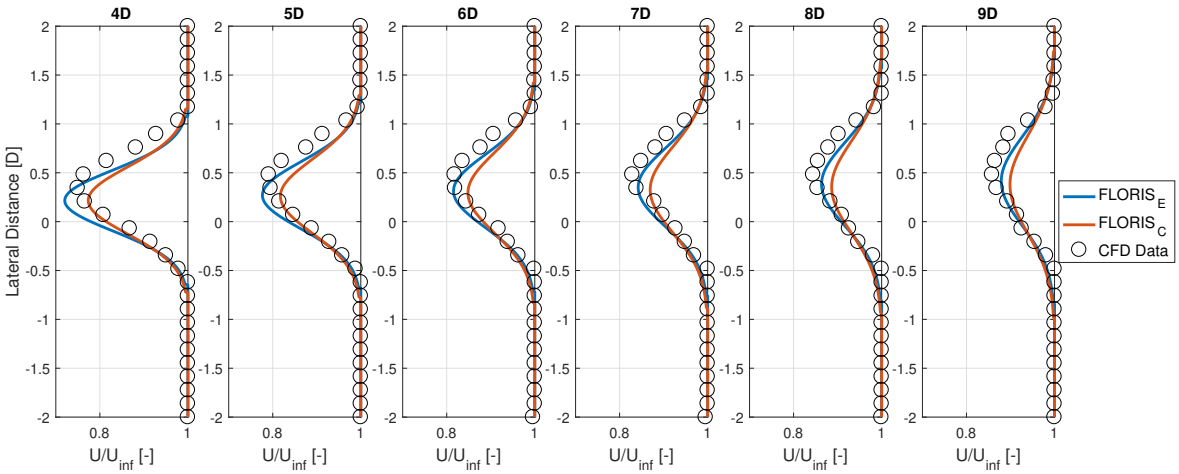

Figure 65. Porté-Agel flow velocity predictions and CFD data for high-TI, $\gamma = -30°$

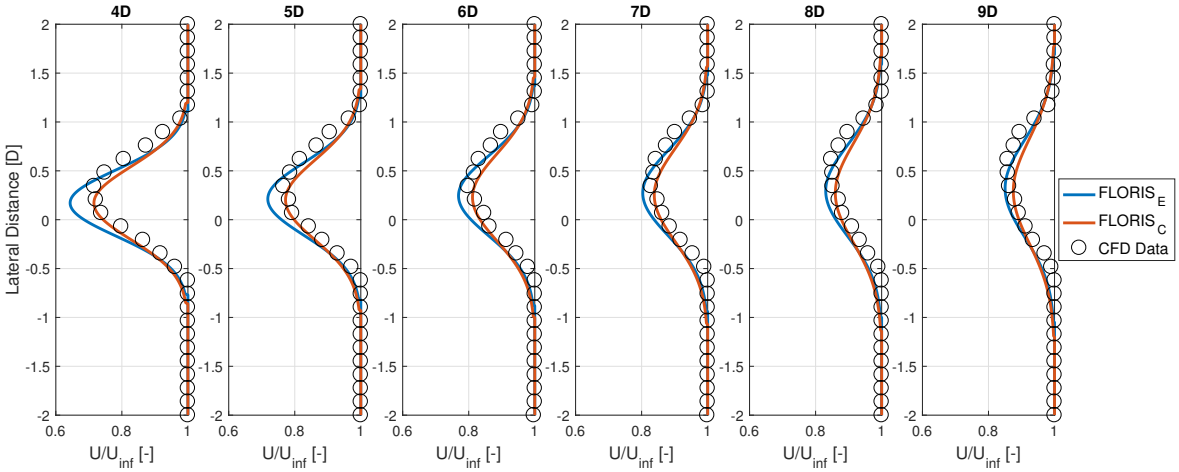

Figure 66. Porté-Agel flow velocity predictions and CFD data for high-TI, $\gamma = -20°$

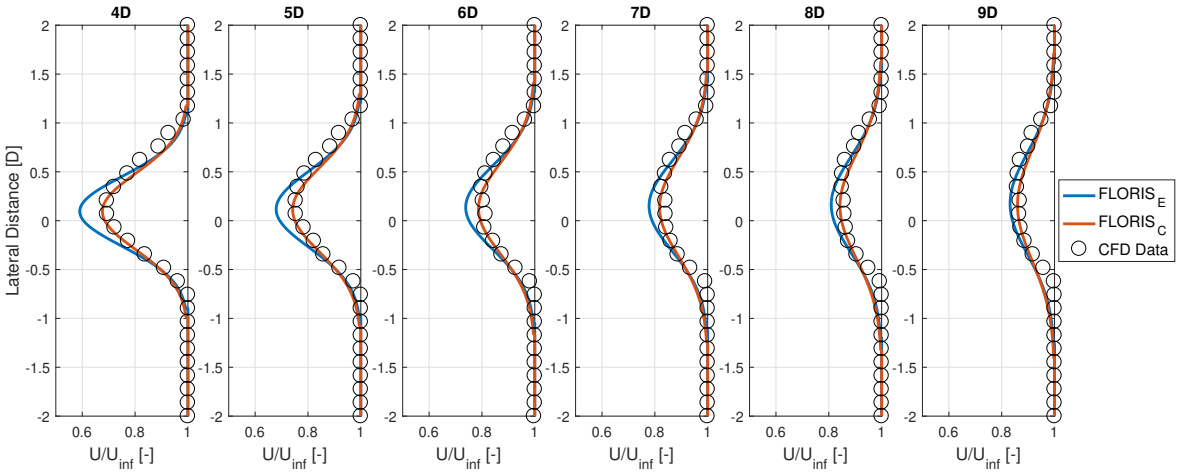

Figure 67. Porté-Agel flow velocity predictions and CFD data for high-TI, $\gamma = -10°$

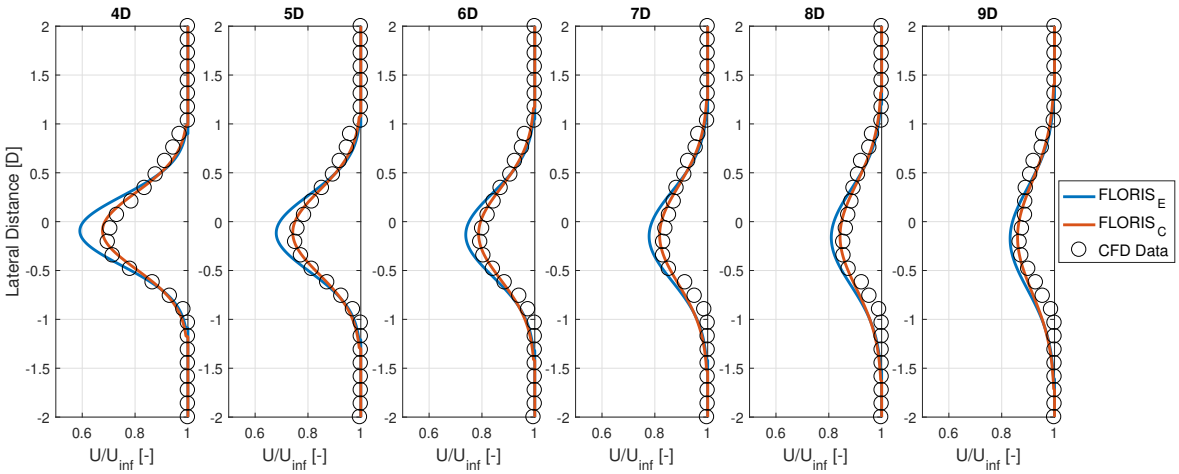

Figure 68. Porté-Agel flow velocity predictions and CFD data for high-TI, $\gamma = 10°$

6.3.5 Comparison between CFD and FLORIS-predicted turbulence intensity.

Table 15 reports the output of the tuning process for the parameters of the turbulence intensity sub-model.

Table 15. Parameters of the Porté-Agel turbulence sub-model after calibration.

Turbulence Intensity			
TI_a	TI_b	TI_c	TI_d
0.7703	0.7659	−0.1191	−0.7083

The FLORIS flow model predictions with tuned parameters, as well as the CFD data, are shown in Fig. 69-81 separately for each wind turbine operating condition, with the turbulence intensity reported on the x-axis as function of the lateral distance from the rotor center.

The turbulence intensity sub-model of Porté-Agel model delivers quite satisfactory results after parametrization for the high-TI inflow cases, while for the mid-TI inflow cases, the Porté-Agel model seems to under estimate the turbulence intensity, specially for downwind distances close to the rotor disk.

The overall results can be assumed to be quite satisfactory, considering the capability of the turbulence intensity model as well as that, differently from the wake velocity model, the impact of mismatches on the predictions of turbulence intensity is pretty moderate. Indeed, a mismatch on the prediction of the turbulence intensity in the wake is weighted by the factor k_a when it comes to the computation of the rate of decay for the wake shed by the immediately downstream wind turbine. However, there is definitely space for improvement and other turbulence intensity sub-models should be considered.

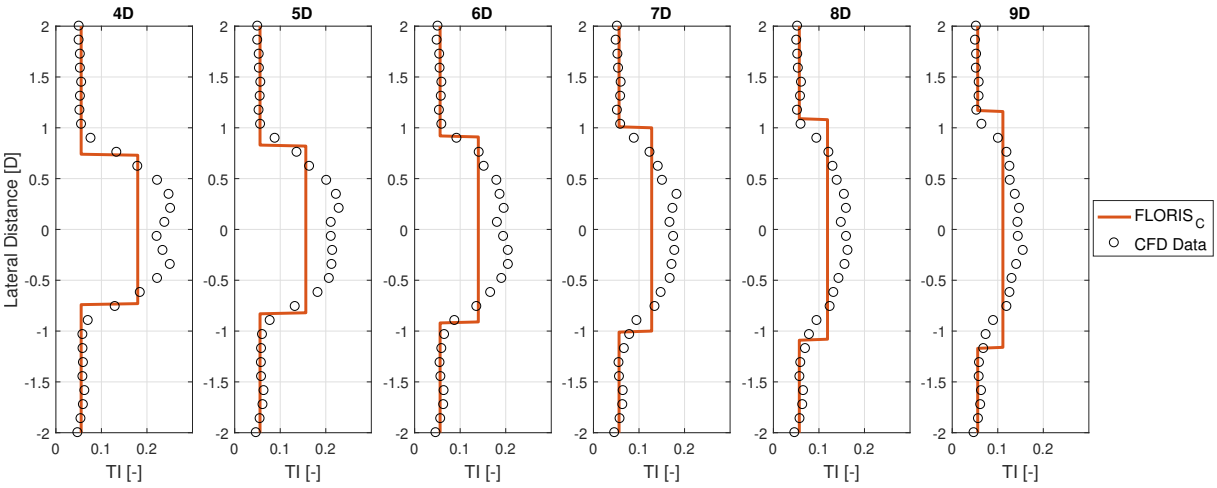

Figure 69. Porté-Agel turbulence intensity predictions and CFD data for mid-TI, $\gamma = 0°$, $C_T = 0.902$.

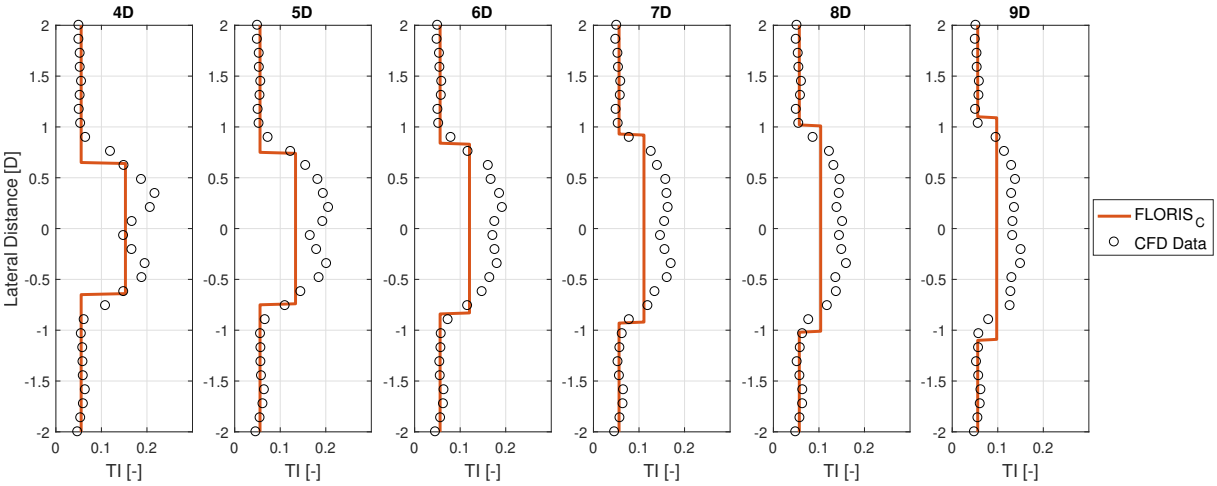

Figure 70. Porté-Agel turbulence intensity predictions and CFD data for mid-TI, $\gamma = 0°$, $C_T = 0.789$.

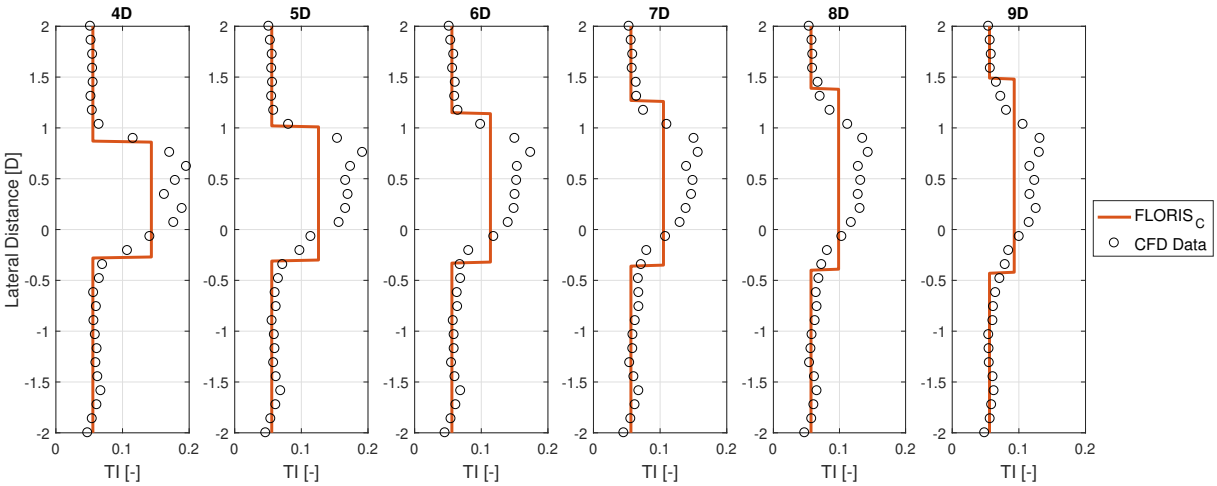

Figure 71. Porté-Agel turbulence intensity predictions and CFD data for mid-TI, $\gamma = -30°$

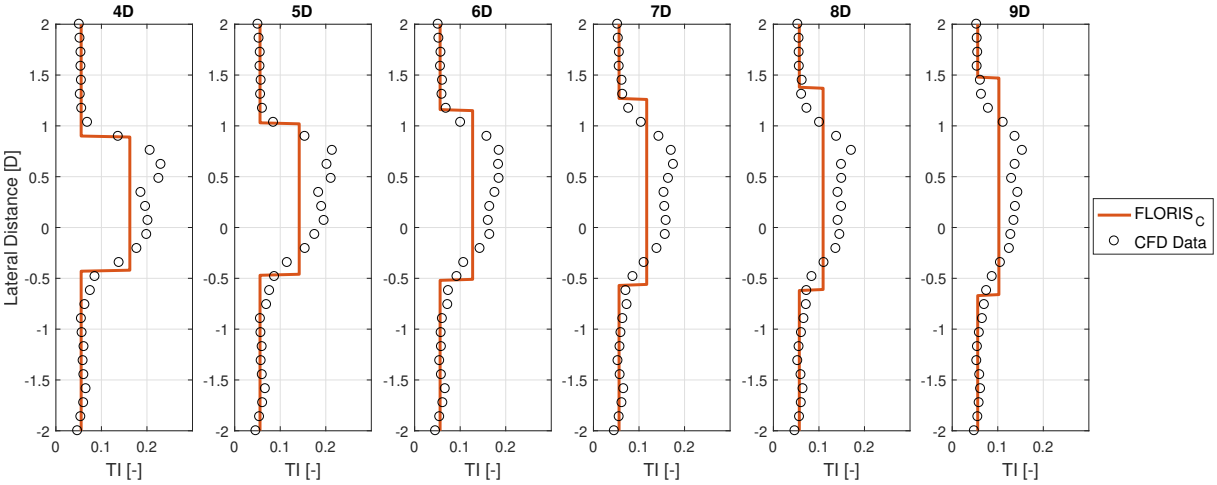

Figure 72. Porté-Agel turbulence intensity predictions and CFD data for mid-TI, $\gamma = -20°$

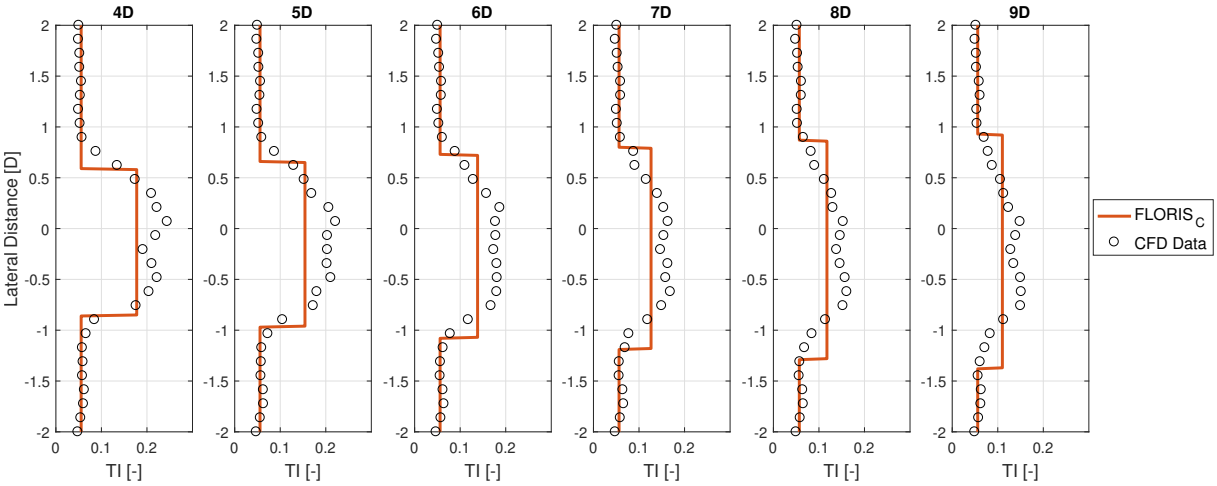

Figure 73. Porté-Agel turbulence intensity predictions and CFD data for mid-TI, $\gamma = 10°$

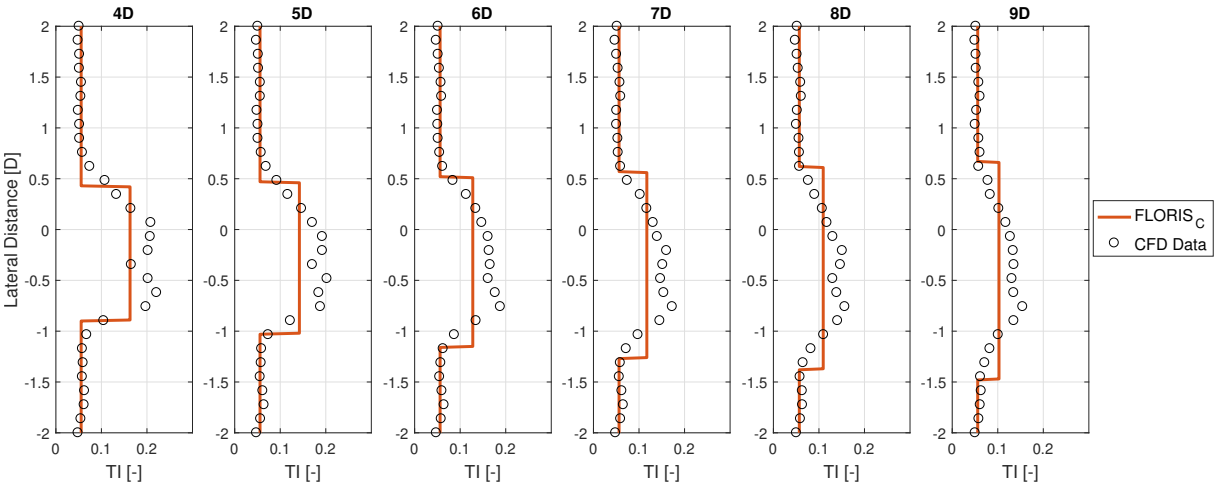

Figure 74. Porté-Agel turbulence intensity predictions and CFD data for mid-TI, $\gamma = 20°$

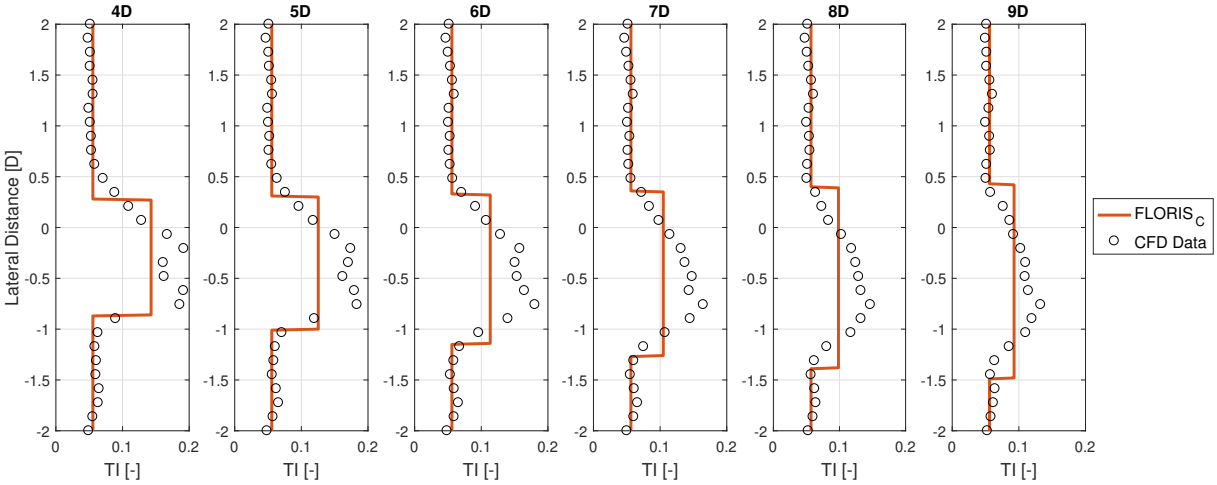

Figure 75. Porté-Agel turbulence intensity predictions and CFD data for mid-TI, $\gamma = 30°$

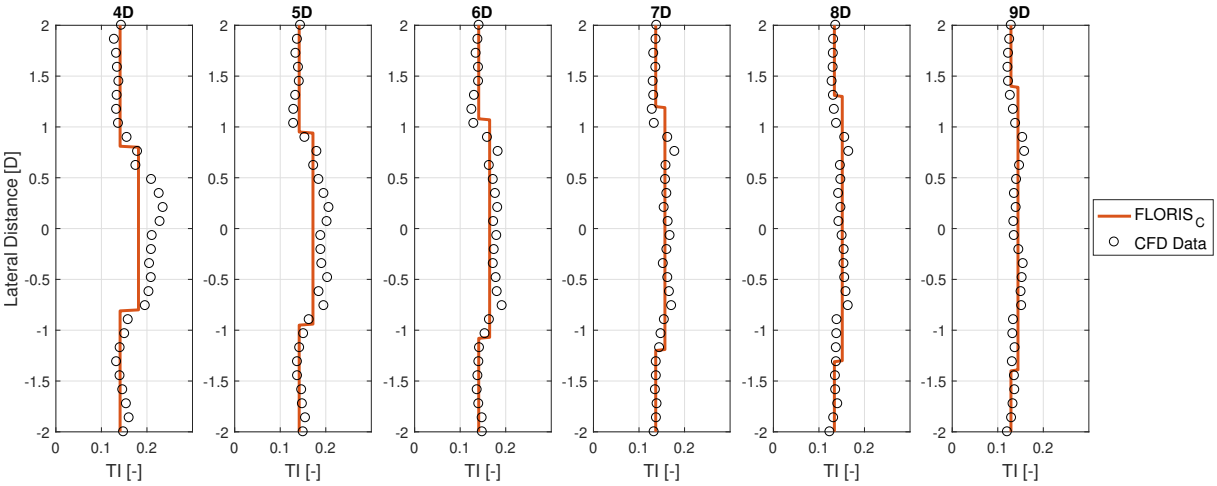

Figure 76. Porté-Agel turbulence intensity predictions and CFD data for high-TI, $\gamma = 0°$, $C_T = 0.718$.

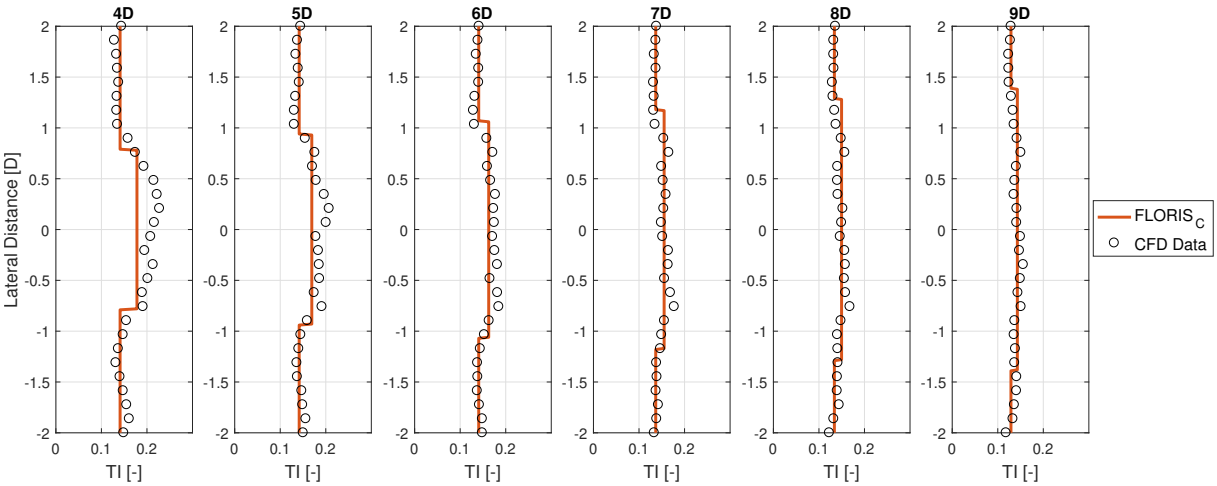

Figure 77. Porté-Agel turbulence intensity predictions and CFD data for high-TI, $\gamma = 0°$, $C_T = 0.686$.

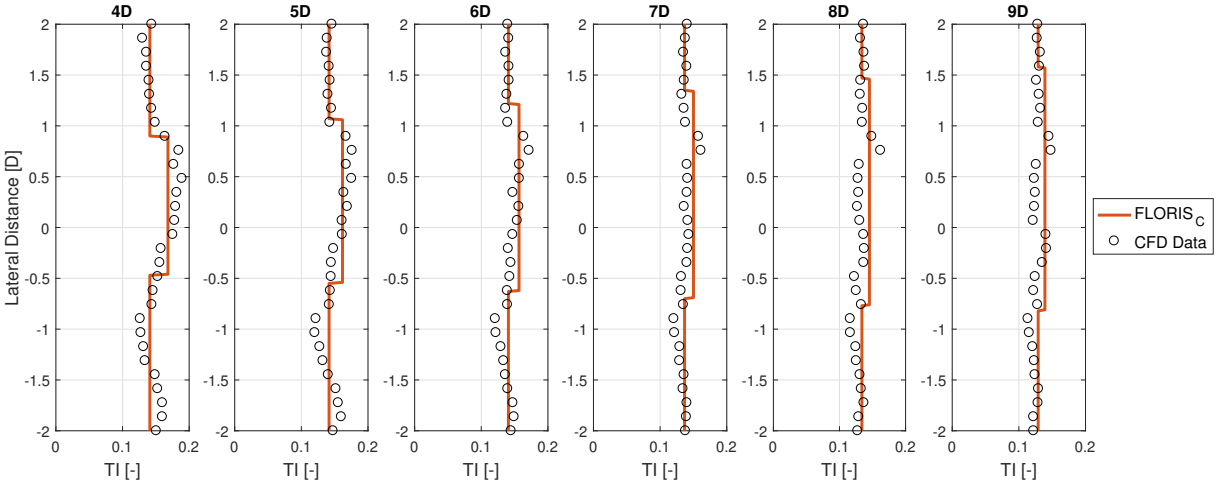

Figure 78. Porté-Agel turbulence intensity predictions and CFD data for high-TI, $\gamma = -30°$.

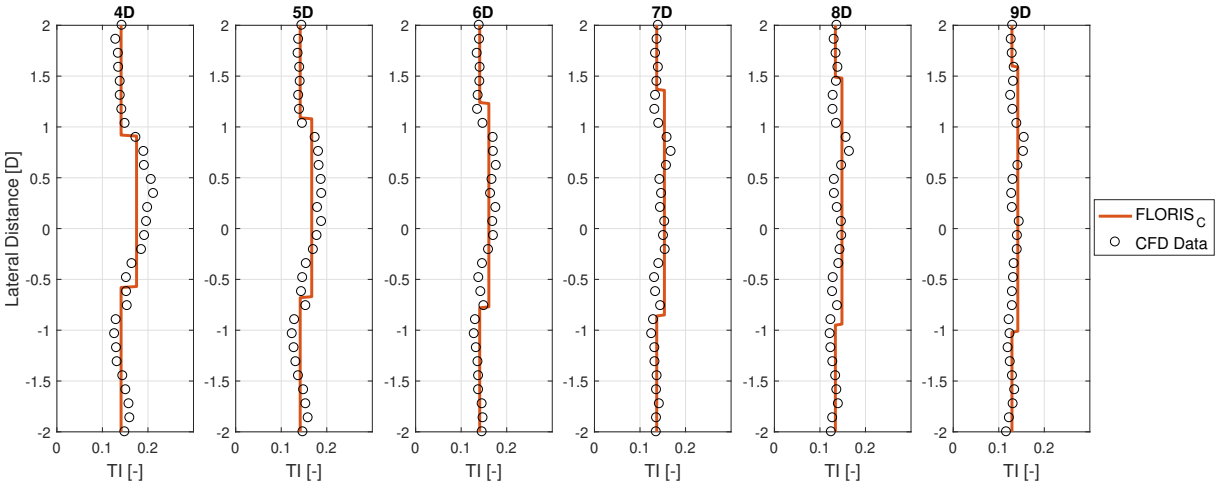

Figure 79. Porté-Agel turbulence intensity predictions and CFD data for high-TI, $\gamma = -20°$.

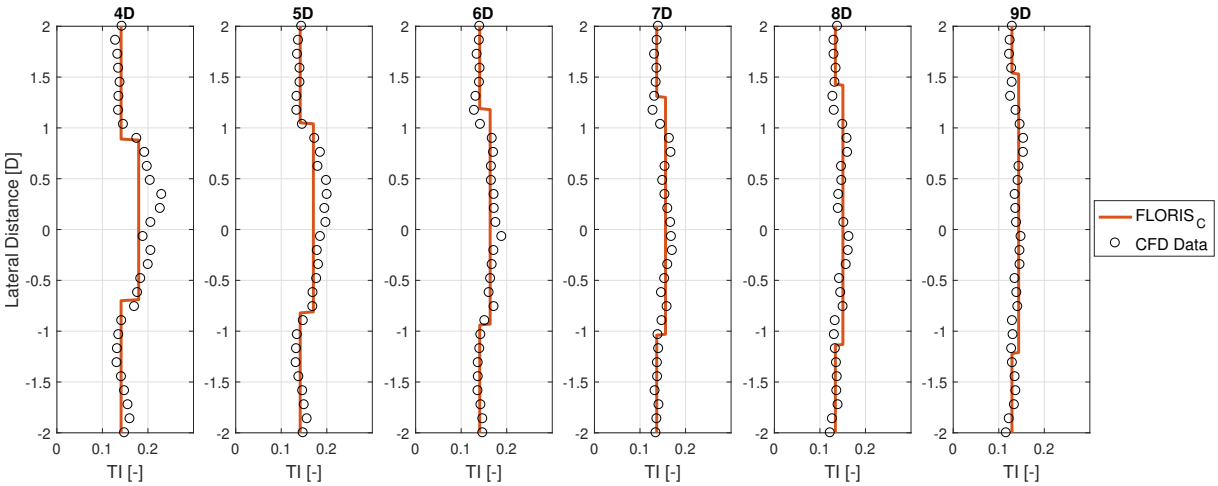

Figure 80. Porté-Agel turbulence intensity predictions and CFD data for high-TI, $\gamma = -10°$.

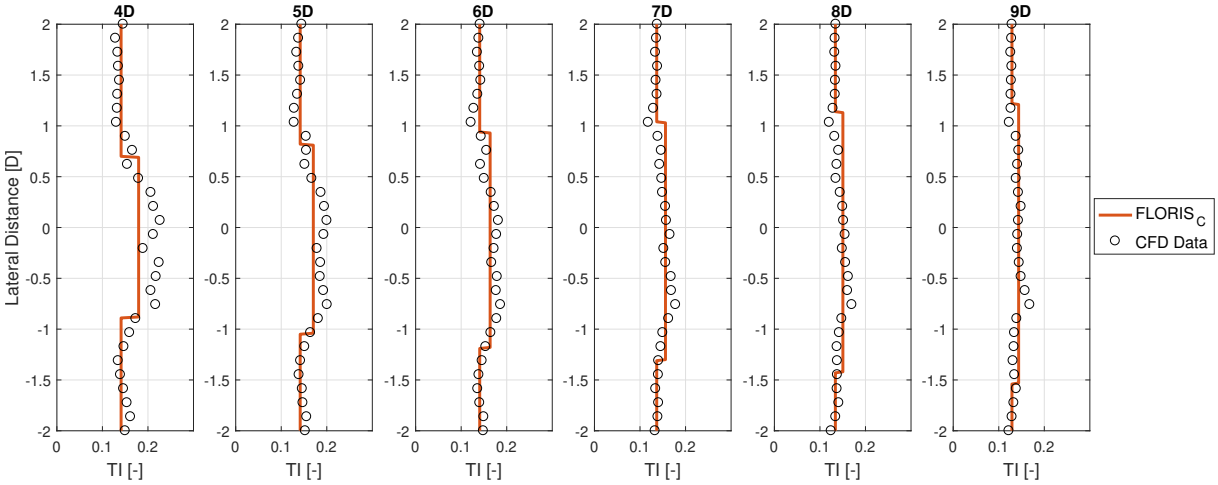

Figure 81. Porté-Agel turbulence intensity predictions and CFD data for high-TI, $\gamma = 10°$.

6.4 Conclusions

In this chapter, a comprehensive comparison between state-of-the-art CFD simulations and FLORIS is given. In details, the comparison aims at assessing the capability of the FLORIS model in predicting the velocity deficit, deflection and turbulence intensity of the wake shed by a scaled wind turbine model conceived for wind tunnel testing. After properly tuning the governing parameters of the considered wind farm model, the comparison highlights that the FLORIS model predictions of the wake velocity deficit and wake deflection are very accurate and well match the CFD outputs, specially for yaw misalignment within the range -20° and 20°. The prediction of the turbulence intensity within the wake, despite satisfactory, could instead be improved, specially in the case of moderate inflow turbulence intensities.

7 VALIDATION OF A MODEL BASED ON DATA REDUCTION TECHNIQUES

7.1 Introduction

The models based on data-reduction techniques developed at TUM are reduced-order models (ROMs) intended to support the design of wind farm control algorithms which require low computational costs to be real-time executed. The governing equations of these models, as well as the numerical procedures required for their synthesis, are given in deliverable D1.2. In the following, a comparison between high-fidelity CFD-SOWFA simulations and predictions obtained using the developed ROMs is given. The comparison also highlights the improvements obtained by embedding in the ROMs state observers, based on Kalman filters, that feeds the model with both wind turbines power and the output of observers of the sectors effective wind speed (SEWSs), described in Deliverable 2.2 and implemented within the CFD framework. Additionally, the ROMs output are compared to wind tunnel experiments, including the capability of the model to partially correct for an intentionally built-in model mismatch.

In order to marry the contrasting requirements of high-fidelity and low computational cost, in Deliverable 1.2 it has been proposed an approach that is based on the idea of compressing high-fidelity CFD data into a reduced-order model (ROM). This is obtained through a data-driven model-identification procedure, based on the proper orthogonal decomposition (POD). The resulting ROMs capture the dominant dynamics of wind turbine wakes and their interactions, while showing at the same time a high degree of data compression. This way, the computationally intensive part of the process is performed offline and, once a ROM has been identified, one is left with a small size state-space model that is ideally suited for the design of model-based control laws. The models are able to predict the deflection experienced by the wake shed by a wind turbine that is rotated out of the wind, as well as the impact that such a technique has on the performance of downstream wind turbines. The implementation of these models requires the availability of detailed flow data, obtained by means of CFD simulations performed with SOWFA (high-fidelity large-eddy simulation tool), as well as several ROMs should be derived, i.e. one for any specific configurations (wind farm layout, wind speed, TI), to enable their use in a real wind farm. However, the use of state observers can enable a strong reduction of the number of required ROMs, as highlighted in the next pages.

7.2 Validation of ROMs with respect to CFD data

The model-compression procedure discussed in Deliverable 1.2 was applied to raw CFD data in order to obtain the desired ROM. To this end, an APRBS signal was designed to excite the system by changing the upwind turbine yaw angle. The length of the training simulation was set to 60 s, which was considered long enough to appropriately excite the system within the range of ± 30 deg, while limiting the computational costs. Then, the procedure explained in Deliverable 1.2 was applied, resulting

in a ROM with 22 POD modes. The order of the model was chosen as a best compromise between model size and error between high-fidelity and reduced-order-reconstructed ow and power outputs.

Subsequently, a second CFD simulation was performed with a different input signal to validate the prediction capabilities of the previously obtained ROM. The ROM was verified for this validation test case in three different variants: in open loop, in conjunction with a Kalman filter (KF) state observer (Kalman, 1960), which uses the power of the wind turbines to estimate and update the model state vector, and in conjunction with a KF state observer which uses the power of the wind turbines and the output of observers of the sectors effective wind speed (SEWSs).

The three comparisons mentioned before can be summarized in short as follows:

- Open Loop
- KF with power outputs
- KF with power outputs + SEWSs

In the following figures, comparison involving Open Loop ROMs (i) will be noted as “w/o KF”, comparisons with ROMs equipped with a KF which feeds power measurements (ii) will be noted as “KF-p”, and comparisons with ROMs equipped with a KF which feeds power and SEWSs measurements (iii) will be noted as “KF-p,sews”.

The process noise covariance matrix of the KF (Qk) was tuned by differently weighting each element of the reduced-order state, i.e. each POD mode. Specifically, modes with higher energies and better resolution (low frequency spectra) were assigned smaller covariances. The measurement noise covariance matrix Rk was set to a low value, since the measured data can be assumed to be highly accurate.

The comparison is done between the CFD and ROM wind turbine powers, SEWSs outputs and flow mapping at hub height for some specific time instants. The SEWSs consist in an estimation, based on the shaft loads, of the stream-wise velocities experienced by four sectors of the rotor disk, shown in Figure 82. The number of sectors and their position is in principle arbitrary, but the wind speeds sensed by this four sectors are useful to infer specific wind features. Indeed, sector 1 (S1) and sector 3 (S3) stream-wise velocities could be used to provide knowledge about the wake position, while sector 2 (S2) and sector 3 (S3) could be used to provide knowledge about the wind shear. More details about this approach and its validation can be found in deliverable D2.2 and D3.3, as well as in [8].

7.2.1 Simulation environment

Simulations were run here using a simulation tool based on SOWFA [9], which is a lifting-line-based large-eddy simulation (LES) tool developed at the National Renewable Energy Laboratory (NREL), using OpenFOAM and coupled with NREL’s FAST wind turbine structural-dynamics model [20]. The implementation used here features an immersed boundary formulation [28] to model the effects

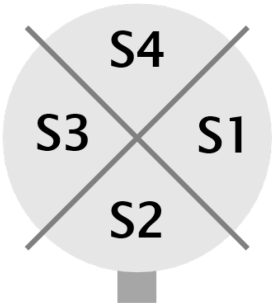

Figure 82. Rotor disk partitioned into four sectors or quadrants (S1, S2, S3, and S4) as defined by the SEWS wake observer.

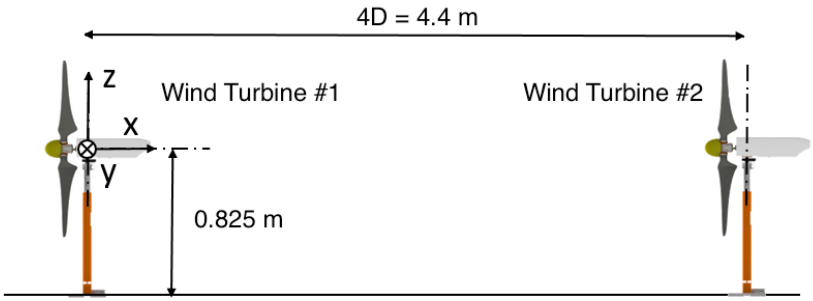

Figure 83. Wind farm layout. Two-turbine cluster aligned with the incoming wind.

of nacelle and tower, which may have a significant influence on wake development and behavior. Typical simulations last for several days, and were run on the 'SuperMUC' cluster of the Leibniz Supercomputing Centre (LRZ, Germany). The simulations considered here reproduce experiments conducted in the boundary layer wind tunnel of the Politecnico di Milano in Italy, using the G1 (Generic 1m diameter rotor) scaled wind turbine models described in Deliverable 3.1. The LES-CFD environment was validated with respect to experimental data in previous studies [35]. The simulation setup considers a two-turbine cluster, shown in Figure 83, where the machines are longitudinally spaced at a distance of 4D and aligned with the prevailing wind flow direction. The free stream flow has an average speed of 5.7 m/s with a turbulence intensity (TI) of about 6% at hub height. Simulations were run with a time step of 0.0004 s and data was collected in snapshots sampled every 0.01 s (snapshot frequency of 100 Hz). The stored data includes the power and SEWSs output of both wind turbines, the prescribed upwind turbine yaw control input, and the three velocity components recorded at all grid points on two planes: the first one is a horizontal plane at hub height (termed XY), while the second is a vertical plane going through the center of the two turbine towers (termed XZ). Clearly, although data was collected only at these two planes, simulations consider the full 3D computational domain. A finer mesh was used closer to the turbines and in their wakes, while a coarser one was used elsewhere to reduce computational cost.

7.2.2 Comparisons ROM - CFD SOWFA simulation

A comparison of the power outputs of the validation case CFD simulation and ROM reconstruction is shown in Figure 84. The power variations of both turbines predicted by the model is given directly in the model output vector. The use of the Kalman filter - which feeds power measurements from the plant back to the ROM - improves the quality of predictions. Indeed, the time-averaged percentage error between CFD and ROM-predicted power outputs reduced from 3.83%, 6.68% and 3.64% for the open loop case, to 1.81%, 3.98% and 1.89% for the case with KF-p, where the three values refer to the upstream turbine (WT1), the downstream one (WT2) and the whole cluster, respectively. In open-loop, the model does not receive any information from the plant regarding power changes due to flow fluctuations. This appears clearly in the figure where, for constant yaw angles, the model cannot accurately predict the fluctuating behavior of power other than the intrinsic dynamics contained in the ROM. However, the use of KF-p,sews, i.e. the Kalman filter which feeds power measurements and SEWSs output from the plant back to the ROM, does not provide major specific benefits in terms of quality of power predictions.

However, major improvements can be observed by looking at Figure 85 and Figure 86, which report comparison of the SEWSs outputs, for the downstream wind turbine, of the validation case CFD simulation and ROM reconstruction. The use of the KF-p,sews, indeed, improves the quality of predictions not only with respect to the open-loop case, but also with respect to the case with KF-p. In this last case, indeed, the model does not receive any information from the plant regarding the flow fluctuations along the horizontal and vertical directions, meanly due to the meandering of the wake shed by the upstream wind turbine. This appears clearly in the figure where, even for the case with KF-p and for constant yaw angles, the model cannot accurately predict the fluctuating behavior of the speed experienced by the several sectors other than the intrinsic dynamics contained in the ROM.

The reconstructed full-order flow produced by the ROM can be approximated as explained in Deliverable 1.2. A comparison between CFD high-fidelity data and ROM-based reconstructed flow is shown in Figure 87 and Figure 88 for a given instant in time. ROM predictions, with and without state observer, match the average wake shape and position. On the other hand, smaller scale fluctuations and wake meandering are not captured. Notice further that the Kalman filter is capable of enhancing the behavior of the model in terms of power predictions, without visually substantially affecting the macroscopic flow behavior in the wake.

7.3 Validation of ROMs with respect to wind tunnel experiments

The same ROM validated with respect to CFD data was also tested with data from a wind tunnel experiment that made use of two G1 models, under very similar conditions in terms of yaw dynamic changes, inflow speed and turbulent intensity of the numerical test conducted so far. However, crucially, in the wind tunnel experiments two different setup were tested: one with the two aligned

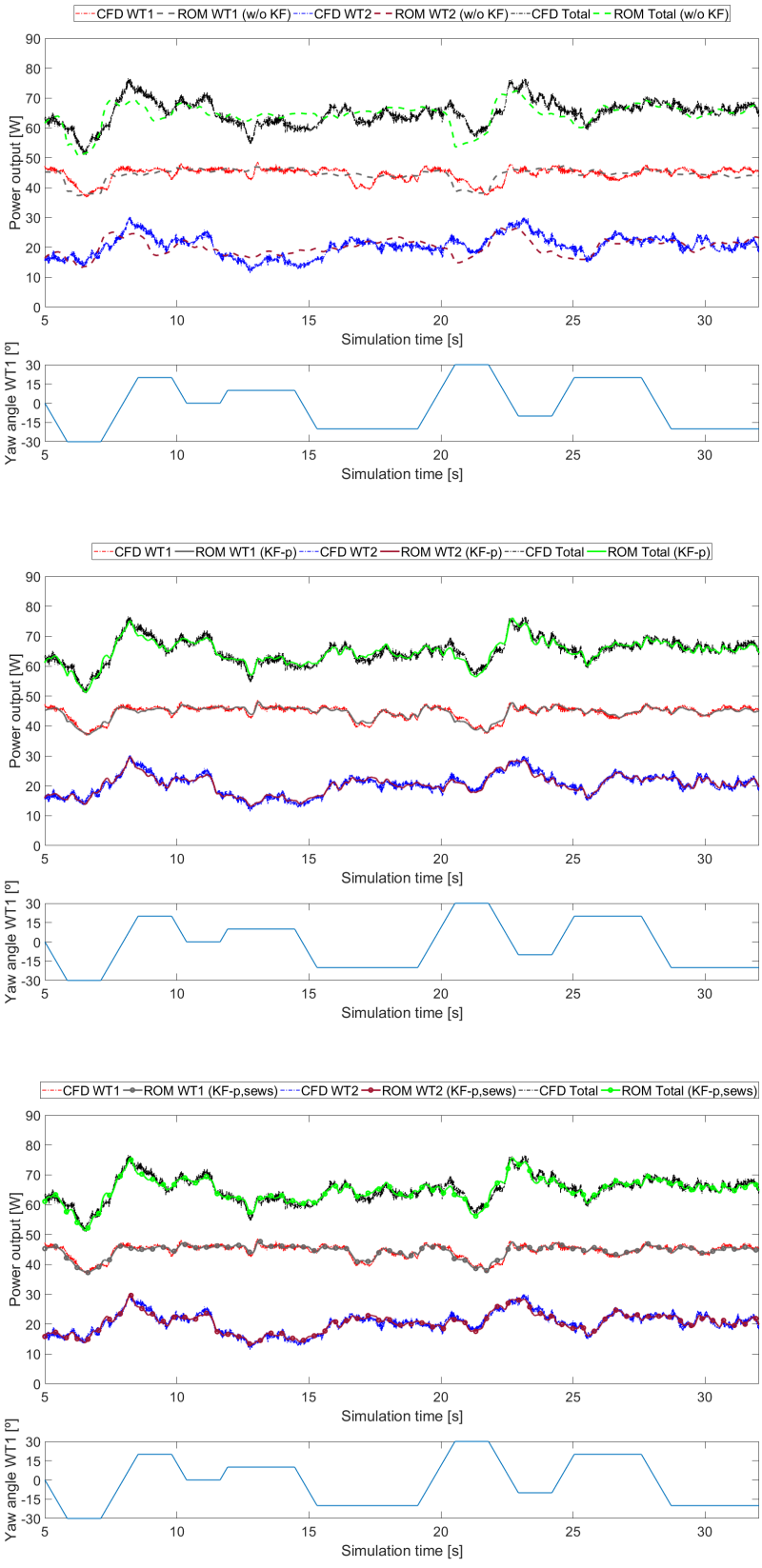

Figure 84. Comparison between ROM-reconstructed and CFD-obtained power outputs

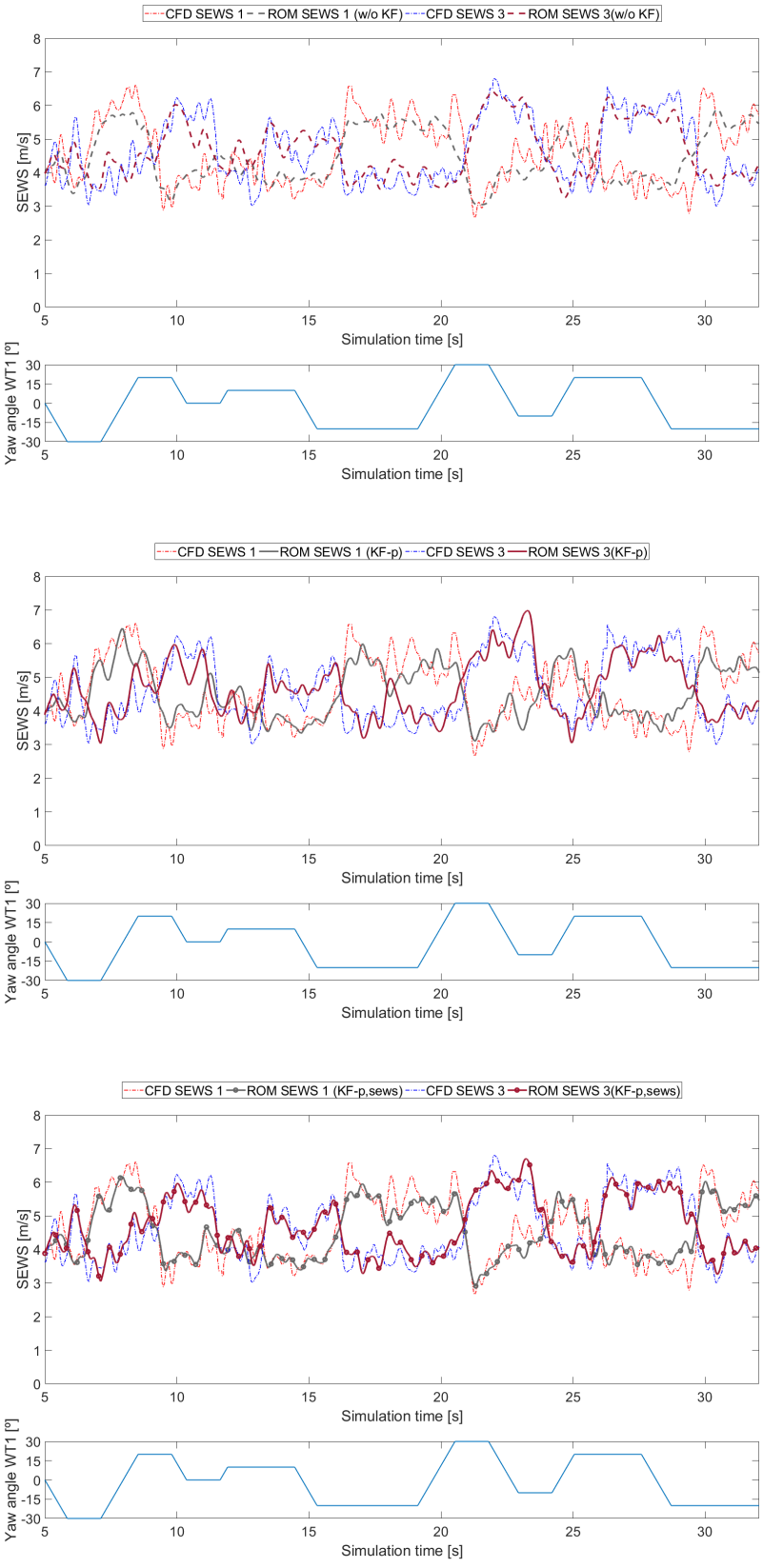

Figure 85. Comparison between the SEWSs output of ROM and CFD for the S1 and S3 sectors of WT2

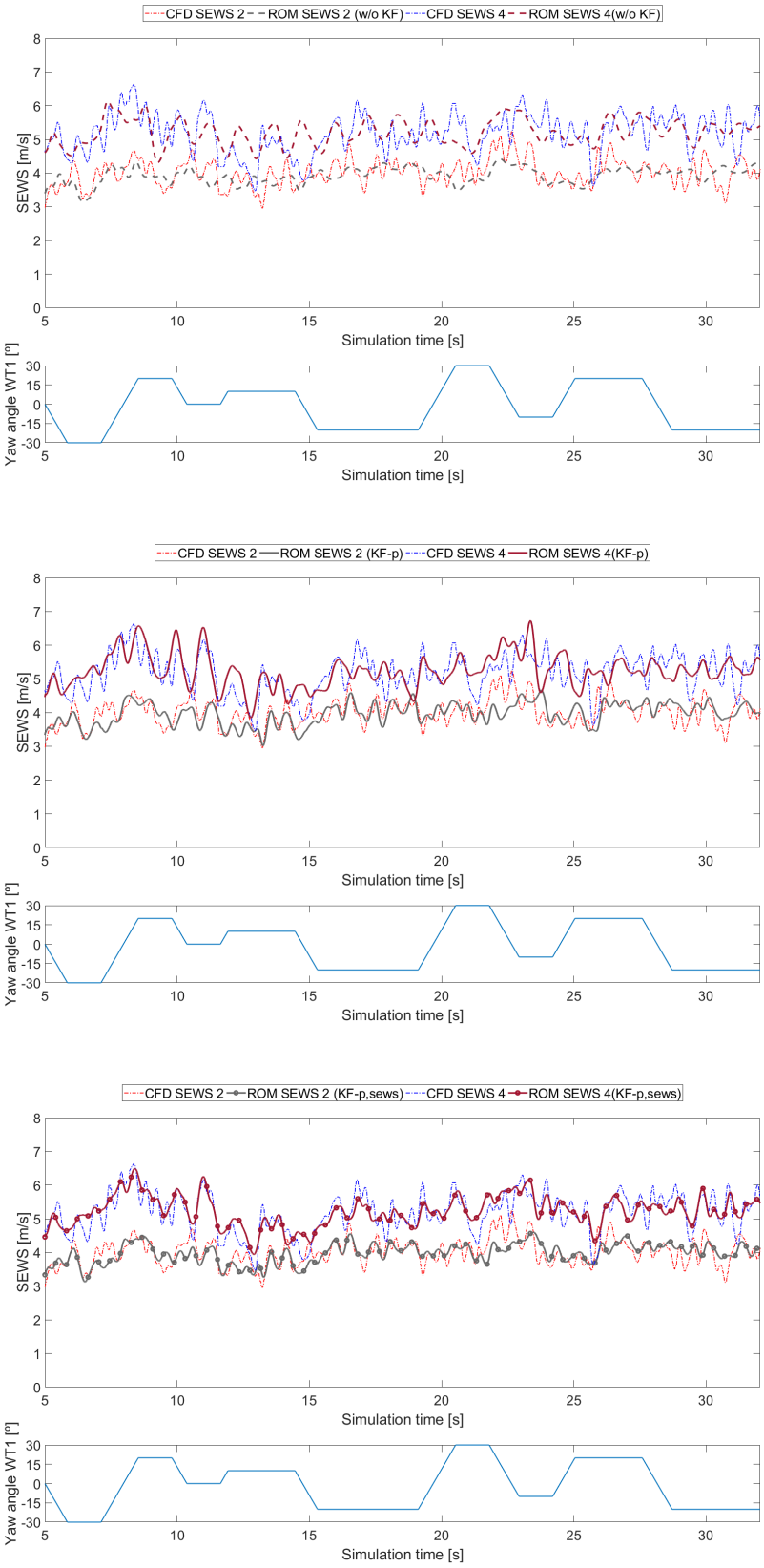

Figure 86. Comparison between the SEWSs output of ROM and CFD for the S2 and S4 sectors of WT2

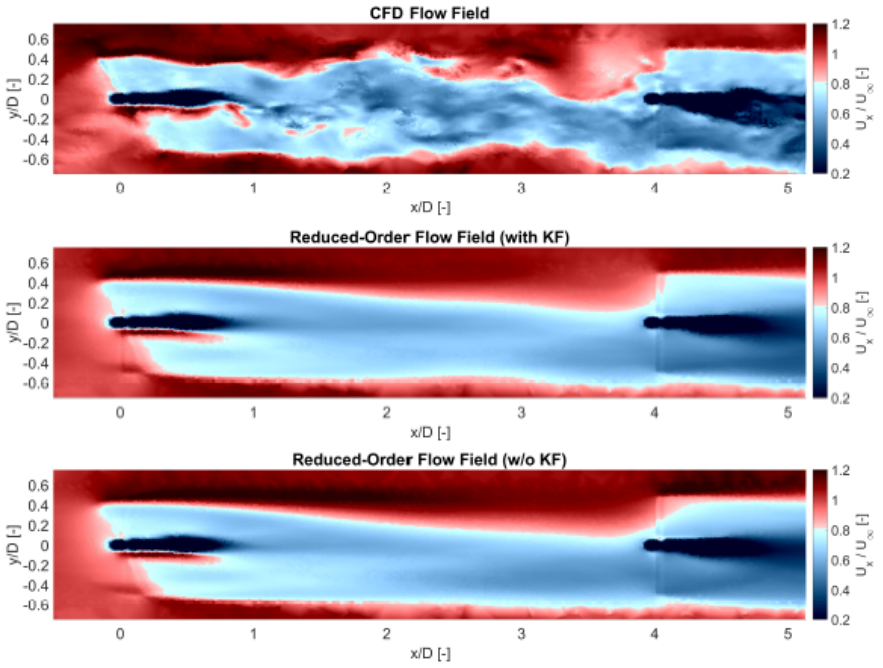

Figure 87. Comparison of the stream-wise velocity component on the horizontal plane between the CFD flow (top), ROM-predicted flow with KF-p state observer (middle), and ROM-predicted flow without state observer (bottom) at one instant in time (γ = 23 deg)

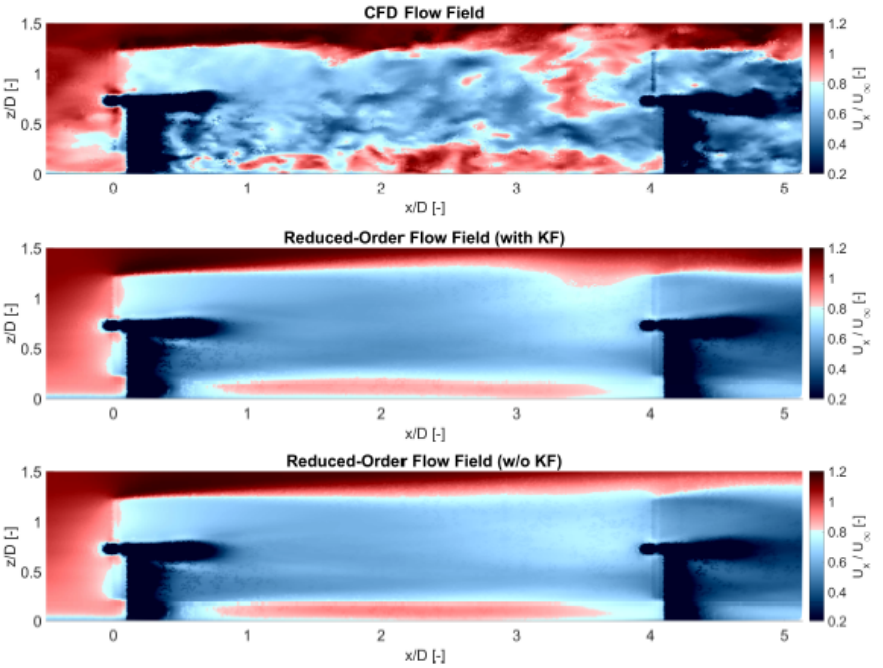

Figure 88. Comparison of the stream-wise velocity component on the vertical plane between the CFD flow (top), ROM-predicted flow with KF-p state observer (middle), and ROM-predicted flow without state observer (bottom) at one instant in time ($gamma$ = 23 deg)

ROM - Wind tunnel (case 0D lateral displacement) ROM - Wind tunnel (case +0.2D lateral displacement)	Open Loop KF with power outputs KF with power outputs + SEWSs

Table 16. Cases used for comparisons with wind tunnel experiments

turbines spaced 4D and another with the two turbines longitudinally spaced 4D as well as laterally spaced 0.2D, while the simulations used to generate the ROM used aligned wind turbines. In other words, the ROM was created on purpose with a significant built-in model mismatch. The cases compared are therefore the ones indicated in Table 16, which also reports the type of comparison that were performed for both cases: i.e. between exp. data and ROM in open loop, in conjunction with a KF state observer which uses the power of the wind turbines and in conjunction with a KF state observer which uses the power of the wind turbines and the output of observers of the sectors effective wind speed (SEWSs).

As mentioned before, the objective of performing a comparison between ROM and wind tunnel for these cases is to test the capability of the model to still accurately predict the desired outputs assuming that modeling errors are present, thus providing valid indications concerning the possibility of using the model for controlling a real wind farm, whose operating conditions, like TI and wind direction, are constantly changing and could therefore be quite different from the ones used to derive the ROM. For instance, the second case allows to address the performance of the ROM in case of a built-in model mismatch in the layout associated to a different wind direction.

The ROM predictions are first compared with the experimental data and for the case with aligned turbines in terms of turbine power outputs. The comparison, shown in Figure 89, highlights that, when the upstream wind turbine is yawed of ± 30 deg, the predicted power for the downwind wind turbine is generally lower than the actual one, while the predicted power of the upstream wind turbine is generally higher than the measured one, thus enhancing a model-plant mismatch for high yaw misalignments. The KF is able to correct for this model defect, no matter if only the turbines power is fed to the model or if both powers and SEWSs output are. However, the comparison between the SEWSs output of WT2 for the same case, shown in Figure 90, indicates that the sole use of the KF-p state observer would lead to an improper estimation of the flow field. Indeed, the plots in the figure show that the ROM with KF-p over predicts the speed sensed by the left sector (S3) and underestimates the speed sensed by the right sector (S1), thus resulting in a modeled wake, shed by the upstream wind, that is not representative of the reality. The use of the KF-p,sews state observer, instead, leads to a much proper estimation of the flow field.

The results shown in Figure 91 and Figure 92, related to the case with laterally shifted wind turbines, highlight even more the importance of the use of state observer in order to compensate for eventual plant-model mismatch.

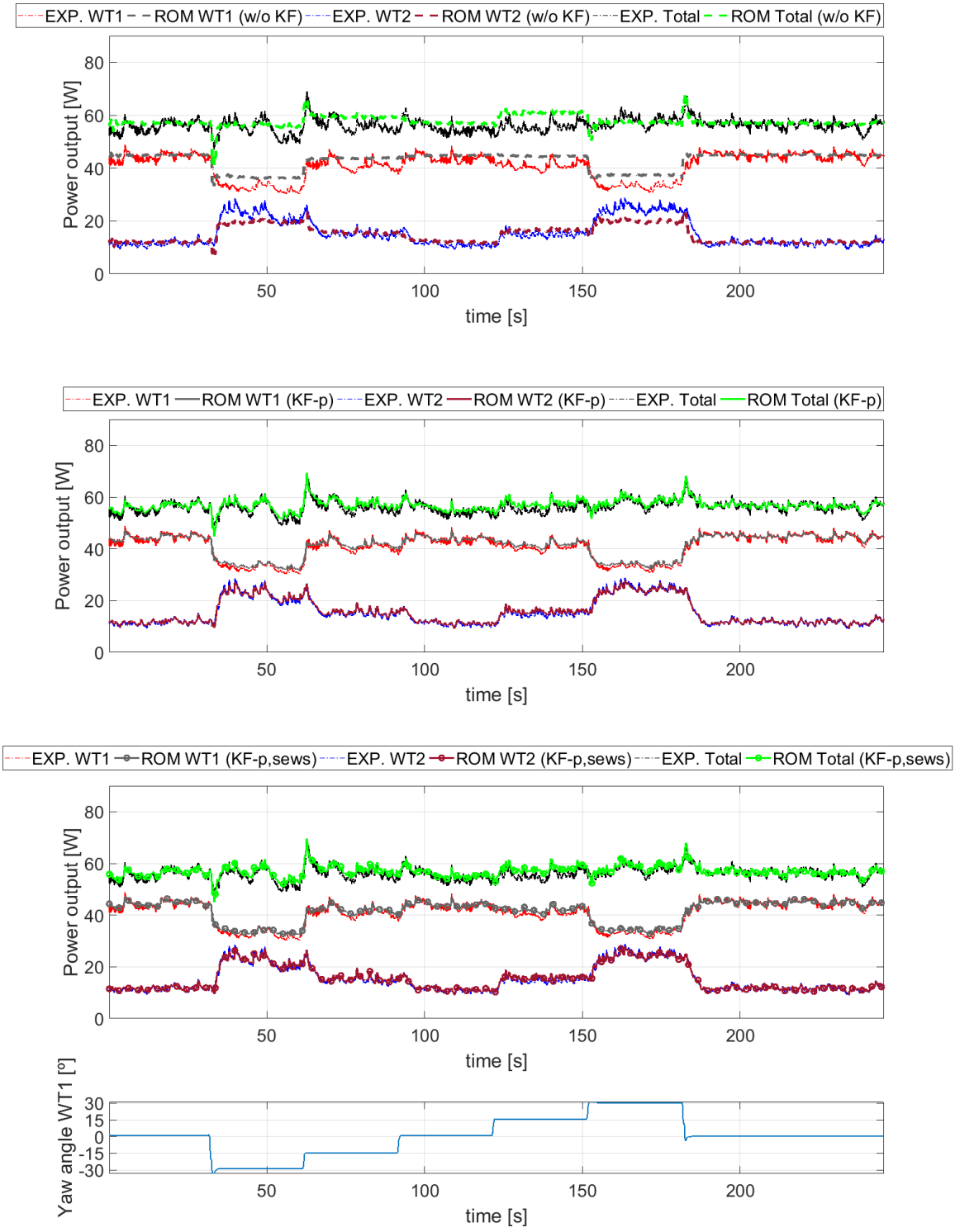

Figure 89. Case with aligned wind turbines: comparison between ROM and Wind tunnel (EXP.) power outputs.

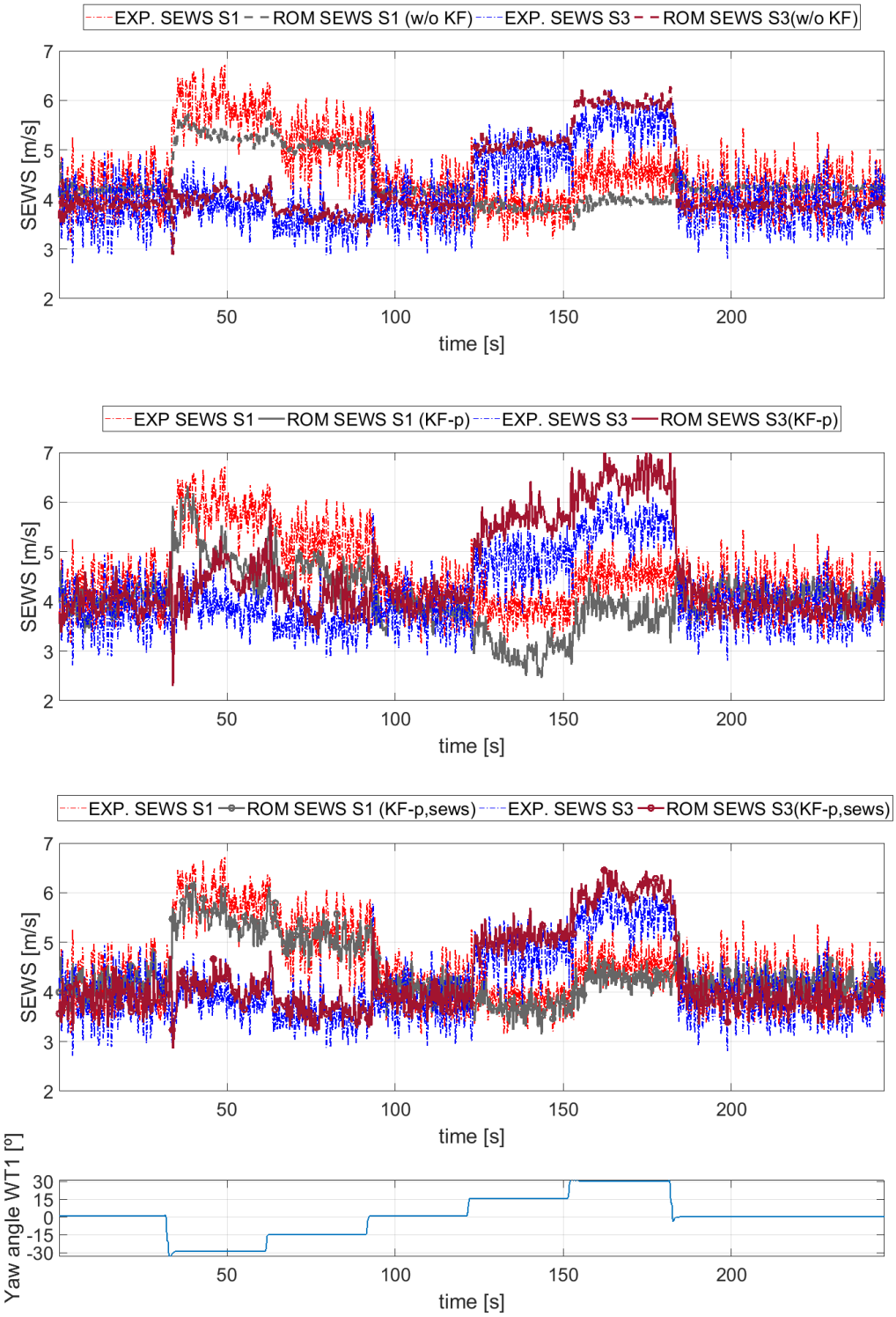

Figure 90. Case with aligned wind turbines: comparison between the SEWSs output of ROM and Wind tunnel (EXP.) for the S1 and S3 sectors of WT2

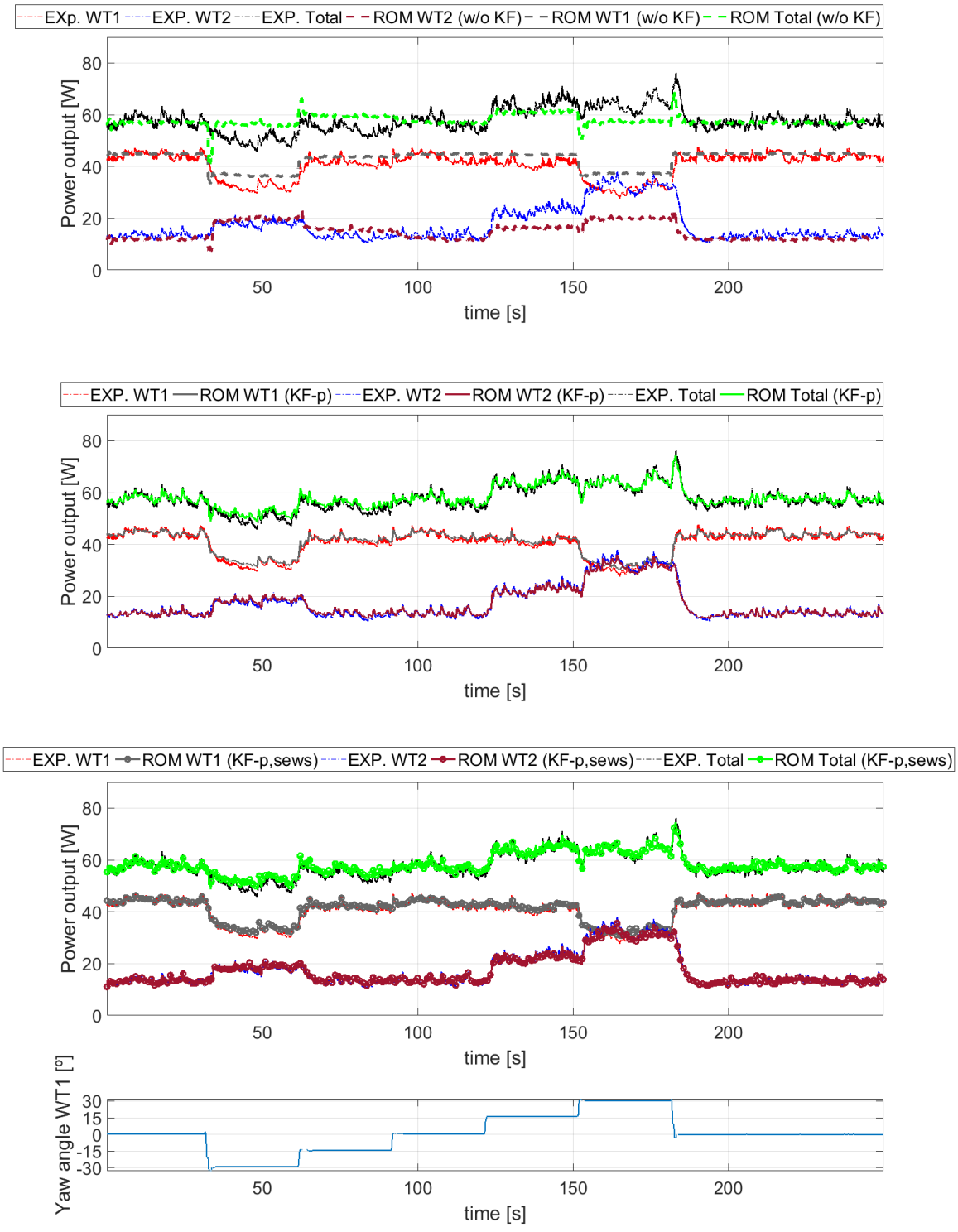

Figure 91. Case with laterally displaced wind turbines: comparison between ROM and Wind tunnel (EXP.) power outputs.

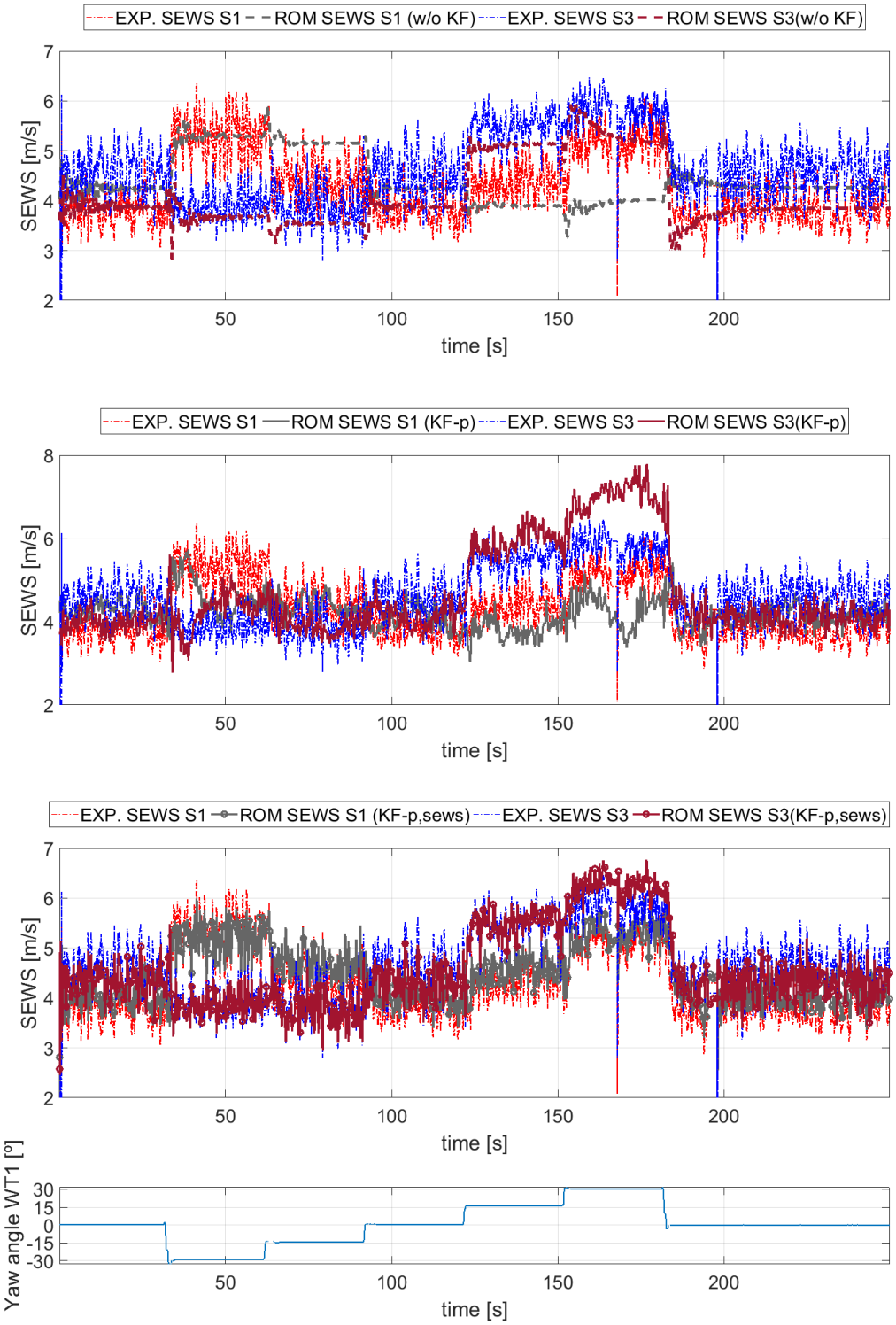

Figure 92. Case with laterally displaced wind turbines: comparison between the SEWSs output of ROM and Wind tunnel (EXP.) for the S1 and S3 sectors of WT2

7.4 Conclusions

In this chapter, a reduced-order model based on data reduction techniques is compared to CFD and wind tunnel data, with the goal of assessing if it could support the development of model-based wind farm control strategies that could be real-time executed at low computational cost.

The present study has focused on a two-turbine cluster, where yaw misalignment of the front machine is used for wake steering. To further improve the quality of predictions, the resulting ROM has been optionally equipped with a KF, which feeds power and sector effective wind speed measurements from the plant back onto the model. Results indicate that the proposed method is able to represent well, when compared to high-fidelity CFD-simulated data, the wake characteristics of both turbines and their respective power outputs. Regarding flow predictions, a proper deflection and development of the wake is observed. With respect to power outputs, the predictions are also accurate and correlate well with changes in the upwind turbine yaw angle. When compared to wind tunnel experiments, acceptable results are also obtained, including the capability of the model to partially correct for an intentionally built-in model mismatch.

Additional work will try to improve the generality of the approach. In fact, since the method is based on system identification, ROMs are derived for a particular configuration and operating condition (wind farm layout, wind speed, TI, etc.). If other conditions are desired, additional high-fidelity CFD simulations are required. While this problem cannot be completely bypassed, the use of KF that feeds power and sector effective wind speed measurements back onto the model could be an effective tool for reducing the complexity of the approach and its associated computational effort.

8 SINGLE WAKE MODEL BENCHMARK WITH FIELD DATA

8.1 Introduction

A single-wake model benchmarking study was carried out to assess the capability of engineering wake models to accurately predict the mean wake velocity defict across a large range of atmospheric conditions and different operational settings of the turbine. For wind farm control, this capability of the models is of critical importance for a reliable control setpoint optimization across the farm and that model based estimates of the benefit of such strategies lead to realistic results. For this exercise, an existing data set provided by GE was leveraged. The benchmark data set contains wake measurements for a single turbine in normal operation, as well as for operation with reduced rotor thrust/induction. The operation modes with reduced rotor thrust pertain to operation strategies as may be used as part of a wind farm control strategy to reduce wake losses.

Several project partners contributed to the study by generating model predictions corresponding to the measured conditions in the field. The models included in the benchmark are FarmFlow and the two FLORIS packages maintained by TU Delft and NREL, respectively. The input data necessary for calculating model predictions for 36 cases pertaining to different atmospheric conditions and turbine operation were provided to the partners. A limited set of measurement data for baseline turbine operation was provided for model calibration/tuning. Partners then reported back model predictions for a set of measured wind conditions and turbine operation using their respective models. Eventually, no tuning of the model parameters was performed and all results were generated with default parameter settings.

The remainder of this chapter is organized as follows. First, the benchmark data set is described along with the instrumentation and the postrocessing applied to the measurement data. Then, the models included in the benchmark are introduced and the corresponding parameter settings are provided. After outlining the approach for comparing the wake model predictions with the lidar data, results are provided with a focus on the ability of the models to accurately predict the wake velocity deficit across different atmospheric conditions and operation modes.

8.2 Description of benchmark data set

8.2.1 Setup of the experiment and instrumentation

The wake measurements used in the present model benchmark study were acquired for a turbine installed in an operational wind plant in South Texas. The turbine under study is exposed to undisturbed free stream inflow wind conditions for the dominant wind direction sector as shown in fig 93. Data from three operational settings was used in this study. The three operational modes includes baseline operation and two modes with reduced rotor thrust. The reduced rotor thrust was achieved by operating at reduced tip speed ratio and the corresponding power-optimal blade pitch.

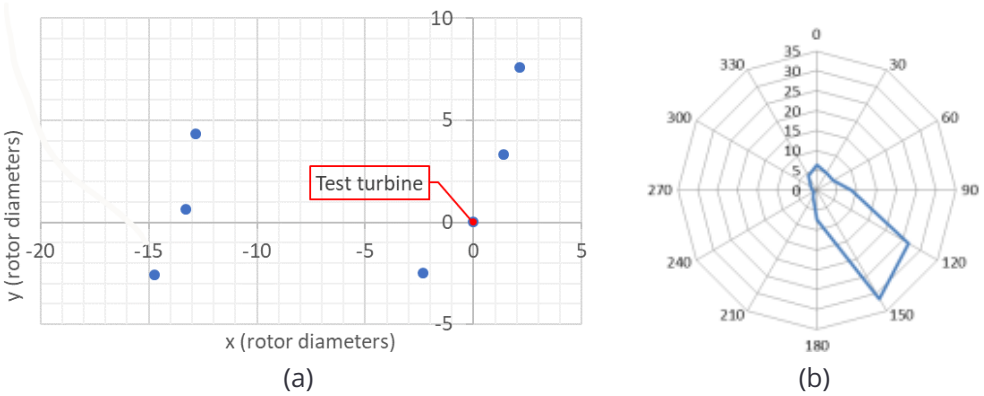

Figure 93. (a) Layout of the test turbine and its immediate neighbors (b) Wind direction distribution at the test site

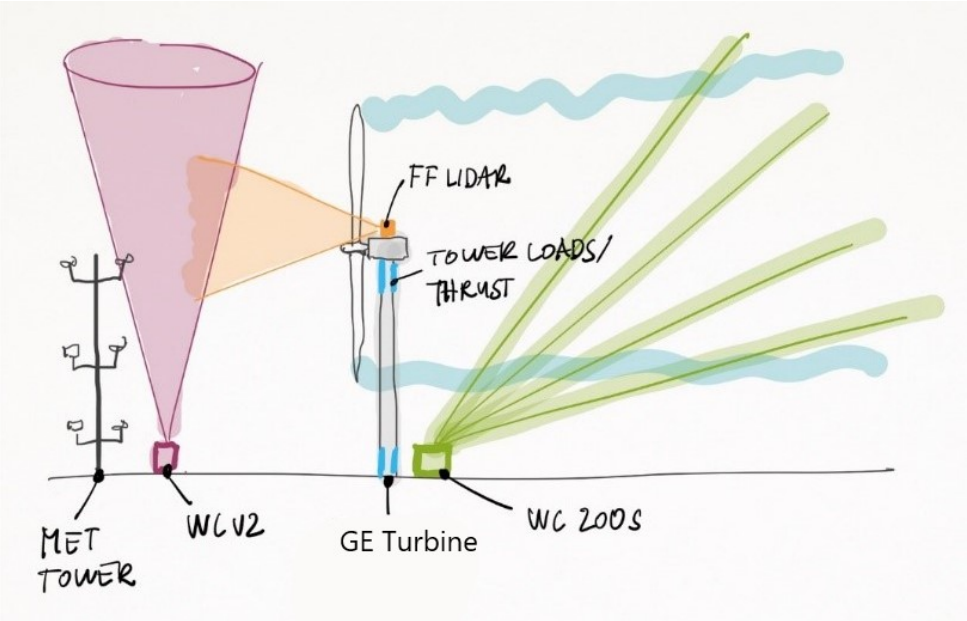

Figure 94. Sketch of the instrumentation setup for the test turbine

The measurement setup available for the test is sketched in fig. 94 and includes the following instrumentation:

- **Inflow wind conditions:** Met mast (wind speed and direction with cups, sonics and vanes, temperature gradient) upstream of test turbine (IEC compliant), WindCube V2 lidar vertical wind profiler next to mast, nacelle-mounted forward-facing lidar
- **Turbine:** Rotor thrust measurements + high frequency performance and operational data
- **Wake:** Windcube 200s scanning lidar at tower base, performs 4 PPI scans of 40 deg azimuth range at 4 elevation angles; scanner speed: 5 deg/s, 500ms accumulation time, 25m range gates

8.2.2 Postprocessing

In order to extract time averaged wake velocity deficits from the measurement setup as described above, four main postprocessing steps were applied to the data

1. Project the lidar wake measurements into a reference frame attached to the present wind direction and reconstruct the downstream component of the wind speed
2. Filter out periods with undesired effects in inflow conditions and/or turbine operation
3. Bin the measurement according to turbine inflow conditions and turbine operation mode
4. Compute bin mean values and confidence intervals of the bin means

In step 1, the instantaneous lidar measurements are tagged with 10-min sliding window averaged quantities of the inflow (centered time stamp), and the calibrated hub-height wind direction measured at the mast is used to project the data into a wind direction attached coordinate frame. The same wind direction is also used to reconstruct the downstream wind speed along with the assumption of a negligible vertical component of the velocity vector. Normalization of the wind speeds in the wake is done with the wind speed measurement from the mast. Due to issues with the primary sensor on the mast, the secondary anemometer located 2 meters below hub-height had to be used for normalization. The rotor thrust coefficient is also computed at in this step and uses nacelle lidar inflow wind speed for normalization.

The main filters applied in step 2 remove data where

- the wind direction is from outside the sector of 100-150 deg.
- the absolute wind veer is > 0.13 deg/m
- the immediate neighbor turbines are not operating normally

In step 3, the data is divided into bins based on hub-height wind speed, atmospheric stability and turbine operation. The split on atmospheric conditions is primarily based on the Bulk Richardson number and vertical wind shear determined based on the measurements at the mast. In order to retain sufficient data in the bins, the data was split in only 3 classes pertaining to stable, neutral and unstable atmospheric conditions.

Step 4 finally provides the averaged wake velocity profiles as reported in this study.

8.2.3 Benchmark cases

The benchmark data set comprised a matrix of 36 cases covering 3 operation modes for 4 wind speed bins ranging from 4-12 m/s, and stable, neutral, and unstable atmospheric conditions. The information provided to the partners for running the model predictions included the rotor diameter

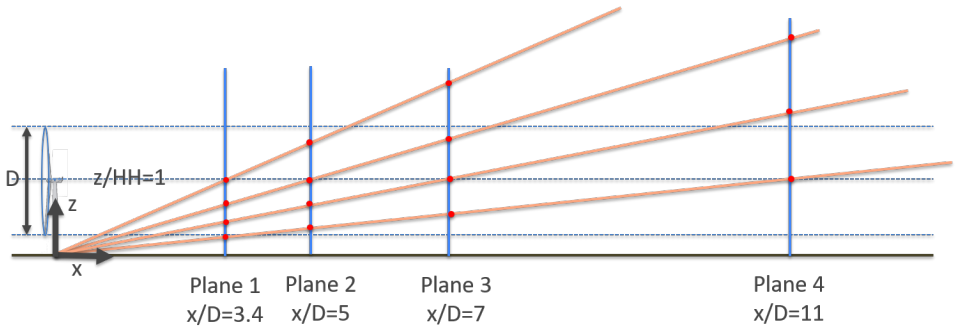

Figure 95. Sketch of the locations where measurement data and model predictions are compared (red dots).

and hub-height of the test turbine, the locations of neighboring turbines, and the following measured mean quantities for each of the 36 cases:

- wind speed
- rotor thrust coefficient
- turbulence intensity
- veer
- shear exponent

The accuracy of the models was assessed by comparing predictions in 4 downstream planes and the corresponding measurement locations of the lidar as sketched in fig. 95.

8.3 Models included in the benchmark and procedure followed to generate predictions

Three partners contributed model predictions for the present benchmarking study: ECN provided results from their inhouse tool FarmFlow , CENER reported prediction results from TUDelft's matlab version of FLORIS , and GE contributed results from the python FLORIS implementation maintained by NREL. In the following, detailed information is provided on how the predictions were obtained with the respective tools.

8.3.1 FarmFlow

ECN contributed model predictions using their inhouse tool FarmFlow which is developed for energy yield calculations of large offshore wind farms [7, 32]. The wind turbine rotors are modelled by prescribing the pressure gradients from the induced velocities by an actuator disk (pre-calculated with a free-vortex wake model), based on the measured thrust coefficient and measured wind speed at hub height as provided in the description of the benchmark cases. Atmospheric stability is included by means of the Monin-Obukhov length, which is calculated from the measured turbulence intensity and shear exponent provided for each of the cases. From these inputs, the velocities in the wake are

calculated by solving the parabolized Navier Stokes equations together with a k-epsilon turbulence model. No neighboring turbines have been included in the predictions, and there was no tuning applied to the data provided upfront.

The coefficients for the standard k-epsilon model are empirically derived for fully turbulent flow fields. The standard k-epsilon model is therefore valid for fully turbulent flows only, like in the far wake of a wind turbine. The main problem of using the standard k-epsilon model in the near wake region of a wind turbine is strong overestimation of the production of turbulence, which results in overestimated recovery of the wake. FarmFlow therefore makes use of adjusted k-epsilon coefficients in the near wake region and in the transition region (between the near wake and the far wake), in order to reduce turbulence. The objective of this tuning was to improve the accuracy of single and multiple wake profiles between 5 and 10 rotor diameters downstream (consistent with the general distance in arrays of wind turbines for which, consequently, enough empirical data was available for the tuning).

Detailed analysis of the LiDAR measurement data has indicated that the wind direction at the measurement site is very stable and does not vary significantly on a 10-min basis. As such, the wind conditions during the measurement differ from the those that have been used for tuning the FarmFlow model wherein more variability of the wind direction is present. As a consequence of this, the wake profile predictions by FarmFlow tend to be somewhat wider and less deep compared to the LiDAR measurements in this study.

8.3.2 FLORIS

CENER used the FLORIS Matlab tool from TUDelft's github repository[1] and tested the "Larsen", "Jensen Gaussian", and "Zones" wake velocity deficit models. In order to launch the 36 test cases, C_pC_t tables were created accordingly to measured data, and several files containing the turbine (specifications.m) and site's characteristics (siteDefinitions/GE_Blindtest.m) were updated. The first file contains the rotor diameter and hub height of the wind turbine, and the second file includes the turbine location, initial yaw, pitch, air density and the input conditions such as inflow wind speed, direction and ambient turbulence. The parameter settings used for the 3 different models are provided in Tables 17, 18, and 19.

GE used the Python implementation of FLORIS maintained by NREL[2] and ran predictions with the "Porté-Agel" model. Turbine specifications and site characteristics were updated in the model input file (xxx_input.json). C_p, and C_t tables for the 36 test cases (to be specified in the model input file) were used from the measured data. Model parameters were set to their default values as maintained in NREL repository at the time of making predictions and are provided in 20. Predictions were made for a single turbine without yaw offset (0 deg).

[1] https://github.com/TUDelft-DataDrivenControl/FLORISSE_M
[2] https://github.com/WISDEM/FLORIS

modelData.adjustInitialWakeDiamToYaw	=	false
modelData.ad	=	-4.5/RotorDiameter
modelData.bd	=	-0.01
modelData.at	=	0.0
modelData.bt	=	0.0
modelData.KdY	=	0.17
modelData.useWakeAngle	=	true
modelData.kd	=	deg2rad(1.5)
modelData.useaUbU	=	true
modelData.aU	=	deg2rad(12.0)
modelData.bU	=	1.3
modelData.Ke	=	0.075
modelData.KeCorrCT	=	0.0
modelData.baselineCT	=	4.0 ∗ (1.0/3.0) ∗ (1.0-(1.0/3.0))
modelData.me	=	[-0.5, 0.22, 1.0]
modelData.MU	=	[0.5, 1.0, 5.5]

Table 17. Parameter settings used for the "Zones" model in FLORIS

modelData.adjustInitialWakeDiamToYaw	=	false
modelData.ad	=	-4.5/RotorDiameter
modelData.bd	=	-0.01
modelData.at	=	0.0
modelData.bt	=	0.0
modelData.KdY	=	0.17
modelData.useWakeAngle	=	true
modelData.kd	=	deg2rad(1.5)

Table 18. Parameter settings used for the "Larsen" model in FLORIS

8.4 Approach for comparing the wake models with lidar data

Results from the models comprised of the velocity field data extracted at pre-specified elevations and streamwise locations in the turbine wake. These results were compared with lidar measurements to determine the prediction capabilities of each model. Following a description of the approach adopted in comparing the models is reported.

As a first step, the hub-height velocity deficit profiles from the models were compared with the lidar profile at different streamwise locations to get a qualitative understanding of the wake recovery prediction from different wake models. Lidar velocity deficit profiles inherently had a spread in the data as these came from measurements in the field and hence had associated uncertainty. Throughout this study, the averaged lidar measurement results are plotted along with 95% confidence intervals of the mean.

Figure 96 shows an example of the hub-height velocity deficit profiles from lidar measurements at different streamwise distances for different atmospheric stability conditions. A notable feature observed in the hub-height velocity deficit profiles from lidar is the undulating movement of the

modelData.adjustInitialWakeDiamToYaw	=	false
modelData.ad	=	-4.5/RotorDiameter
modelData.bd	=	-0.01
modelData.at	=	0.0
modelData.bt	=	0.0
modelData.KdY	=	0.17
modelData.useWakeAngle	=	true
modelData.kd	=	deg2rad(1.5)
modelData.Ke	=	0.075
modelData.KeCorrCT	=	0.0
modelData.baselineCT	=	4.0*(1.0/3.0)*(1.0-(1.0/3.0))

Table 19. Parameter settings used for the "Jensen Gaussian" model in FLORIS

ka	=	0.3
kb	=	0.004
alpha	=	0.58
beta	=	0.077
ad	=	0.0
bd	=	0.0
aT	=	0.0
bT	=	0.0
veer	=	0.0

Table 20. Parameter settings used for the "Porté-Agel" model in FLORIS

mean wake center for increasing downstream distance. The reasons that could be attributed to this movement include the effects of neighboring turbine blockage/wakes and slight modulations of terrain elevation. For the comparison of the lidar data with the model prediction in this study, the lateral offset of the measured velocity deficits is corrected for each downstream distance such that a Gaussian fit to the profiles at hub-height is centered at $y/D = 0$.

Next, the wake center-line peak deficit and the wake width were used as the wake characteristics to make a quantitative comparison of the models with lidar data. The wake center-line peak deficit could be directly read out from the velocity deficit profiles. For the wake width computation, an orthogonal regression curve was fit to the velocity deficit profile from each model. The ratio of standard deviation of the fit to the turbine diameter was used as a measure of the wake width. An example case is shown below in fig. 97 where the actual velocity deficit profile from lidar data and the orthogonal regression fit are co-plotted. Results from the models and the lidar data were then compared based on variations in atmospheric conditions and turbine operation.

8.5 Results

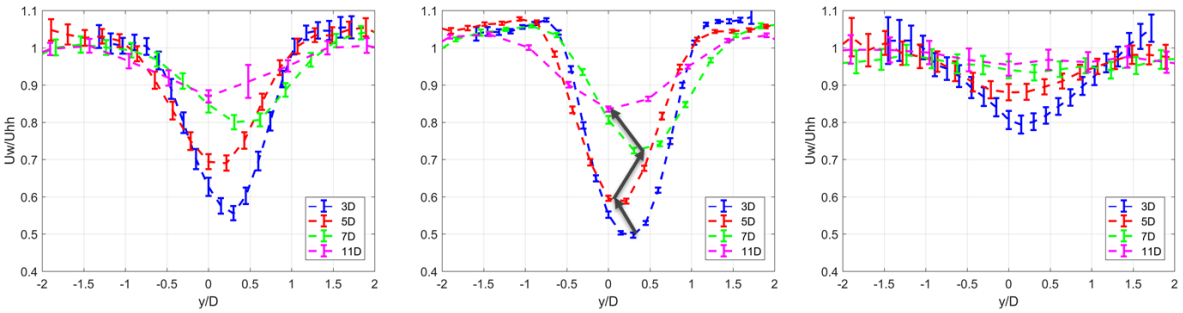

Figure 96. Example of hub-height velocity deficit profiles from lidar measurements at different downstream distances for neutral (left), stable (center) and unstable (right) atmospheric conditions. Black arrows indicate the observed s-shaped path of the center of the time averaged velocity deficit and error bars provide the 95% confidence interval for the mean of the measurements

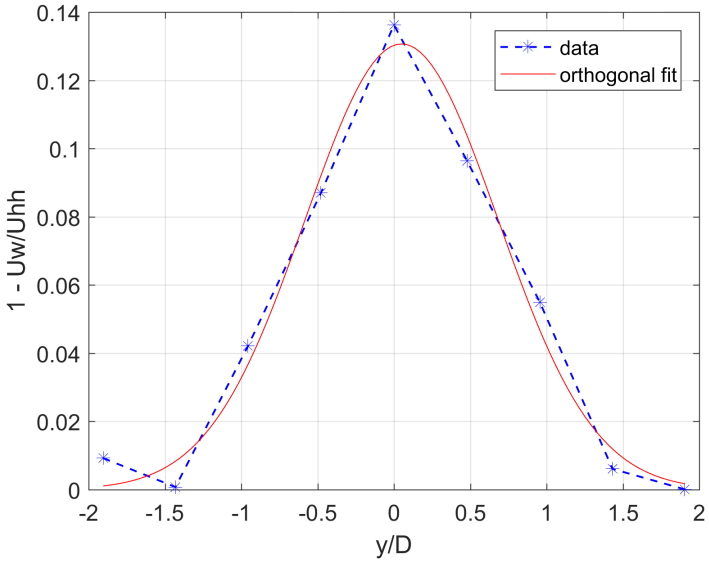

Figure 97. Example of orthogonal regression fit of a Gaussian curve to a measured velocity deficit profile

8.5.1 Wake recovery

For the sake of comparing the hub-height velocity deficit profiles from the models with the measurements, the lidar profiles were shifted in the lateral direction to center the peak of the velocity deficit with zero of the transversal axis (y/D). Figures 98 and 99 show the hub-height velocity deficit profiles from the models and the lidar data for neutral, stable and unstable atmospheric conditions respectively for baseline operation and wind speeds of 6-8 m/s. The hub-height velocity deficits are plotted at 4 different downstream distances in the wake from 3.4 to 11 rotor diameters (D). Clearly, all the models capture the wake recovery, albeit with varying degrees of accuracy in comparison to the lidar data. Figure 100 provides the velocity deficits at different elevations in a vertical plane at a distance of 5 rotor diameters downstream of the turbine. Plots show the wake velocity deficits in the wind speed bin of 6-8 m/s and baseline operation for neutral, stable and unstable atmospheric

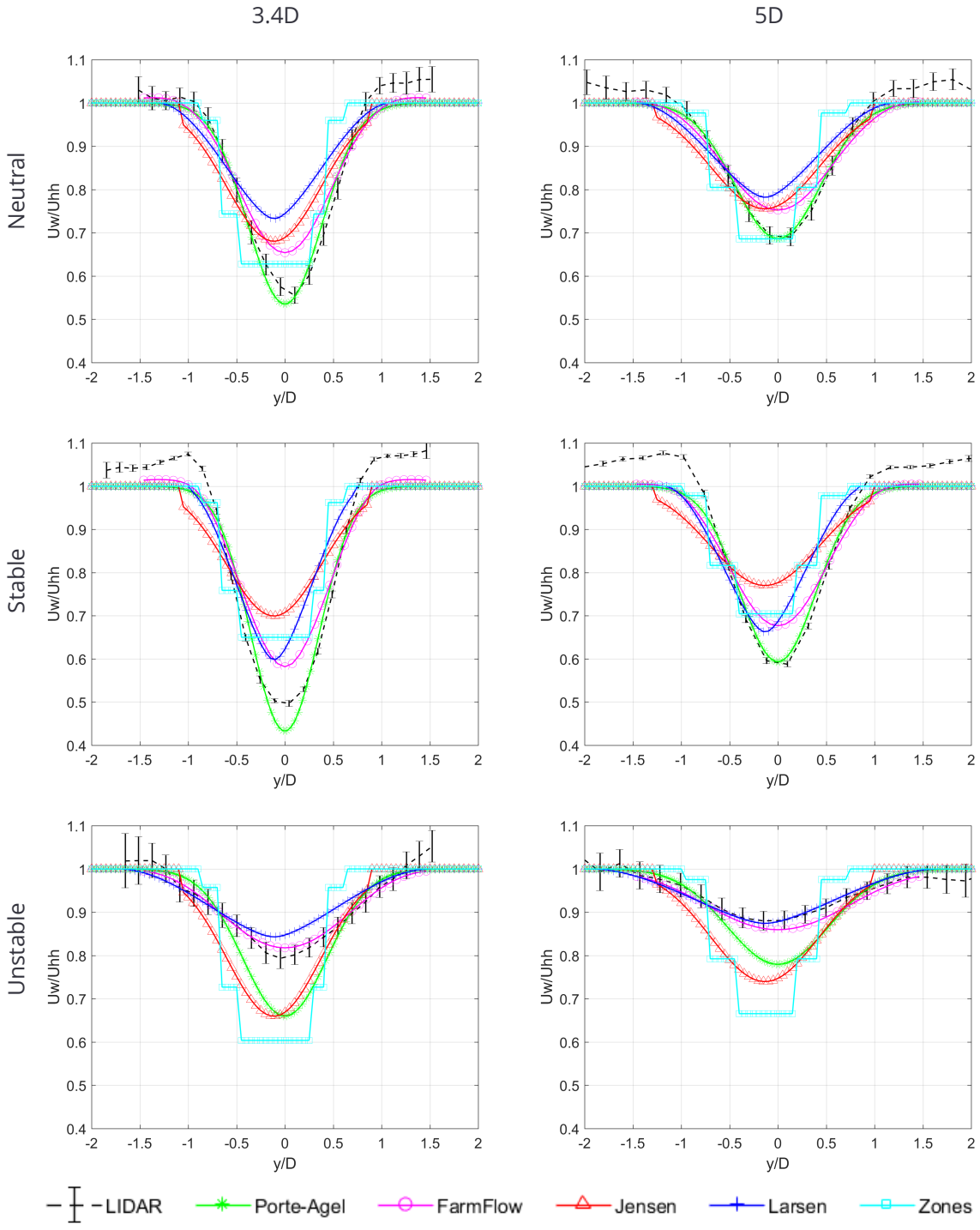

Figure 98. Hub-height velocity deficit profiles for 6-8m/s at 3.4 and 5D downstream for neutral, stable, and unstable atmospheric conditions.

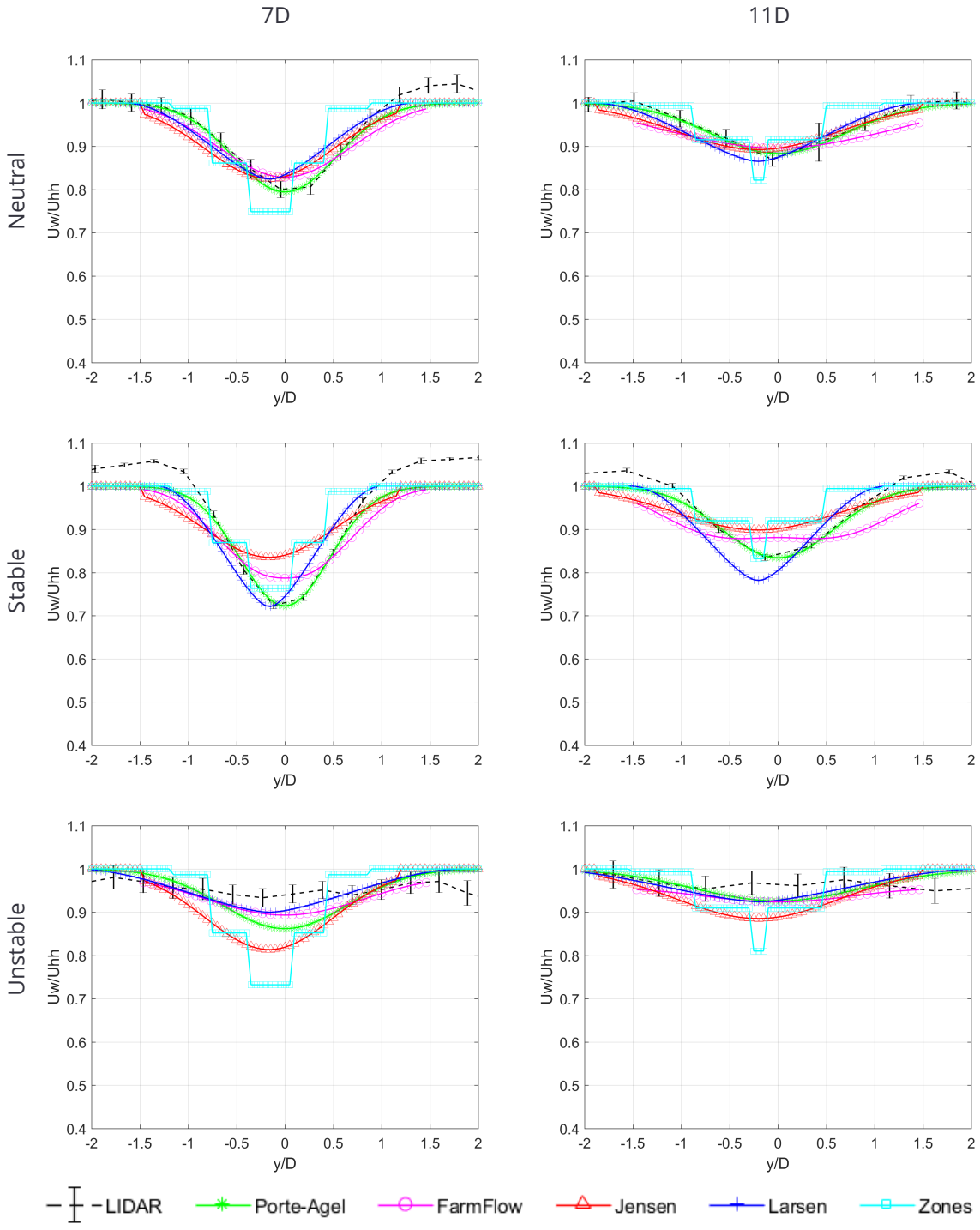

Figure 99. Hub-height velocity deficit profiles for 6-8m/s at 7 and 11D downstream for neutral, stable, and unstable atmospheric conditions.

conditions respectively. Again, all the models show good sensitivity to the variation of velocities in the wake with respect to elevation. Trends from the models follow the lidar data except that the measurements show lateral displacement of the wake center-line with changing elevation also. This is clearly notable from the shift in the lidar peak velocity deficits in the plots and is most pronounced for stable conditions, which also are subject to the largest average wind veer.

8.5.2 Variation of atmospheric conditions

A quantitative assessment of the different wake models in predicting the single turbine wake was done by first comparing their performance with varying atmospheric conditions. Figure 101 shows the comparison of hub-height wake center-line peak velocity deficits with varying wind speed for different atmospheric stability conditions. Clearly, for neutral and stable atmospheric conditions, the Porté-Agel model shows superior performance in comparison to the other models. For unstable atmospheric conditions, FarmFlow and the Larsen model show better agreement with the lidar data. Also, almost all models over-predict the wake velocity deficits for the unstable atmospheric condition. Another notable feature is that the Jensen and Zones models show little sensitivity to variations in wind speed. Figure 102 shows the variation of wake width with varying wind speed for different atmospheric stability conditions at hub-height. Contrary to the trend in wake velocity deficit predictions, models predict the wake width more accurately at the downstream distances of 3.4D and 5D. There appears to be a general trend for the models to under-predict the wake width for the unstable atmospheric condition in comparison to lidar measurements. For the Porté-Agel, Jensen and Zone models, this underprediction in wake width for unstable conditions is substantial with deviations > 20-30%. Again, the width predictions from Jensen and Zones models show little sensitivity to variations in wind speed.

8.5.3 Variation of turbine operation

The ability to accurately predict the change of the velocity deficit with a change of the turbine operation is essential for those farm control strategies that aim at increasing farm power output by reducing wake losses. In the following, hub-height wake center-line peak deficits from the models and the lidar data are compared for baseline operation and operation with reduced thrust. Results for a wind speed range of 6-8 m/s and different atmospheric stability conditions are provided in fig. 103. Hub-height wake center-line peak deficits (Uw/Uhh) are plotted against the streamwise distance (x/D).

The agreement of the model predictions for the thrust reduced operation show comparable trends to baseline operation with the Porté-Agel agreeing best for neutral and stable atmospheric conditions. Looking at the capability of the models to accurately predict the change of the hub-height centerline wake velocity deficit, a couple of observations stand out:

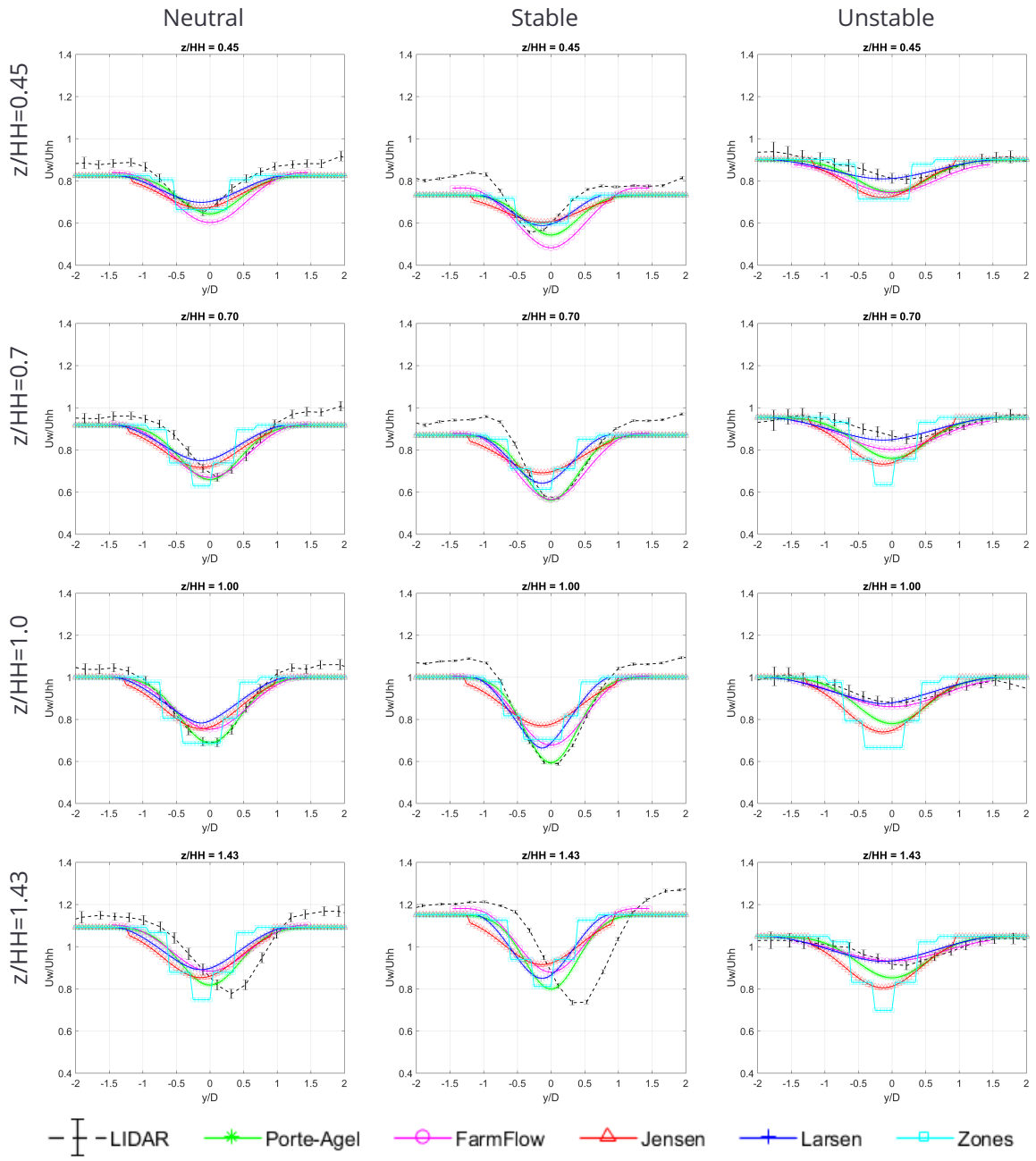

Figure 100. Hub-height velocity deficit profiles for 6-8m/s at 5D for different elevations above ground (z/HH) and neutral, stable, and unstable atmospheric conditions.

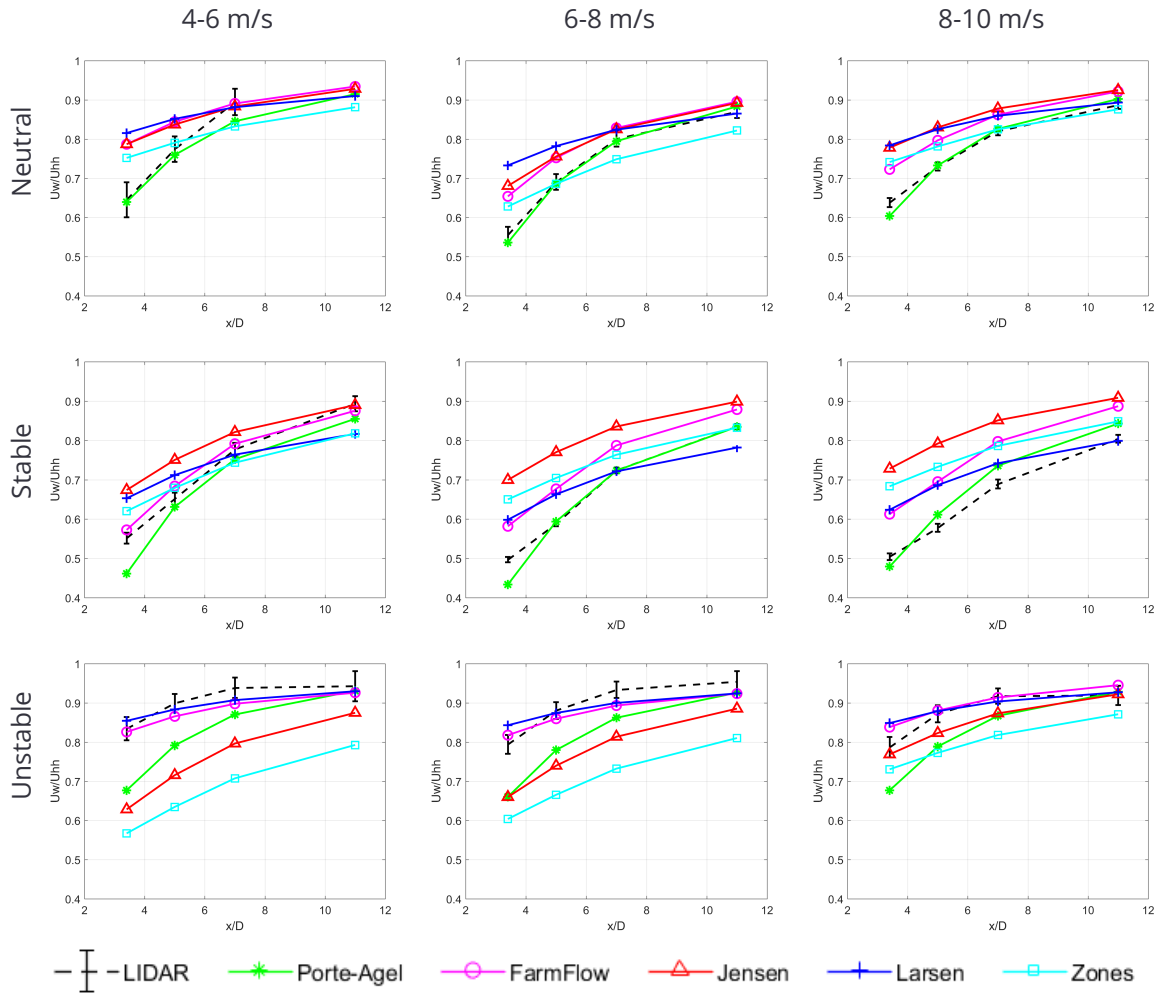

Figure 101. Variation of hub-height wake center-line peak velocity deficit with atmospheric conditions.

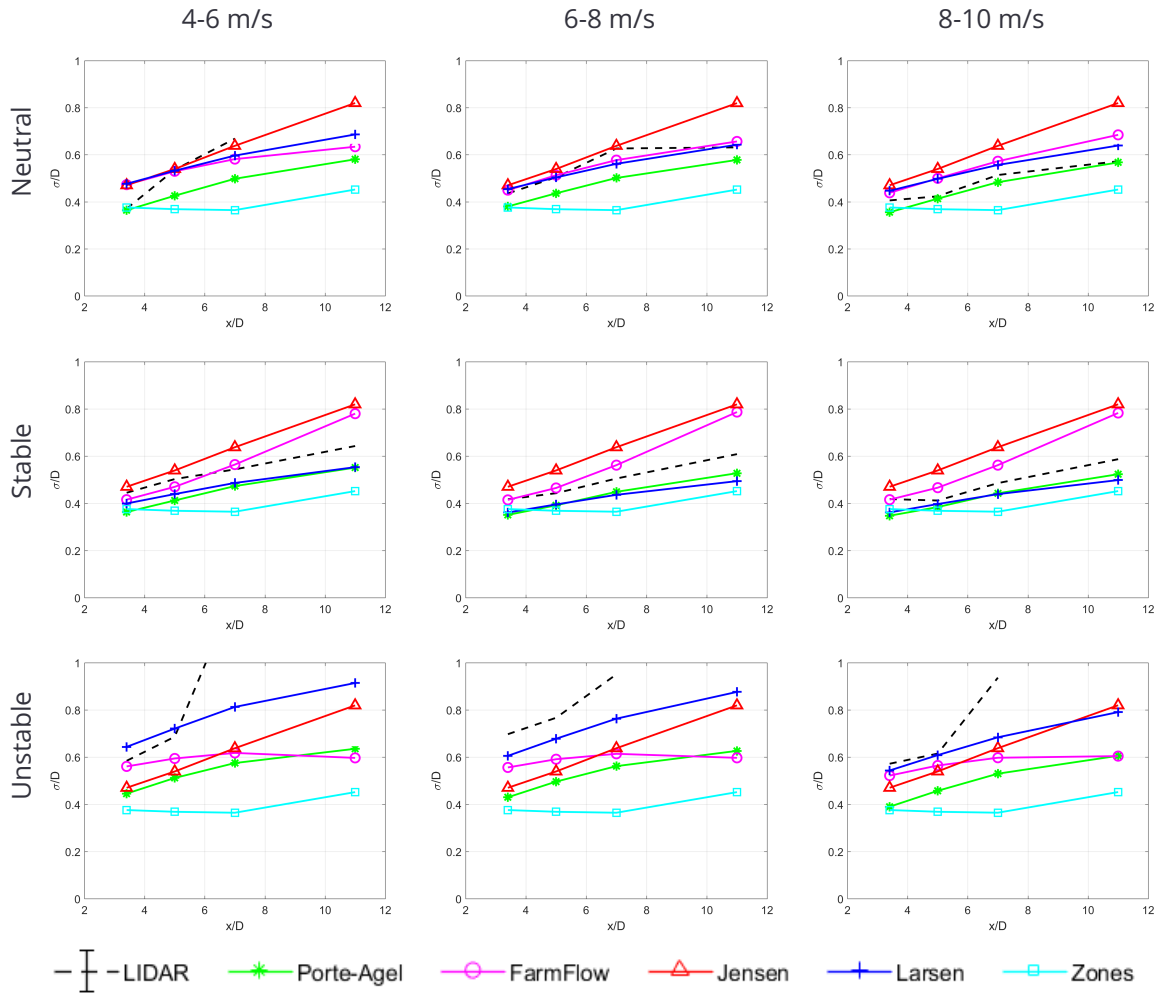

Figure 102. Variation of hub-height wake width with atmospheric conditions.

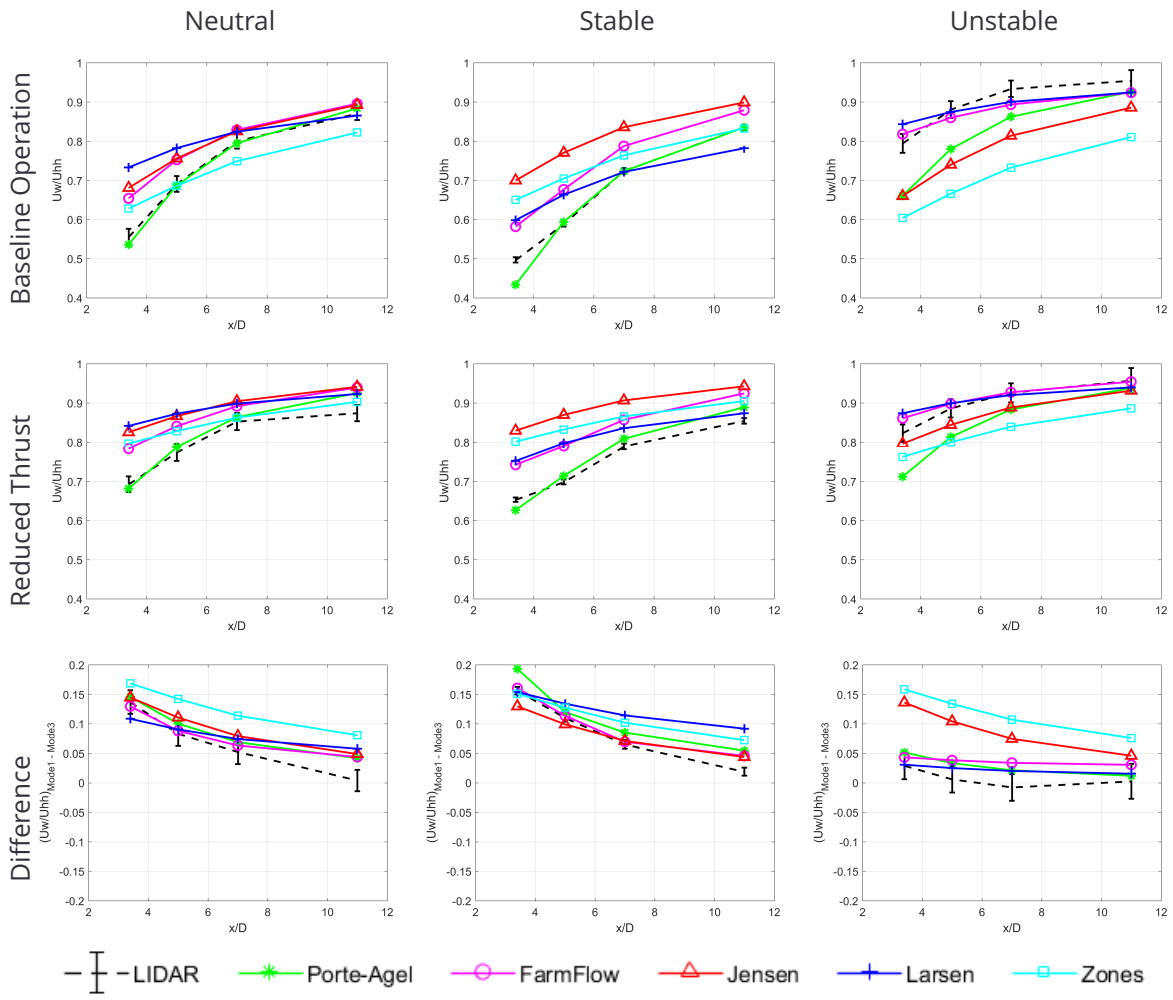

Figure 103. Variation of hub-height wake centerline peak velocity deficit with turbine operation at 6-8m/s. The top row shows results for baseline operation, the second row shows results for thrust-reduced operation, and the bottom row quantifies the delta centerline peak velocity deficit between the two operation modes.

- The Porté-Agel and Jensen models, as well as FarmFlow provide a fair prediction of the delta wake velocity deficit between operation modes for neutral and stable atmospheric conditions up to 7D downstream.
- All models appear to overpredict the control authority over the mean velocity deficit at 11D. The lidar data suggests that only for stable conditions the impact of reducing the rotor thrust can still be felt at 11D.
- For unstable conditions, the lidar data suggest the influence of turbine operation on the velocity deficit is very limited while the Jensen and the Zones model grossly overestimate the control authority over the velocity deficit using rotor thrust.

Figure 104 shows the impact of turbine operation on wake width at hub-height for the 6-8 m/s wind speed bin under different atmospheric stability conditions. The lidar data suggest that a reduction

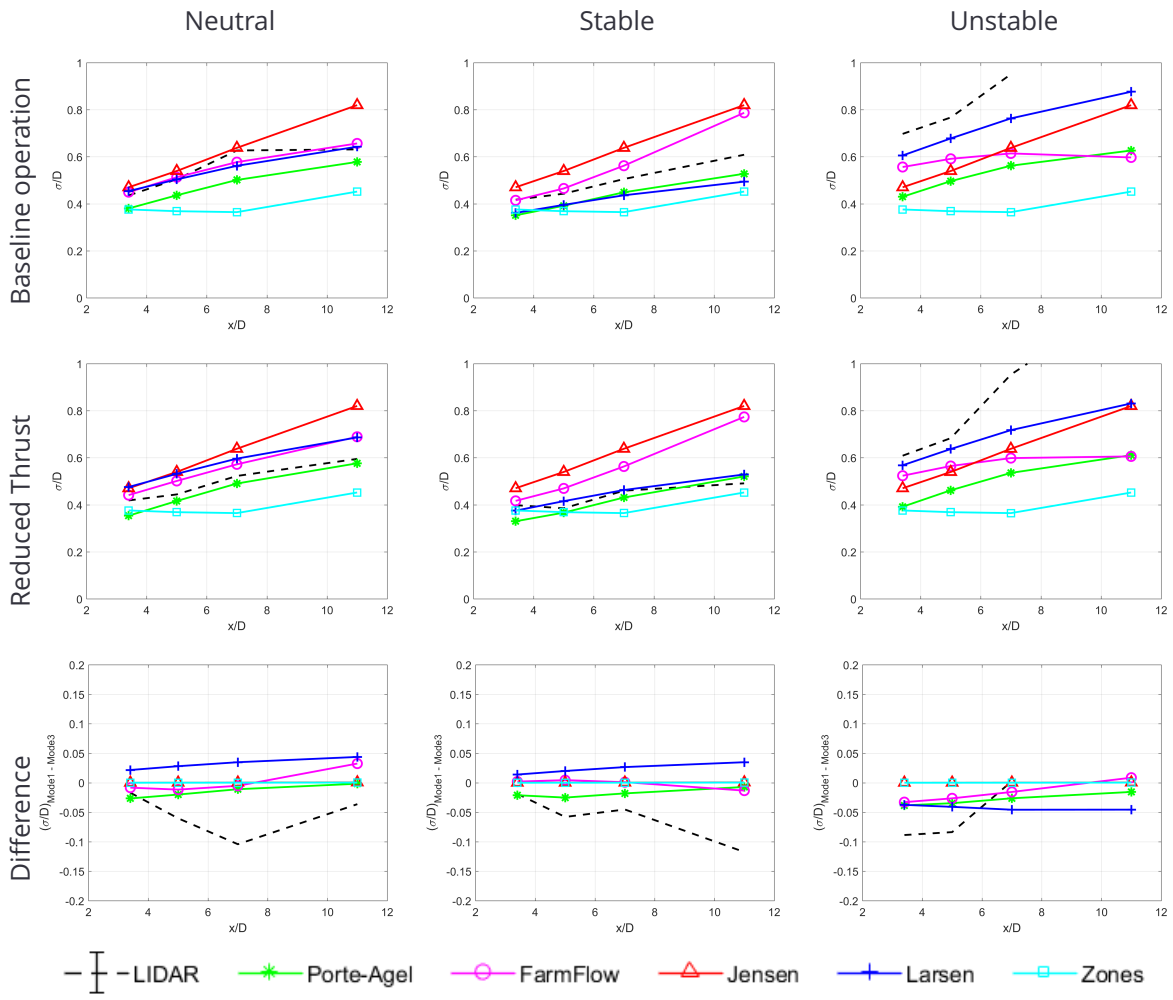

Figure 104. Variation of hub-height wake width with turbine operation at 6-8m/s. The top row shows results for baseline operation, the second row shows results for thrust-reduced operation, and the bottom row quantifies the delta wake width between the two operation modes.

in rotor thrust leads to a reduction in wake width, which is generally reflected in the model results except for the Larsen model for neutral and stable conditions. Overall, changes in predicted and measured wake width as a function of a change in turbine operation is relatively small. At the same time, the trend of the models to (substantially) underpredict wake width for unstable condtions persists also for thrust reduced operation.

8.6 Conclusions

This benchmarking study involved the investigation of five different wake models, viz. Porté-Agel, Jensen, Larsen, Zone (as implemented in FLORIS) and FarmFlow in predicting a single turbine wake velocity deficit. Results from these models were validated against scanning lidar wake measurements performed on a GE turbine in an operational wind farm in South Texas. The model parameters were retained as their defaults and were not tuned in this study for the site-specific conditions.

The study assessed the predictive capabilities of the models specifically for the use in farm control applications where farm energy yield shall be increased by optimizing the individual rotor thrust/induction set points of each turbine. Hence, the models were mainly assessed in terms of their ability to accurately capture the recovery of wind velocities in the wake across a large range of atmospheric conditions and for different turbine operational settings pertaining to thrust/induction control. Two primary wake characteristics were used to compare the performance of models against the lidar measurements: The wake center-line peak velocity deficit and the wake width. The key findings of this study can be summarized as follows:

- The models were, in general, able to capture the trends in wake velocity deficit distributions as compared to the lidar measurements, albeit with varying degrees of accuracy. The Porté-Agel model was found to be the most accurate model for predicting the wake velocity deficits and wake widths for the neutral and stable atmospheric conditions.
- Almost all the models overpredict the wake velocity deficit and underpredict wake width for unstable atmospheric conditions, and hence require tuning of model parameters specifically for these conditions. However, FarmFlow and Larsen show some promise for the unstable atmospheric conditions.
- The lidar data shows that the control authority over the wake velocity deficit using rotor thrust is largest for stable atmospheric conditions and practically vanishes for unstable conditions (except close to the rotor). Also, for distances >10D, the potential to reduce the wake velocity deficit is diminishing except for stable conditions. The degree to which the models are able to capture these trends vary substantially. The Porté-Agel model and FarmFlow perform best while the Zones and Jensen models substantially overpredicts the control authority over the wake velocity deficit using rotor thrust .
- Uncertainty in the lidar measurements was higher for unstable atmospheric conditions due to increased turbulence and associated mixing of flow. This could pose a challenge for the accurate tuning of model parameters for site-specific conditions.

9 CONCLUSIONS

The presented report has described and classified the different wake models being available to the CL-Windcon project. In fact, wakes represent a major interaction between wind turbines and the wind flow. The relevant consideration of the interaction is of high importance to describe well the wake behavior and to predict the impact of the wake interaction.

In the deliverable, first, the models are reviewed and classified with several aspects, but mainly their capabilities for wind farm control applications. A spreadsheet is presented which analyzes and compares the models with their dedicated validity.

Then, different aspects of validation and tuning have been studied. Parameter tuning, estimation and calibrating of the FLORIS and WFSim wake model have been studied. In both cases to ensure that the model calibration procedure was successful the calibrated model is compared with high fidelity models, SOWFA in the FLORIS case and FLORIS and PALM in the WFSim. Both programs, FLORIS and WFSim can capture the wake and power for the wind farm in study. Further, a sensitivity study is performed with the FAST.Farm model. The influence of several parameter of the model on the wake prediction has been studied in the sensitivity study.

The validity of two wake models at the wind tunnel scale have been tested. This aspect is very important for further investigations in the wind tunnel and the assessment of the predictability of the wake by the studied models. In conclusion the models can predict the wake after being tuned properly. Altogether various aspects of the models have been stated and their capabilities have been evaluated and compared.

Finally, a wake model blind benchmark has been presented. In this work the models were compared to predict the wake from a field-testing experiment. Taking the fact into account that field experiments and real measurements include several uncertainties, this investigation has allowed to see the capabilities of the models to capture the wake characteristics without being tuned.

Altogether, various aspects of model classification, tuning aspects and procedures to validate the results have been presented. This deliverable helps partners to choose the model and tuning procedure to apply the dedicated model in the wind farm control applications.

REFERENCES

[1] J Annoni, P. M. O. Gebraad, A. K. Scholbrock, P. A. Fleming, and J. W. van Wingerden. "Analysis of axial-induction-based wind plant control using an engineering and a high-order wind plant model." In: *Wind Energy* 19.6 (2016), pp. 1135–1150. ISSN: 1099-1824.

[2] M. Bastankhah and F. Porté-Agel. "Experimental and theoretical study of wind turbine wakes in yawed conditions." In: *Journal of Fluid Mechanics* 806 (2016), 506––541.

[3] M. Bastankhah and F. Porté-Agel. "Experimental and theoretical study of wind turbine wakes in yawed conditions." In: *Journal of Fluid Mechanics* 806 (2016), pp. 506–541.

[4] S. Boersma, B. M. Doekemeijer, M. Vali, J. Meyers, and J. W. van Wingerden. "A control-oriented dynamic wind farm model: WFSim." In: *Wind Energy Science* (2018).

[5] E Bossanyi. "Dynamic wind power plant simulator for wind farm controller testing." In: *Proceedings of the Wind Energy Science conference*. 2017.

[6] E Bossanyi, T Delouvrié, and S Lindahl. "Long-term simulations for optimising yaw control and start-stop strategies." In: *EWEA-European Wind Energy Association Annual Event, Vienna, Austria* (2013).

[7] E Bot. *FarmFlow validation against fulll scale wind farms*. 2015.

[8] C. Bottasso and J Schreiber. "Online model updating by a wake detector for wind farm control." In: *2018 Annual American Control Conference (ACC)*. IEEE. 2018, pp. 676–681.

[9] M Churchfield and S Lee. *NWTC design codes (SOWFA) http://wind. nrel. gov/designcodes/simulators*. 2012.

[10] M. Churchfield, S. Lee, P. J. Moriarty, L. Martinez, S. Leonardi, G. Vijayakumar, and J. Brasseur. "A Large-Eddy Simulation of Wind-Plant Aerodynamics." In: *50th AIAA Aerospace Sciences Meeting*. January. Nashville, Tennessee: American Institute of Aeroenautics and Astronautics, 2012, pp. 1–19.

[11] M. J. Churchfield, S. Lee, J. Michalakes, and P. J. Moriarty. "A numerical study of the effects of atmospheric and wake turbulence on wind turbine dynamics." In: *Journal of Turbulence* 13.October 2014 (2012), N14. ISSN: 1468-5248. URL: http://www.tandfonline.com/doi/abs/10.1080/14685248.2012.668191.

[12] A Crespo, J Herna, et al. "Turbulence characteristics in wind-turbine wakes." In: *Journal of wind engineering and industrial aerodynamics* 61.1 (1996), pp. 71–85.

[13] A Crespo and J Hernández. "Numerical modelling of the flow field in a wind turbine wake." In: *Proceedings of the 3rd Joint ASCE/ASME Mechanics Conference*. 1989, pp. 121–127.

[14] B. M. Doekemeijer, P Fleming, and J. W. van Wingerden. "Synthesis and validation of a closed-loop wind farm controller using a steady-state surrogate model." In: *American Control Conference (ACC)* (2019). In review.

[15] B. M. Doekemeijer and R Storm. *FLORISSE_M Github repository*. English. https://github.com/TUDelft-DataDrivenControl/FLORISSE_M. 2018.

[16] P. A. Fleming, P. M. Gebraad, S. Lee, J. W. van Wingerden, K. Johnson, M. Churchfield, J. Michalakes, P. Spalart, and P. Moriarty. "Evaluating techniques for redirecting turbine wakes using SOWFA." In: *ICOWES*. Vol. 70. June. Lyngby, Denmark, 2013, pp. 211–218. ISBN: 0960-1481.

[17] P. A. Fleming, P. M. Gebraad, S. Lee, J.-W. van Wingerden, K. Johnson, M. Churchfield, J. Michalakes, P. Spalart, and P. Moriarty. "Evaluating techniques for redirecting turbine wakes using SOWFA." In: *Renewable Energy* 70 (2014), pp. 211–218.

[18] D. GL. *WindFarmer Theory Manual v5.3*. 2014.

[19] S. Guntur, J. M. Jonkman, B. Jonkman, Q. Wang, M. A. Sprague, M. Hind, R. Sievers, and S. J. Schreck. "FAST v8 verification and validation for a MW-scale wind turbine with aeroelastically tailored blades." In: *34th wind energy symposium*. 2016, p. 1008.

[20] J. M. Jonkman and M. L. Buhl. *FAST v6.0 User's Guide*. English. Technical Report. National Renewable Energy Laboratory (NREL), 2005.

[21] J. Jonkman and M. Sprague. *FAST v8 and the transition to OpenFAST*. Tech. rep. Golden, CO: NREL, 2017. URL: https://nwtc.nrel.gov/OpenFAST.

[22] N. Kelley. *Full vector (3-D) inflow simulation in natural and wind farm environments using an expanded version of the SNLWIND (VEERS) turbulence code*. Tech. rep. November 1992. 1992, pp. 1–8.

[23] W.-w. Kim and S. Menon. "A New Dynamic One-Equation Subgrid- Scale Model for Large Eddy Simulations." In: *33rd Aerospace Sciences Meeting and Exhibit*. Atlanta, Georgia, USA.: School of Aerospace Engineering, 1995.

[24] M. Klein, A. Sadiki, and J. Janicka. "A digital filter based generation of inflow data for spatially developing direct numerical or large eddy simulations." In: *Journal of Computational Physics* 186.2 (2003), pp. 652–665. ISSN: 00219991.

[25] J. Mann. "The Spatial Structure of Neutral Atmospheric Surface-Layer Turbulence." In: *Journal of Fluid Mechanics* 273 (1994), pp. 141–168. ISSN: 14697645.

[26] J. Mann. "Wind field simulation." In: *Probabilistic Engineering Mechanics* 13.4 (1998), pp. 269–282. ISSN: 02668920. URL: http://linkinghub.elsevier.com/retrieve/pii/S0266892097000362.

[27] L. A. Martínez-Tossas, J. Annoni, P. A. Fleming, and M. J. Churchfield. "The Aerodynamics of the Curled Wake: A Simplified Model in View of Flow Control." In: *Wind Energy Science Discussions* 2018 (2018), pp. 1–17.

[28] R. Mittal and G. Iaccarino. "Immersed boundary methods." In: *Annu. Rev. Fluid Mech.* 37 (2005), pp. 239–261.

[29] OpenFOAM. *OpenFOAM, the open source CFD toolbox*. 2013. URL: http://www.openfoam.com/.

[30] H. A. Panofsky and J. Dutton. *Atmospheric turbulence: models and methods for engineering applications, 397 pp*. 1984.

[31] S. Raach, D. Schlipf, F. Beyer, and P. W. Cheng. "Wake redirecting using feedback control to improve the power output of wind farms." In: *2016 American Control Conference (ACC)*. IEEE, 2016, pp. 1387–1392.

[32] J. Schepers and S. van der Pijl. "Improved modelling of wake aerodynamics and assessment of new farm control strategies." In: *Journal of Physics, Conference Series 75*. 2007.

[33] J. N. Sorensen and W. Z. Shen. "Numerical Modeling of Wind Turbine Wakes." In: *Journal of Fluids Engineering* 124.2 (2002), p. 393. ISSN: 00982202. URL: http://fluidsengineering.asmedigitalcollection.asme.org/article.aspx?articleid=1429525.

[34] P. S. Veers. *Technical report. Three-Dimensional nd Simulation*. Tech. rep. Albuquerque, NM, USA: Sandia National Labs., 1988.

[35] J Wang, S Foley, E. Nanos, T Yu, F. Campagnolo, C. L. Bottasso, A. Zanotti, and A. Croce. "Numerical and experimental study of wake redirection techniques in a boundary layer wind tunnel." In: *Journal of Physics: Conference Series*. Vol. 854. 1. IOP Publishing. 2017, p. 012048.

[36] A. Yoshizawa and K. Horiuti. "A Statistically-Derived Subgrid-Scale Kinematic Energy Model for the Large-Eddy Simulation of Turbulent Flows." In: *Journal of the Physical Society of Japan* 54.8 (1985), pp. 2834–2839.